Study on Electrochemical Hydrogen Penetration into Iron and Steel with Sinusoidal Perturbation

正弦波変調を用いた
鉄鋼への電気化学的水素侵入の研究

Yudai Yamamoto

Graduate School of Chemical Sciences and Engineering
Hokkaido University

Table of Contents

Chapter 1: Introduction 1

1.1. Hydrogen in iron and steel

1.2. Hydrogen penetration into metal from environment

1.3. Transportation of hydrogen in metal

1.4. Measurement of hydrogen diffusion coefficient

1.5. Devanathan-Stachurski cell

1.6. Step method and sinusoidal perturbation method

1.7. Purpose and outline of this dissertation

1.8. References

Chapter 2: Past Studies on Hydrogen Penetration into Iron and Steel with Devanathan-Stachurski Cells 26

2.1. Introduction

2.2. Hydrogen diffusion coefficient in iron measured by electrochemical method using Devanathan-Stachurski cell

2.3. Modified Devanathan-Stachurski cells

2.3.1. Devanathan-Stachurski cell with corrosion cell

2.3.2. Devanathan-Stachurski cell combined with other hydrogen detection methods

2.3.3. Devanathan-Stachurski cell with a flow cell

2.3.4. Devanathan-Stachurski cell combined with a micro-capillary cell

2.4. Conclusions

2.5. References

Chapter 3: FEM Analysis for Hydrogen Penetration as Multi-dimensional Diffusion 46

3.1. Introduction

3.2. Governing equations and boundary conditions for hydrogen penetration

3.3. FEM calculation

3.4. Results and discussion

3.4.1. One-dimensional diffusion problem

3.4.2. Local measurement with a micro-capillary cell

3.4.3. Two-dimensional diffusion problem

3.5. Conclusions

3.6. References

Chapter 4: Time-Dependent Measurement of Hydrogen Penetration into Iron Sheets from a Borate Buffer Solution Using FFT Analysis 67

4.1. Introduction

4.2. Experimental

4.2.1. Measurement of hydrogen penetration into iron by sinusoidal perturbation method

4.2.2. Derivation of the diffusion coefficient using FFT

4.3. Results and discussion

4.3.1. Actual illustration of FFT processing

4.3.2. Frequency dependence

4.3.3. Dependence of D on specimen thickness and potential

4.3.4. Flow-rate dependence

4.3.5. Time-dependent measurement

4.3.6. Temperature dependence

4.3.7. X-ray photoelectron spectroscopy

4.4. Conclusions

4.5. References

Chapter 5: Summary **97**

Appendix **99**

List of publications **111**

Acknowledgements **112**

Chapter 1: Introduction

1.1. Hydrogen in iron and steel

Metal is an essential structural material because of its hardness, toughness and workability. Steel, which is an iron alloy with carbon, is the most commonly used metal and constitutes around 90% of total global metal production by weight. This is due to its abundance [Ober, 2018] and highly controllable mechanical properties [Urabe and Hosoya, 2005; Yasuno et al., 1992], as depicted in Fig. 1.1 showing the relationship between tensile strength and breakdown elongation. High tensile strength steel (HTSS) possesses superior specific strength (strength-to-weight ratio) and therefore, its importance is increasing from the viewpoint of sustainability [Sugiyama, 2005; Lesch et al., 2017]; its superior specific strength allows for lighter automobiles, resulting in improvement of fuel efficiency without affecting safety. However, the problem of so-called hydrogen embrittlement is also growing.

Hydrogen is the smallest atom, with an atomic radius of 25 pm [Greenwood and Earnshaw, 1984] and penetrates into almost everything; iron and steel are no exception. Hydrogen in a metal is capable of deteriorating the toughness of the metal [Nagumo, 2008]. Hydrogen atoms accumulate in crystallographic defects in metal and form metal-hydrogen clusters that work as origins of cracks. HTSS is known to be especially susceptible to hydrogen embrittlement owing to its higher content of crystallographic defects, including dislocations and grain boundaries [Liu et al., 2016]. Therefore, the development of an efficient way to prevent hydrogen penetration into metallic materials for the safe use of steel is required [Sakairi, 2016]. For such development, it is very important to comprehend the mechanisms and kinetics of hydrogen penetration, i.e. hydrogen diffusion in metal and its durability.

1.2. Hydrogen penetration into metal from environment

Hydrogen is capable of penetrating into metal both from gas phase and from liquid phase. In both cases, hydrogen atoms are adsorbed on one side of the metal surface (hereafter referred to as the entry side) as intermediates. In the case of penetration from gas phase, hydrogen adatoms are produced by dissociation of hydrogen molecules on the surface. In the case of penetration from liquid phase, hydrogen adsorption occurs because of cathodic reactions, such as the hydrogen evolution reaction. The detail of the process of the hydrogen evolution reaction on metals is expressed by the Volmer-Heyrovsky-Tafel mechanism [Bockris, 1952; Lasia et al., 1995]. A hydrogen atom is adsorbed from chemical species in an electrolyte on a metal by a one-electron transfer reaction (Volmer reaction). In an acidic solution, a hydrogen adatom is produced from a proton:

$$H^+ + M + e^- \rightleftharpoons M\text{-}H_{ads}, \qquad \text{Eq. 1.2.1}$$

where M and M-H_{ads} represent an empty adsorption site on a metal and a hydrogen adatom on a metal, respectively. In a basic solution, on the other hand, a water molecule works as a reactant due to the deficiency of protons, as follows:

$$H_2O + M + e^- \rightleftharpoons M\text{-}H_{ads} + OH^-. \qquad \text{Eq. 1.2.2}$$

There are two reaction pathways to hydrogen evolution: One is the electrochemical reaction of a hydrogen adatom and another hydrogen ion in an acidic solution:

$$M\text{-}H_{ads} + H^+ + e^- \rightleftharpoons H_2 + M. \qquad \text{Eq. 1.2.3}$$

In a neutral or basic solution:

$$M\text{-}H_{ads} + H_2O + e^- \rightleftharpoons H_2 + M + OH^-. \qquad \text{Eq. 1.2.4}$$

These reactions are called Heyrovsky reactions. The other pathway is a chemical reaction of two hydrogen adatoms called a Tafel reaction:

$$M\text{-}H_{ads} + M\text{-}H_{ads} \rightleftharpoons H_2 + 2M. \qquad \text{Eq. 1.2.5}$$

No matter whether hydrogen comes from gas phase or from liquid phase, a hydrogen atom adsorbed on metal is capable of being absorbed into metal according to the following reaction:

$$\mathrm{M\text{-}H_{ads}} \rightleftharpoons \mathrm{H_{abs}} + \mathrm{M}, \qquad \text{Eq. 1.2.6}$$

where $\mathrm{H_{abs}}$ represents absorbed hydrogen.

Since the hydrogen evolution reaction is the electrochemical process, the total reaction rate per unit electrode area can be evaluated from current density. For a simple redox reaction, current density i is described by the Butler-Volmer equation as follows:

$$i = i_0 \left(\exp\left(\frac{\alpha_\mathrm{a} z F \eta}{RT}\right) - \exp\left(-\frac{(1-\alpha_\mathrm{a}) z F \eta}{RT}\right)\right), \qquad \text{Eq. 1.2.7}$$

where i_0 is the exchange current density, α_a is the electron transfer coefficient of the oxidation reaction, z is the number of electrons transferred by the reaction, η is the overpotential (the deviation of the electrode potential E from the equilibrium potential E_0), R is gas constant and T is absolute temperature. Here, positive current is defined as the current enhanced by anodic polarization, like the oxygen revolution reaction current. However, Eq. 1.2.7 cannot simply be applied to the hydrogen evolution reaction since the reaction contains multi-step processes. To obtain an equation describing the current density, kinetic equations of relating steps (Eqs. 1.2.1-1.2.6) should be considered.

The rate v_V of the forward reaction of the Volmer step in an acidic environment can be written as follows:

$$v_\mathrm{V} = k_\mathrm{V}\left(1 - \theta_\mathrm{coverage}\right) a_{\mathrm{H^+}} \exp\left(-\frac{(1-\alpha_\mathrm{a}) F \eta}{RT}\right), \qquad \text{Eq. 1.2.8}$$

where k_V is the rate constant of the forward Volmer reaction, θ_coverage is the surface coverage of $\mathrm{H_{ads}}$, and $\alpha_{\mathrm{H^+}}$ is the activity of $\mathrm{H^+}$ in the solution. Similarly, the rate $v_{-\mathrm{V}}$ of the backward reaction of the Volmer step can be written as follows:

$$v_{-\mathrm{V}} = k_{-\mathrm{V}} \theta_\mathrm{coverage} \exp\left(\frac{\alpha_\mathrm{a} F \eta}{RT}\right), \qquad \text{Eq. 1.2.9}$$

where $k_{-\mathrm{V}}$ is the rate constant of the backward Volmer reaction. Moreover, the forward and

backward Volmer reaction rates v'_{V} and v'_{-V} in a neutral or basic solution are described using the rate constants k'_{V} and k'_{-V}, respectively, as follows:

$$v'_{V} = k'_{V}\left(1 - \theta_{\text{coverage}}\right)a_{H_2O}\exp\left(-\frac{(1-\alpha_a)F\eta}{RT}\right), \quad \text{Eq. 1.2.10}$$

$$v'_{-V} = k'_{-V}\theta_{\text{coverage}}a_{OH^-}\exp\left(\frac{\alpha_a F\eta}{RT}\right), \quad \text{Eq. 1.2.11}$$

where α_{H2O} and α_{OH-} are the activities of H_2O and OH^- in the solution, respectively. The rate v_H and v_{-H} of the forward and the backward reactions of the Heyrovsky step are described as follows:

$$v_H = k_H\theta_{\text{coverage}}a_{H^+}\exp\left(-\frac{(1-\alpha_a)F\eta}{RT}\right), \quad \text{Eq. 1.2.12}$$

$$v_{-H} = k_{-H}(1 - \theta_{\text{coverage}})a_{H_2}\exp\left(\frac{\alpha_a F\eta}{RT}\right), \quad \text{Eq. 1.2.13}$$

where k_H and k_{-H} are the rate constants of the forward and the backward Heyrovsky reactions, respectively, and α_{H2} is the activity of H_2 dissolved in the solution. In the case of a neutral or basic environment, the rates v'_{H} and v'_{-H} of the forward and the backward reactions of the Heyrovsky step are described using the rate constants k'_{H} and k'_{-H}, respectively, as follows:

$$v'_{H} = k'_{H}\theta_{\text{coverage}}a_{H_2O}\exp\left(-\frac{(1-\alpha_a)F\eta}{RT}\right), \quad \text{Eq. 1.2.14}$$

$$v'_{-H} = k'_{-H}(1 - \theta_{\text{coverage}})a_{H_2}a_{OH^-}\exp\left(\frac{\alpha_a F\eta}{RT}\right), \quad \text{Eq. 1.2.15}$$

In the same way, the reaction rates v_T and v_{-T} of the forward and the backward reactions of the Tafel step are expressed as follows:

$$v_T = k_T\theta_{\text{coverage}}^{\,2}, \quad \text{Eq. 1.2.16}$$

$$v_{-T} = k_{-T}\left(1 - \theta_{\text{coverage}}\right)^2 a_{H_2}, \quad \text{Eq. 1.2.17}$$

where k_T and k_{-T} are the rate constants of the forward and the backward Tafel reactions, respectively.

Hydrogen entry into metal can also be considered as dissolution. From this viewpoint, the hydrogen dissolution reaction is described as follows:

$$\frac{1}{2}H_2 \rightleftharpoons H_{abs}. \quad \text{Eq. 1.2.18}$$

Under equilibrium, the chemical potential of H_2 and H_{abs} is equivalent:

$$\frac{1}{2}\mu_{H_2} = \mu_{H_{abs}}. \quad \text{Eq. 1.2.19}$$

Chemical potential μ_i and the activity a_i of a chemical species i are expressed by standard chemical potential $\mu_{0,i}$ as follows:

$$\mu_i = \mu_{0,i} + RT \ln a_i. \quad \text{Eq. 1.2.20}$$

From Eqs. 1.2.19-1.2.20, standard Gibbs free energy change ΔG_0 of the hydrogen dissolution reaction (Eq. 1.2.18) is written as follows:

$$\begin{aligned}\Delta G_0 &= \mu_{0,H_{abs}} - \frac{1}{2}\mu_{0,H_2} \\ &= \left(\mu_{H_{abs}} - RT \ln a_{H_{abs}}\right) - \frac{1}{2}\left(\mu_{H_2} - RT \ln a_{H_2}\right) \\ &= \left(\mu_{H_{abs}} - \frac{1}{2}\mu_{H_2}\right) + RT\left(\ln \sqrt{a_{H_2}} - \ln a_{H_{abs}}\right) \\ &= RT \ln \frac{\sqrt{a_{H_2}}}{a_{H_{abs}}}. \quad \text{Eq. 1.2.21}\end{aligned}$$

Gibbs free energy change is also expressed by enthalpy change ΔH and entropy change ΔS:

$$\Delta G_0 = \Delta H_0 - T\Delta S_0, \quad \text{Eq. 1.2.22}$$

where ΔH_0 and ΔS_0 are the standard enthalpy change and the standard entropy change of the reaction, respectively. Combining Eqs. 1.2.21-1.2.22, the following equation is yielded:

$$a_{H_{abs}} = \sqrt{a_{H_2}} \exp\left(-\frac{\Delta G_0}{RT}\right) = \sqrt{a_{H_2}} \exp\left(-\frac{\Delta H_0}{RT}\right) \exp\left(\frac{\Delta S_0}{R}\right), \quad \text{Eq. 1.2.23}$$

The solubility of hydrogen in metal depends on the temperature, and the temperature dependence is determined by the standard enthalpy change ΔH_0 of the dissolution. ΔH_0 is positive (endothermic) for some metals, such as iron, nickel and platinum. On the other hand, ΔH_0 is negative (exothermic) for some other metals, such as titanium, vanadium, and palladium. The temperature dependence of the hydrogen solubility is shown in Fig. 1.2 [Huang et al., 1979].

Hydrogen absorbed in a metal lattice exists in an interstitial site due to its small atomic

radius. Hydrogen is also trapped by any lattice defects. Fig. 1.3 schematically illustrates the energy level of hydrogen in metal. Hydrogen is considered to exist in a trough of the energy level. In order to move to an adjacent trough, hydrogen needs to pass over a potential hill as activation energy E_a. Defects in the lattice form troughs whose depths are different from that of ordinary interstitial sites. Troughs deeper than the ordinary interstitial sites work as trapping sites for hydrogen due to the need for larger activation energy for escape. Trapping sites are roughly classified into two types according to their depths. Relatively shallow troughs correspond to reversible trap sites, from which hydrogen can escape at the temperature of interest. Deep troughs work as irreversible trap sites, where trapped hydrogen cannot escape.

Hydrogen penetration from gas phase occurs on metal materials in contact with hydrogen gas, for example, in an H_2 gas reservoir. The safety of an H_2 reservoir is of paramount importance for systems using high-pressure H_2 gas such as fuel cell vehicles. On the other hand, hydrogen penetration from liquid phase occurs on most metal materials subjected to corrosion, since corrosion processes are often proceeded by cathodic hydrogen evolution reactions (Eqs. 1.2.1-1.2.5) and/or oxygen reduction reactions. If research interests are on the hydrogen transportation process in metal, both methods are acceptable because the hydrogen absorption process (Eq. 1.2.6) after hydrogen adsorption is substantially equivalent for both methods. In this way, both penetration from gas phase and from liquid phase are industrially important and have been studied in past researches on hydrogen penetration (see Chapter 2).

1.3. Transportation of hydrogen in metal

Hydrogen atoms absorbed from the (entry side) metal surface have an inhomogeneous distribution, which is a concentrated region of absorbed hydrogen atoms. However, the state is thermodynamically unstable. The hydrogen atoms are gradually diluted into the metal bulk by diffusion to form a homogeneous distribution.

Fick explained that the diffusive flux **J** of substances is in proportion to the concentration gradient ∇C formed in the substrate, as follows:

$$\mathbf{J} = -D\nabla C, \qquad \text{Eq. 1.3.1}$$

where the proportional coefficient D is called the diffusion coefficient whose value generally depends on both substance and substrate. Eq. 1.3.1 is called Fick's first law. The concentration change at a point in a substance is related to mass valance depending on changes in flux $\nabla \cdot \mathbf{J}$ and reaction rate ν at the point and is described in the following second law:

$$\frac{\partial C}{\partial t} + \nabla \cdot \mathbf{J} = \nu, \qquad \text{Eq. 1.3.2}$$

It is commonly thought that diffusion of hydrogen in steel completely obeys these two laws of Eqs. 1.3.1 and 1.3.2. For hydrogen diffusion in metal, the hydrogen-trapping reaction is included in the reaction term. In hydrogen diffusion under ideal conditions such as hydrogen diffusion in a well-annealed pure metal, the reaction term in Eq. 1.3.2 is negligible:

$$\frac{\partial C}{\partial t} + \nabla \cdot \mathbf{J} = 0. \qquad \text{Eq. 1.3.3}$$

For a system in a steady state, Eq. 1.3.3 can be simplified as follows:

$$\nabla \cdot \mathbf{J} = -D\nabla^2 C = 0. \qquad \text{Eq. 1.3.4}$$

As mentioned in Section 1.2, hydrogen atoms in a metal lattice exist in troughs of the energy level (Fig. 1.3). In the process of diffusion, the atoms jump to the adjacent troughs passing over the hills of energy as activation energy. It is dependent on the energy of the hydrogen atom whether the atom can pass over the hill or not. Since the energy distribution of the atoms in the system is described by Boltzmann distribution, the probability of jump is dependent on temperature. Therefore, the hydrogen diffusion coefficient D exhibits an Arrhenius-type temperature dependence, as shown in the following equation [Nagumo, 2008]:

$$D = D_0 \exp\left(\frac{-E_a}{RT}\right), \qquad \text{Eq. 1.3.5}$$

where D_0 is the maximum value of D at high temperature, and E_a is the activation energy for the diffusion of hydrogen. Temperature dependence of the hydrogen diffusion coefficient is one of the important factors to represent hydrogen penetration behavior because it reflects the strength of the interaction between hydrogen and the metal lattice.

In specimens with trap sites such as dislocations, impurity atoms, lattice vacancies and grain boundaries, on the other hand, hydrogen trapping also affects the behavior of hydrogen in metal. McNabb and Foster proposed a model with reversible trapping by modification of Eq. 1.3.2, as follows [McNabb and Foster, 1963]:

$$\frac{\partial C}{\partial t} + N\frac{\partial n}{\partial t} + \nabla \cdot \mathbf{J} = 0, \qquad \text{Eq. 1.3.6}$$

$$\frac{\partial n}{\partial t} = kC(1-n) - pn, \qquad \text{Eq. 1.3.7}$$

where N is concentration of trapping site, n is occupancy of trapping site, k is probability of trapping, and p is probability of de-trapping. A model with irreversible trapping can also be described by these equations with p = 0. Eqs. 1.3.6-1.3.7 can be referred to as a simple deformation of Eq. 1.3.2 assuming the trapping sites and the trapped hydrogen atoms as chemical species with D = 0. This model is an archetype for analysis of hydrogen transport with trapping, since the model can be generally applicable and is difficult to solve analytically. Oriani proposed an approximated model by introducing a thermodynamic interpretation of McNabb-Foster's theory [Oriani, 1970]. Assuming local equilibrium for trapping/de-trapping, an effective hydrogen diffusion coefficient in a specimen with reversible trap is derived as follows:

$$D_{\mathrm{eff}} = \frac{C_{\mathrm{lattice}}}{C_{\mathrm{lattice}} + C_{\mathrm{trap}}(1-n_{\mathrm{trap}})} D_{\mathrm{lattice}}, \qquad \text{Eq. 1.3.8}$$

where C_{lattice} and C_{trap} are hydrogen concentration in interstitial positions of a regular lattice and in trap sites, respectively, n_{trap} is fractional occupancy of hydrogen trap sites and D_{lattice} is the hydrogen diffusion coefficient in a regular lattice. If the specimen has no trapping sites, D_{eff} is equal to D_{lattice} and D in Eq.1.3.2 but becomes smaller according to the significance of the trapping effect.

1.4. Measurement of hydrogen diffusion coefficient

As mentioned in Sections 1.2 and 1.3, hydrogen penetrates into metal from the environment via the absorbed state (entry reaction) and diffuses inside the metal. Hydrogen

absorbed in metal can also escape from the metal by desorption, which is the backward reaction of Eq. 1.2.6, called the exit reaction. If the hydrogen entry reaction and the exit reaction occur on different sides of a metal sheet, hydrogen atoms need to diffuse through the whole thickness of the sheet from the entry side to the exit side. This behavior of hydrogen entry and exit reactions is utilized to measure a hydrogen diffusion coefficient as follows.

Assuming that hydrogen atoms diffuse in a sheet-type homogeneous specimen, the thickness of which is sufficiently smaller than lengths in the plane direction, the diffusion of hydrogen can be expressed by a one-dimensional form of Eq. 1.3.3 as follows:

$$\frac{\partial C}{\partial t} = D\frac{\partial^2}{\partial x^2}C, \qquad \text{Eq. 1.4.1}$$

where x represents a coordinate in the thickness direction of the sheet. Here, hydrogen penetration from gas phase into the sheet with thickness L is assumed. Hydrogen is introduced on one side (the entry side) of the specimen by exposure to hydrogen gas. Simultaneously, the other side (the exit side) of the specimen is put into an environment where adsorbed hydrogen atoms are forcibly removed, such as a vacuum. Hydrogen atoms absorbed into the specimen diffuse from the entry side to the exit side and are then desorbed from the exit side. Since it is thought that hydrogen diffusion is quite slow compared with the surface reaction (Eq. 1.2.6), absorbed hydrogen concentration $C_{x=0}$ at the entry side is regarded as constant due to the equilibrium or quasi-equilibrium reaction of Eq. 1.2.6:

$$C_{x=0} = C_0, \qquad \text{Eq. 1.4.2}$$

where C_0 is the hydrogen concentration at the entry side surface of the sheet. Absorbed hydrogen concentration at the exit side can be regarded as zero, when the desorption reaction is significantly fast compared with diffusion. The hydrogen concentration $C_{x=L}$ at the exit side surface can be written as follows:

$$C_{x=L} = 0. \qquad \text{Eq. 1.4.3}$$

In addition, the initial hydrogen concentration before starting hydrogen penetration is zero, therefore, the initial condition is defined as follows:

$$C_{t=0} = 0. \qquad \text{Eq. 1.4.4}$$

Under the boundary condition of Eqs. 1.4.2-1.4.4, Eq 1.4.1 can be solved algebraically and the hydrogen mass flux passing through the exit side surface is expressed as follows:

$$\mathbf{J}_{x=L} = \frac{DC_0}{L}\left[1 + 2\sum_{m=1}^{\infty} \exp(-1)^m \exp(-\frac{Dm^2\pi^2}{L^2}t)\right] . \qquad \text{Eq. 1.4.5}$$

According to Eq. 1.4.5, $\mathbf{J}_{x=L}$ exhibits some characteristic values at specific times which can be utilized to represent the hydrogen diffusion coefficient as depicted in Fig. 1.4. The breakdown time t_{break} of $\mathbf{J}_{x=L}$ has a relationship with D as follows:

$$t_{\text{break}} = \frac{0.5L^2}{\pi D} . \qquad \text{Eq. 1.4.6}$$

t_{break} can be obtained as a t-intercept of extrapolation of $\mathbf{J}_{x=L}$ transient. In addition, the time lag t_{lag} for $\mathbf{J}_{x=L}$ to reach 63.2% of the steady-state value (= (1–1/e) $\mathbf{J}_{t=\infty}$) has a relationship with D as follows:

$$t_{\text{lag}} = \frac{L^2}{6D} . \qquad \text{Eq. 1.4.7}$$

1.5. Devanathan-Stachurski cell

Although some electrochemical techniques for measurement of hydrogen penetration were developed before 1962, they were not published openly [Bockris, 1959; Bockris and Devanathan, 1961]. Devanathan and Stachurski produced the first publication about the electrochemical method to measure the hydrogen diffusion coefficient according to the principle mentioned in Section 1.4 [Devanathan and Stachurski, 1962]. Fig. 1.5 shows the double electrochemical cell to measure the hydrogen diffusion coefficient, which is nowadays referred to as a Devanathan-Stachurski (DS) cell. A metal sheet specimen is placed between two independent cells to conduct different electrochemical reactions on each interface simultaneously. One side of the specimen (the entry side) is cathodically polarized to induce hydrogen evolution and absorption reactions (forward reactions of Eqs. 1.3.1-1.3.6), while the other side (the exit side) is anodically polarized to cause the hydrogen desorption reaction

(backward reactions of Eqs. 1.3.6 and 1.3.1). The boundary conditions of Eqs. 1.4.3 and 1.4.4 can be achieved by galvanostatic polarization and potentiostatic polarization for the entry side and the exit side, respectively. A comparison between the currents measured for the entry and exit sides provides information on hydrogen penetration, such as the hydrogen diffusion coefficient (Eqs. 1.4.6, 1.4.7) and hydrogen absorption efficiency φ, as follows:

$$\varphi = \frac{I_{\mathrm{exit}}}{|I_{\mathrm{entry}}|} \ . \qquad \text{Eq. 1.5.1}$$

This electrochemical method using a DS cell is relatively convenient and therefore has become a standard way to measure the hydrogen diffusion coefficient.

The electrochemical hydrogen penetration method using a DS cell has some advantages compared with the penetration from gas phase. The DS cell method does not need a pressure-resistant chamber, a vacuum pump, and a gas bomb of explosive hydrogen gas since the hydrogen entry side reaction is induced via electrochemical polarization instead. For these reasons, the DS cell method has been widely utilized for the determination of the hydrogen diffusion coefficient in a metal specimen.

On the other hand, the DS cell method also has substantial disadvantages. Since the method uses aqueous electrolyte solution as the source of hydrogen, it is very difficult to conduct measurement at temperatures higher than 373K (the boiling point of water) or lower than 273K (the freezing point of water). There are very few reports of measurements at temperatures outside of this range; Nagano et al. reported an electrochemical hydrogen penetration measurement at 222K using electrolyte mixed with methanol [Nagano et al., 1981].

1.6. Step method and sinusoidal perturbation method

The method of hydrogen diffusion coefficient measurement using Eq. 1.4.6 or 1.4.7 is called the “step method”. In the step method, the entry side of the specimen is quickly polarized

at a cathodic potential at which hydrogen adsorbs efficiently. The exit side current starts to flow after some delay, which corresponds to the time lag for hydrogen diffusion from the entry side to the exit side inside the metal specimen. The ASTM Standard Practice [ASTM International, 2011] defines the evaluation using a DS cell with Eq. 1.4.7 as a standard way of measuring a hydrogen diffusion coefficient. In the step method, it is necessary to obtain the steady-state value of the exit side current, though it is generally small and involves uncertainty. In case of hydrogen penetration into iron, absorption efficiency is a few percent, in general. In the case where the exit side current is comparable to the background noise, it is difficult to obtain a reliable diffusion coefficient.

Sekine [Sekine, 1975 and 1977] and Boes et al. [Boes et al., 1976] individually reported another method to measure the hydrogen diffusion coefficient. It can be referred to as the "sinusoidal perturbation method", in which a parameter such as polarization potential, current, or electrolyte flow rate at the entry side surface is sinusoidally perturbed. The perturbation induces a sinusoidal perturbation in the surface coverage of hydrogen via the changes in the reaction rates of the hydrogen evolution reaction (Eqs. 1.2.1-1.2.5). Since hydrogen absorption at the entry side and hydrogen desorption at the exit side (the forward and the backward reaction of Eq. 1.2.6, respectively) are rapid compared with the diffusion of hydrogen in a steel sheet [Iyer et al., 1989], the reactions on both sides are considered to be always in equilibrium. Under this condition, the concentration of the absorbed hydrogen at the entry side surface is also perturbed sinusoidally as follows:

$$C_{x=0} = C_0 + \Delta C \sin(2\pi f t), \qquad \text{Eq. 1.6.1}$$

where ΔC represent the perturbation amplitude of the concentration of absorbed hydrogen at the entry side interface and f is the frequency of the applied perturbation. The sinusoidal signal

induced by the perturbation at the entry side is observed in entry side current. Similar to Eq. 1.4.3, the concentration at the exit side interface is assumed to be zero as hydrogen desorption from the exit side surface is sufficiently fast:

$$C_{x=L} = 0. \qquad \text{Eq. 1.6.2}$$

The signal transmitted through hydrogen diffusion in the sheet to the exit side is detected as the sinusoidal current with attenuated amplitude and a delay. Similar to the time lag in the step method, the delay in the sinusoidal perturbation method can be quantified as a phase shift θ from the entry current to the exit current, as depicted in Fig. 1.6.

Using the boundary conditions of Eqs. 1.6.1 and 1.6.2 and the initial condition of Eq.1.4.4, Eq. 1.4.1 can be solved analytically [Sekine, 1975; Boes et al., 1976] to yield the phase shift θ between hydrogen mass flux passing through the entry side and hydrogen mass flux at the exit side surface:

$$\theta = \tan^{-1}(\tan\alpha \tanh\alpha), \qquad \text{Eq. 1.6.3}$$

$$\alpha = \sqrt{\frac{\pi f L^2}{D}}\ . \qquad \text{Eq. 1.6.4}$$

where θ is a monotonically increasing function of α, as shown in Fig. 1.7. Therefore, the evaluation of θ is capable of determining the value of α and, consequently, D when f and L are provided. On the other hand, the perturbation amplitude ratio A of hydrogen entry flux to the exit flux is as follows:

$$A = \frac{1}{\sqrt{\cosh^2\alpha\cos^2\alpha + \sinh^2\alpha\sin^2\alpha}} = \sqrt{\frac{2}{\cos 2\alpha + \cosh 2\alpha}}\ . \qquad \text{Eq. 1.6.5}$$

It is theoretically possible, but practically almost impossible, to evaluate the value of α from A using Eq. 1.6.5, since the amplitude of the hydrogen entry flux cannot solely be measured. As the perturbation amplitude of the entry side current contains both contributions from the

hydrogen adsorption reaction (Eqs. 1.2.1 and 1.2.2) and from the hydrogen evolution reaction (Eqs. 1.2.3 and 1.2.4), A differs from the amplitude ratio of measured currents. For this reason, evaluation of the hydrogen diffusion coefficient by the sinusoidal perturbation method has been exclusively carried out using the phase shift. The coidentity of the obtained value of D by the step method and the sinusoidal perturbation method has been verified by some researchers [Tahara and Hayashi, 1983; Hagi, 1994].

The sinusoidal perturbation method has noteworthy positive features compared with the step method. The first is a potential for quantitative analysis. A temporal delay due to hydrogen diffusion is analyzed from the phase shift between the entry- and exit side current waveforms, being independent of amplitudes of waveforms. This is advantageous, especially if small current is monitored at the exit side. For example, the sinusoidal perturbation method was applied to measure the exit side current from a small electrode of a microcapillary cell, which was an exit side electrode of a DS cell [Fushimi et al., 2016]. Even though the magnitude of the exit side current was below 100nA, which was a few percent of the exit side current obtained with a conventional macro-cell, the sinusoidal signal of the exit side current enabled the analysis of phase shift, the elucidation of the hydrogen diffusion coefficient, and the interpretation of hydrogen penetration depending on metallographic structure. The hydrogen diffusion coefficient obtained at two single crystals containing a grain boundary was larger than that obtained at a single crystal, indicating that the grain boundary allowed faster diffusion than did a single grain.

The second feature is a potential that the sinusoidal perturbation method provides additional parameters to evaluate hydrogen penetration characteristics. Tada et al. utilized the amplitude ratio of the exit side current to the entry side current for evaluating hydrogen

absorption efficiency [Tada et al., 2016]. It was also reported that the AC absorption ratio was more precise than the DC absorption ratio due to the elimination of the contribution of background current. Sinusoidal perturbation is also utilized to analyze hydrogen penetration in respect of transfer function [Zoltowski, 2001, 2003, 2006, 2010; Gabrielli et al., 2002]. The concept of the analysis is similar to that of electrochemical impedance spectroscopy (EIS): A transfer function of a hydrogen penetration system is evaluated from the comparison of the perturbation in current/potential at the different surfaces, while EIS is done by the comparison of the perturbation in the current and the potential on the same surface. The transfer function therefore reflects the hydrogen diffusion process in the specimen.

As another advantage, the sinusoidal perturbation method is considered to be utilizable for time-dependent measurement of hydrogen penetration. Differing from the step method, this method uses a continuous cyclic signal to evaluate temporal delay. This means that the obtained phase shift is also continuous: this can be useful to evaluate change in temporal delay. To the best of my knowledge, there are no studies on temporal change of hydrogen penetration response. In addition, the phase shift between two waveforms can be easily derived as a phase shift by using Fourier transform. This characteristic could be utilized to speed up and automate the derivation procedure.

The sinusoidal perturbation method also has some problems, since it is not fully matured. The applicability of the sinusoidal perturbation method to interpret diffusion problems is not fully verified. For example, it is unknown whether Eq. 1.6.3 assuming the diffusion in a homogeneous specimen is also applicable to the diffusion in heterogeneous specimens.

1.7. Purpose and outline of this dissertation

As mentioned above, hydrogen penetration measurement is a basic technique to investigate the reliability of metallic structural materials, including iron and steel. Highly quantitative analyses of hydrogen diffusion in materials are important in order to take measures against hydrogen embrittlement, especially in next-generation materials, such as HTSS. This dissertation aims to achieve time-dependent hydrogen penetration measurement by utilization of a sinusoidal perturbation method. Emphasis is also placed on consideration of the verification of the applicability of this method to local measurement and the measurement of heterogeneous specimens.

In this chapter, Chapter 1, the significance of hydrogen penetration measurement in iron and steel has been presented. The mechanism of hydrogen penetration into materials and analytical methods utilizing the mechanism have been described. The sinusoidal perturbation method has been referred to as a possible way to realize time-dependent measurement.

In Chapter 2, previous studies on hydrogen penetration in steel and its measurement with the sinusoidal perturbation method are introduced, with the characteristic design of DS cells developed. The potential problems originating from the peculiarity of the measurement method and the cell design are described in detail.

In Chapter 3, the hydrogen diffusion problem in multi-dimensional geometry is considered to evaluate the applicability of the conventional model of hydrogen penetration measurement using a numerical calculation. A finite element method (FEM) is applied to solve one- and two-dimensional diffusion problems and to simulate the hydrogen concentration gradient in sheet specimens. The prospected values of phase shift by the sinusoidal perturbation method in heterogeneous specimens are discussed.

In Chapter 4, a time-dependent measurement of hydrogen penetration with the sinusoidal perturbation method is developed. A methodology to automate the derivation process of the hydrogen diffusion coefficient by fast Fourier-transform is introduced. The developed method is applied to observe hydrogen penetration into pure iron from pH 8.4 boric acid-borate

buffer solution, and its temperature dependency.

In Chapter 5, the conclusions drawn in each chapter are summarized and the implications of the results of this study are discussed.

1.8. References

J.A. Ober, *Mineral Commodity Summaries 2018*, pp. 82-83, U.S. Geological Survey, Reston (2018).

T. Urabe and Y. Hosoya, *J. Japan Soc. Technol. Plast.* **46**, 560 (2005).

T. Yasuno, K. Kuribayashi and T. Hasegawa, Sen'i Gakkaishi **48**, 489 (1992).

T. Sugiyama, *J. Japan Soc. Technol. Plast*. **46**, 532 (2005).

C. Lesch, N. Kwiaton, and F.B. Klose, *Steel Res. Int*., **88**, 1700210 (2017).

N. N. Greenwood and A. Earnshaw, *Chemistry of the Elements*, 1st ed., p. 32, Pergamon Press, Oxford (1984).

M. Nagumo, *Fundamentals of Hydrogen Embrittlement*, 1st ed., p. 274, Uchida Rokakuho Publishing, Tokyo (2008) (Japanese).

Q. Liu, Q. Zhou, J. Venezuela, M. Zhang, J. Wang, and A. Atrens, *Corros. Rev.*, **34**, 127 (2016).

M. Sakairi, *ISIJ Int.* **56**, 377 (2016).

J.O'M. Bockris and E.C. Potter, *J. Electrochem. Soc*. **99**, 169 (1952).

A. Lasia and D. Grégoire, *J. Electrochem. Soc.* **142**, 3393 (1995).

Y.C. Huang, K. Fujita and H. Uchida, *Bull. Japan Inst. Met.* **18**, 694 (1979).

A. McNabb and P.K. Foster, *Trans. Metall. Soc. AIME* **245**, 618 (1963).

R.A. Oriani, *Acta Metall*. **18**, 147 (1970).

J.O'M. Bockris, Tech. Rep. No.3 ONR/551/22/NR-036-028, Office of Naval Research (1959).

J.O'M. Bockris and M.A.V. Devanathan, Tech. Rep. No.4 ONR/551/22/NR-036-028, Office of Naval Research (1961).

M.A.V. Devanathan and Z. Stachurski, *Proc. R. Soc. A Math. Phys. Eng. Sci.* **270**, 90 (1962).

M. Nagano, Y. Hayashi, N. Ohtani, M. Isshiki and K. Igaki, *Trans. Japan Inst. Met.* **22**, 423 (1981).

ASTM International, G148-97: Standard Practice for Evaluation of Hydrogen Uptake, Penetration, and Transport in Metals by an Electrochemical Technique, ASTM International, West Conshohocken, PA, (2011).

K. Sekine, *Chem. Lett.* **4**, 841(1975).

K. Sekine, *J. Res. St. Catal. Hokkaido Univ*. **25**, 73 (1977).

N. Boes and H. Züchner, *J. Less Common Met.* **49**, 223 (1976).

A. Tahara and Y. Hayashi, *J. Japan Inst. Met. Mater*. **47**, 180 (1983).

H. Hagi, *Mater. Trans. JIM* **35**, 112 (1994).

K. Fushimi, M. Jin, Y. Kitagawa, T. Nakanishi and Y. Hasegawa, *ISIJ Int*. **56**, 431 (2016).

E. Tada and A. Nishikata, *ISIJ Int.* **56**, 424 (2016).

P. Zoltowski, *J. Electroanal. Chem*. **501**, 89 (2001).

P. Zoltowski, *Acta Mater*. **51**, 5489 (2003).

P. Zoltowski, *Electrochim. Acta* **51**, 1576 (2006).

P. Zoltowski, *Electrochim. Acta* **55**, 6274 (2010).

C. Gabrielli, P.P. Grand, A. Lasia and H. Perrot, *J. Electroanal. Chem.* **532**, 121 (2002).

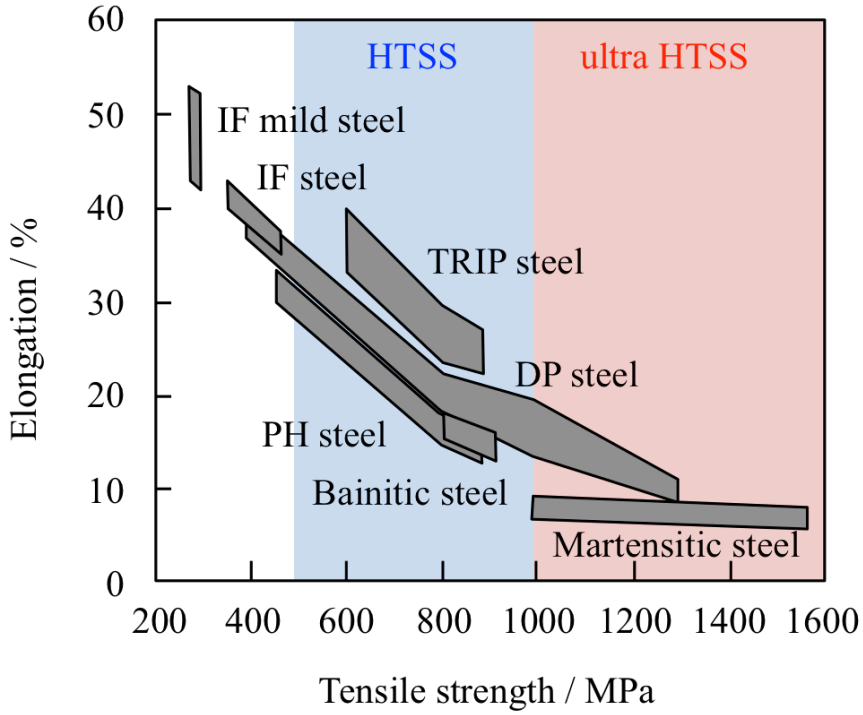

Fig 1.1. Relationship between tensile strength and breakdown elongation of various steels. IF, PH, TRIP, DP are acronyms of interstitial-free, precipitation hardening, transformation-induced plasticity, dual phase, respectively. The steels in the blue area correspond to high tensile strength steels, while the steels in the red area correspond to ultrahigh tensile strength steels. This figure was drawn by replotting the original figure in the following paper: T. Urabe and Y. Hosoya, *J. Japan Soc. Technol. Plast.* **46**, 560 (2005).

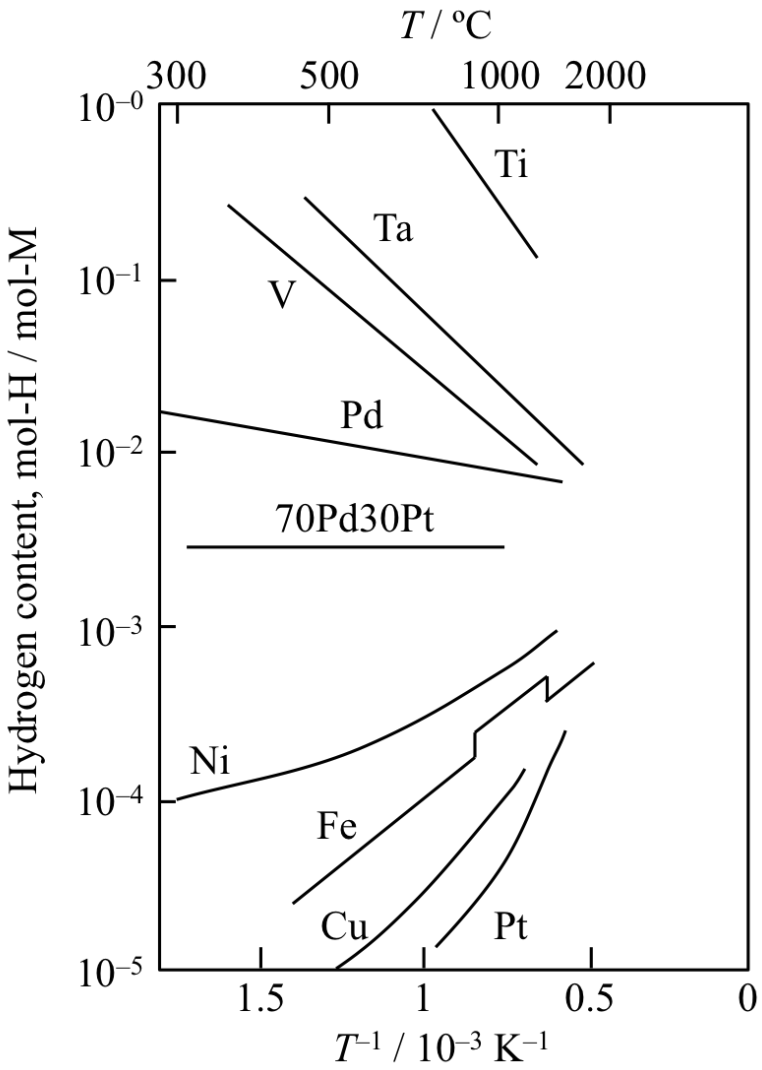

Fig. 1.2. Hydrogen solubility and its temperature dependence for various metals.

This figure was drawn by replotting the original figure in the following paper: Y.C. Huang, K. Fujita and H. Uchida, *Bull. Japan Inst. Met.* **18**, 694 (1979).

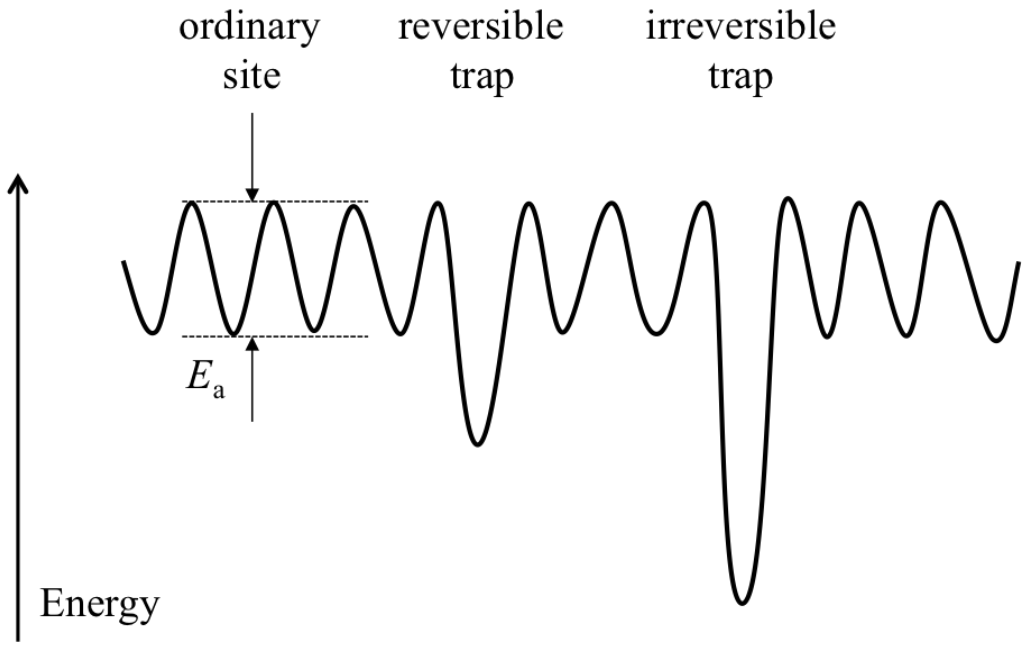

Fig. 1.3. Schematic illustration of hydrogen energy level in a metal lattice containing trap sites with different depths.

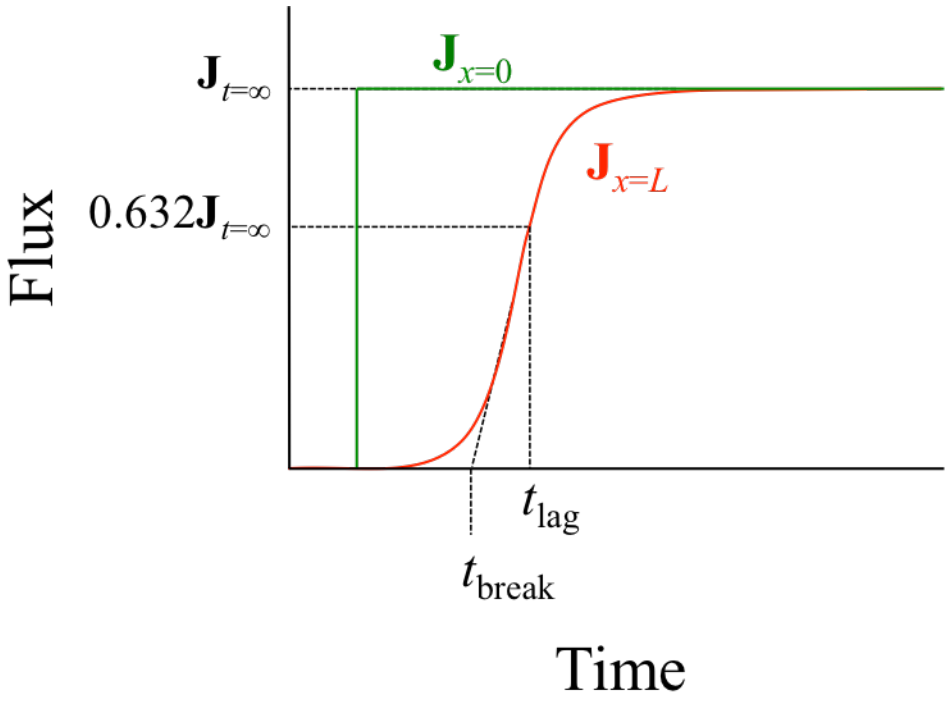

Fig. 1.4. Schematic diagram of hydrogen mass flux transient during hydrogen penetration by step method. Green and red curves denote hydrogen flux passing through the hydrogen entry side surface and the hydrogen exit side, respectively.

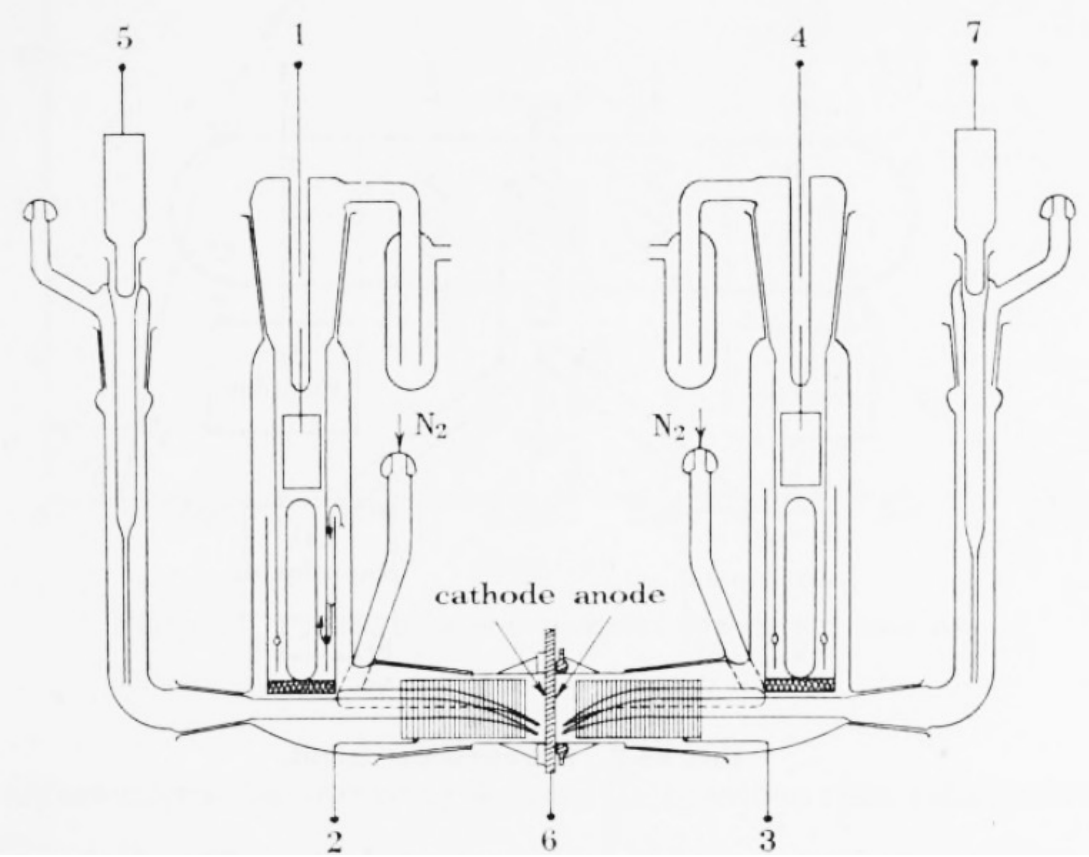

Fig. 1.5. Schematic illustration of Devanathan-Stachurski cell.

This figure was reprinted from the following paper: M.A.V. Devanathan and Z. Stachurski, *Proc. R. Soc. A Math. Phys. Eng. Sci.* **270**, 90 (1962).

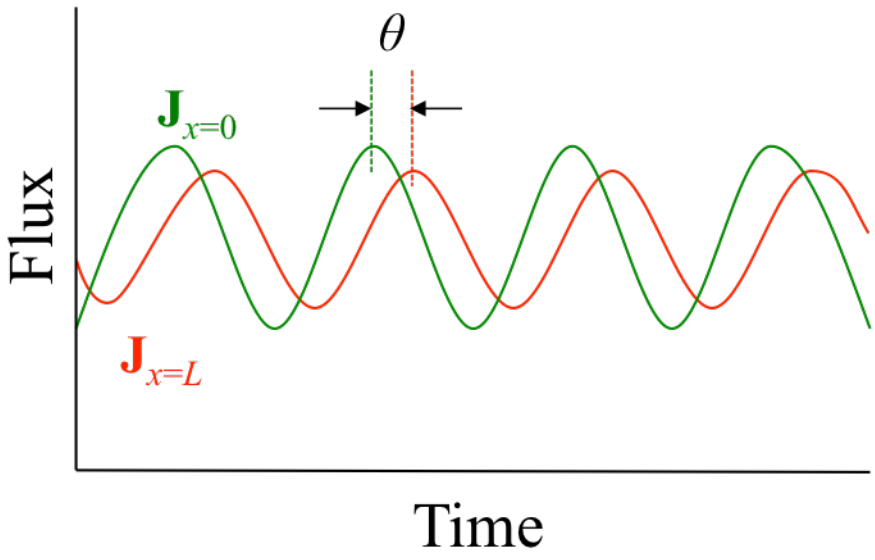

Fig. 1.6. Schematic diagram of hydrogen mass flux transient during hydrogen penetration by sinusoidal perturbation method. Green and red curves denote hydrogen flux passing through the hydrogen entry side surface and the hydrogen exit side, respectively.

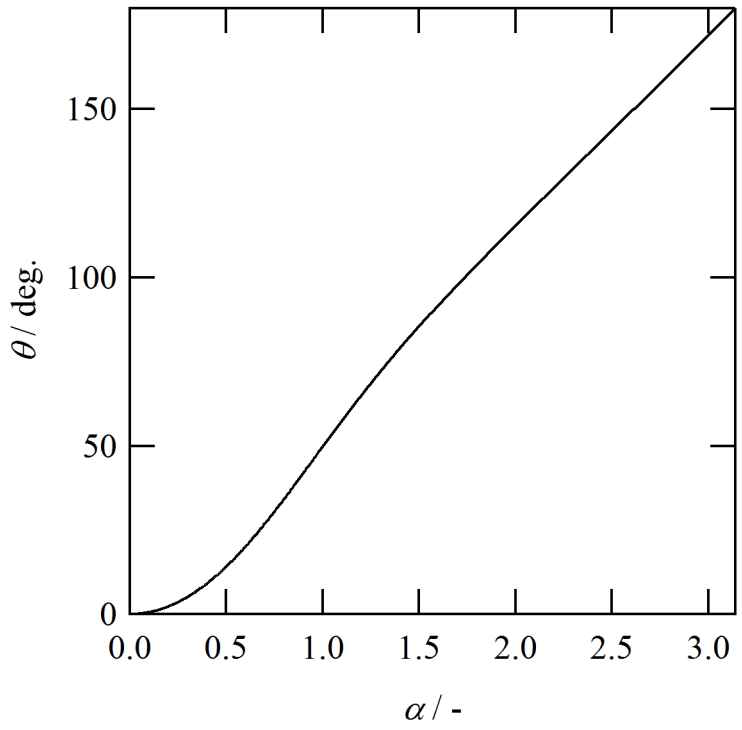

Fig. 1.7. The relationship between θ and α, as described in Eq. 1.6.3.

Chapter 2:
Measurement of hydrogen penetration into iron and steel with Devanathan-Stachurski Cells

2.1. Introduction

As mentioned in Chapter 1, the DS cell is widely utilized for measurement of hydrogen diffusion coefficient D in iron and steel. However, the obtained values of D are strongly dependent on experimental conditions. In this chapter, the previous reports of the hydrogen penetration measurement of iron are reviewed as well as values of D and the experimental conditions suitable for the reproducible measurement are discussed.

It is thought that the design of the DS cell is also one of the experimental conditions of hydrogen penetration measurement and affects the hydrogen penetration phenomena. Conversely, specific factors of hydrogen penetration can be evaluated by the measurement using well-designed DS cells. Up to now, therefore, a wide variety of DS cell has been developed to obtain a unique information upon the hydrogen penetration and to open up a new field of hydrogen penetration measurement. In this chapter, previous studies on hydrogen penetration with modified DS cells are also discussed.

2.2. Hydrogen diffusion coefficient in iron measured by electrochemical method using Devanathan-Stachurski cell

After the development of the original DS cell [Devanathan and Stachurski, 1962], many researchers studied the hydrogen diffusion coefficient in iron and steel. Kiuchi and McLellan summarized the reported values of hydrogen diffusion coefficient D in pure iron in an

Arrhenius-type plot as shown in Fig. 2.1 [Kiuchi and McLellan, 1983]. The annotation "H_2 gas equilibration" denotes the data obtained by the gas-phase penetration where hydrogen penetrates from gas phase, while the annotation "Electrochemical" denotes the data obtained by the liquid-phase penetration where hydrogen entry reaction is induced via electrochemical hydrogen evolution reactions as described in Section 1.2. It was pointed out that the values are widely scattered, especially at low temperatures near room temperature (from 10^{-13} to 10^{-8} m^2 s^{-1}). It was figured out that insufficient annealing of the specimen keeps abundant residual sites of hydrogen trapping inside the specimens and causes extremely (several orders in magnitude) small *D*. Only considering the results for "well-annealed" specimens, on the other hand, it was also found out that the difference of evaluation method of *D* causes the large scattering. The temperature dependence of hydrogen diffusion coefficient obtained by the gas-phase penetration exhibited large deviation while that obtained by electrochemical method were relatively in good agreement. Gas-phase penetration is not suited for the precise evaluation of *D* at low temperatures, since the hydrogen desorption from iron surface is relatively slow due to the relatively strong adsorption of hydrogen atom on iron surface and can determine the rate at the low-temperature condition. To avoid this uncertainty, the use of Pd-coated specimen and ultra-high vacuum for the exit side to accelerate the hydrogen desorption is essential. In this wise, the electrochemical hydrogen penetration is a convenient method for measurement of hydrogen diffusion coefficient at low-temperature condition since it provides the data with high reproducibility even though it does not require large-scaled apparatus (Section 1.5).

Fig. 2.2 shows the temperature dependence of hydrogen diffusion coefficient in annealed iron obtained by the electrochemical method. The data were mainly extracted from Fig. 2.1 and some data not mentioned in the paper [Kiuchi and McLellan, 1983] were also added.

The plotted data show a deviation. To figure out the origin of the deviation, the data plotted in Fig. 2.1 were listed with the experimental conditions in Table 2.1. The highest value at room temperature was reported by Hagi and in good agreement with those reported by Nagano et al. and Yamakawa et al. [Hagi, 1993; Nagano et al., 1981; Yamakawa et al., 1981]. The temperature dependence of D reported by them also agree well each other in spite of the difference in the measurement method and the surface treatment for the exit side, though one of the plots for the specimen with lower purity (99.83 wt% Fe) reported by Hagi shows a small and slightly steep dependence compared with others with higher purity (> 99.9 wt%). It seems that the purity of iron specimen affects the dependence of D. It was also reported that the type of impurities (interstitial or substitutional) does not significantly affect the value of D when the purity is high enough [Hagi, 1993]. The specimens with purities of 99.85 wt% [Beck et al., 1966] and 98.95 wt% [Asano et al., 1974] have obviously smaller values of D. However, the significantly small D and the steep dependence were reported by Kumnick et al. who used the specimen with a purity of 99.85 wt%, suggesting that hydrogen diffusion is dependent on not only the purity of iron but also other factors [Kumnick et al., 1974]. One of the factors may be pH of the solution used in the entry side. Only Kumnick et al. used a basic solution (0.1 M sodium hydroxide) for the entry side solution. Since the elemental reactions of hydrogen evolution in a basic solution (Eqs. 1.2.2, 1.2.4 and 1.2.5) differ from those in an acidic solution (Eqs. 1.2.1, 1.2.3 and 1.2.5), it is likely that the surface reactions might be slower in a basic solution and spend longer time to reach a steady state after the change of the polarization condition. In such a case, the concentration of absorbed hydrogen at just beneath the entry side surface gradually changes over time after the change of the polarization condition. It means that the boundary condition of constant concentration assumed for the entry side surface (Eq. 1.4.2)

is not completely established and the D cannot be evaluated properly by Eq. 1.4.6 or Eq. 1.4.7. The abnormally large value of the activation energy (E_a = 17 kJ mol^{-1}) would be attributed to the temperature dependence of the surface reactions.

In addition to these, some other conditions are also seemed to be essential for the appropriate determination of D. For example, the specimen prepared by the heat treatment at 1123 K for 1 h [Yamakawa et al., 1981] and at 973 K for 3 h [Hagi, 1993] exhibited the almost identical and reasonable temperature dependence as shown in Fig. 2.1. Therefore, both annealing conditions are assumed to meet the minimum requirement for sufficient annealing. Similarly, both electroplating of nickel [Yamakawa et al., 1981] and palladium [Nagano et al., 1981; Hagi, 1993] seem to be acceptable for the surface treatment of the exit side surface by the same reason. It should also be noted that all the referred data obtained in strong basic solutions for the exit side. It is due to the same reason as for the requirement of the entry side solution; the establishment of the constant concentration condition at the exit side (Eq. 1.4.3). In this wise, the use of a basic solution in the exit side cell is also assumed to be crucial to achieve mass transport control at the exit side interface and therefore sodium hydroxide or potassium hydroxide has widely been used.

As a consequence, hydrogen diffusion coefficient in well-annealed pure iron under room temperature is regarded as ~ 9×10^{-9} m^2 s^{-1}, which seems quite large since it is comparable to the diffusion coefficient of H^+ in aqueous solution (9.31×10^{-9} m^2 s^{-1} [Atkins and Paula, 2002]). Actually, hydrogen diffusion coefficient D is strongly dependent on the type of metal as depicted in Fig. 2.3 [Nagano et al., 1981; Yamakawa et al., 1981; Hagi, 1993; Qi et al., 1983; Birnbaum et al., 1972; Robertson, 1973]. Large D is commonly seen for body-centered cubic (bcc) metals such as vanadium, niobium and tantalum. The values of D in face-centered cubic

(fcc) metals such as palladium and nickel, are some orders in magnitude smaller than those in bcc metals. This is mainly originated from the difference of the packing ratio. The packing ratio is lower in bcc (68%) than fcc (74%) and therefore bcc metals provide room for hydrogen to diffuse in the lattice freely.

2.3. Modified Devanathan-Stachurski cells

Similarly to the experimental conditions discussed in the Section 2.2, the design of a DS cell also affects the hydrogen diffusion. Various designs of DS cell have been developed to obtain distinctive information about hydrogen penetration behavior. In this section, some noteworthy variations of the cell are introduced.

2.3.1. Devanathan-Stachurski cell with corrosion cell

DS cells have been utilized not only for measurement of hydrogen diffusion coefficient but also for evaluation of hydrogen uptake under specific conditions. Atmospheric corrosion is one of the most considerable conditions initiating hydrogen embrittlement. In order to evaluate hydrogen penetration during atmospheric corrosion, a DS cell modified as shown in Fig. 2.4 has been developed [Tsuru et al. 2005; Akiyama et al., 2011]. The entry side cell of the modified DS cell is opened to atmospheric environment and capable of simulating the atmospheric corrosion while the exit side cell has not been modified. Wet-and-dry cycling by periodical droppings of electrolyte solution and/or distilled water onto the surface are frequently employed. Ootsuka et al. applied the DS cell method to the in-situ evaluation of hydrogen penetration during “real” corrosion by putting the modified DS cell on an automobile and by driving a potentiostat with a car battery [Ootsuka et al., 2015]. It was observed that the hydrogen uptake increases with decrease in the specimen weight owing to corrosion, confirming

the corrosion-assisted hydrogen penetration.

2.3.2. Devanathan-Stachurski cell combined with other hydrogen detection methods

In Section 2.3.1, the DS cell technique was developed for measurement of hydrogen penetration during the atmospheric corrosion. In the technique, the entry side cell was modified to expose surface to the environment of the interest, while the exit side cell was remained intact. The replacement of the exit side cell for a DS cell by other hydrogen detection method has also been studied. When the entry side cell is exposed to solution and polarized cathodically for the hydrogen entry reaction in the other type of DS cell, the exit side cell for hydrogen detection can be exchanged with other physicochemical method. One of the motives to employ other physicochemical method is to detect hydrogen at the exit side with spatial resolution where hydrogen passed through. One is scanning Kelvin probe (SKP) technique, in which a Kelvin probe senses a work function of the specimen surface. Hydrogen absorbed in metal causes the decrease of working function (Fig. 2.5) [Evers et al., 2013; Katayama, 2016] Tungsten oxide was also utilized to literally visualize the penetrated hydrogen [Sugawara et al., 2018]. The thin layer of WO_3 deposited on the exit side reacts with the penetrated hydrogen and forms H_xWO_3, the color of which changes from blue to dark blue and can be observed even by the naked eye. The application of electrochemical detection method with spatial resolution has also been reported and will be introduced in the following two sections.

2.3.3. Devanathan-Stachurski cell with a flow cell

Fushimi and Jin et al. developed a modified DS cell that had a flow channel of the electrolyte solution in the entry side cell (hereinafter referred to as single flow DS cell) [Fushimi

et al., 2014]. The schematic illustration of the single flow DS cell is shown in Fig. 2.6. The single flow DS cell was initially introduced to remove hydrogen gas babbles produced on the entry side surface of a specimen during a measurement, since bubbles screened a part of the specimen surface resulting in the decrease of the effective electrode area of the entry side. The introduction of electrolyte flow enabled not only removal of the bubbles on the entry side surface but also control of the electrode reaction rates. Controlling hydrodynamic conditions of electrolyte in the entry side cell affects the rate of electrode reactions via promotion of mass transport of the reactants and the products. Fig. 2.7 shows currents of entry and exit sides during the hydrogen penetration measurement into a steel sheet from pH 8.4 boric acid-borate buffer solution at various flow rates of the solution. Faster flow results in increasing the entry side current and decreasing the exit side current. This result clearly shows that the flow promotes the hydrogen evolution reaction (Eqs. 1.2.1-1.2.5) but suppresses the hydrogen absorption reaction (Eq. 1.2.6). Since the decrease in the hydrogen absorption rate is observed as the decrease in the exit side current with a diffusional delay as mentioned in Section 1.3, modulation of flow rate can be utilized for the measurement of hydrogen diffusion coefficient.

Fushimi et al. also applied the sinusoidal perturbation of flow rate in the entry side cell to the hydrogen penetration measurement [Fushimi et al., 2014]. Although the principle of the hydrogen penetration measurement with sinusoidal perturbation was reported by other researcher [Sekine, 1975] as introduced in Section 1.6, the fact that the electrolyte flow rate can also be used as the perturbing parameter was a new discovery. It is also noteworthy that the exit side current exhibited a negative correlation to the entry side current as the hydrogen absorption reaction is suppressed by flow while the hydrogen evolution reaction is promoted by flow. This causes the apparent inversion of the phase of the sinusoidal perturbation in the exit side current.

The single flow DS cell has a flow cell only for the entry side. To evaluate the effect of electrolyte flow in the exit side cell, a DS cell having two equivalent flow cells for both sides was developed [Fushimi et al., 2014]. This type of cell is described in detail with experimental results in Chapter 4.

2.3.4. Devanathan-Stachurski cell combined with a micro-capillary cell

In research of corrosion, a micro-capillary cell (MCC) has been utilized to measure the dependence of corrosion behavior on metallographic structure of a specimen [Suter and Böhni, 1997]. Fushimi et al. combined a single-flow DS cell with an MCC at the exit side as illustrated in Fig. 2.8 [Fushimi et al., 2016] (hereinafter referred to as flow-micro DS cell) and conducted the local hydrogen penetration into a carbon steel sheet from a boric acid-borate buffer solution using the modified DS cell. The local hydrogen penetration measurement on a single crystal and the measurement on a two-crystal grain containing a grain boundary were successfully conducted using the steel sheet with coarse crystal grains larger than the inner diameter of the MCC. It was reported that the phase shift obtained on the single grain was two times larger than that measured on the two-grain, indicating the promotion effect of hydrogen diffusion by the grain boundary.

Almost all of conventional consideration on hydrogen diffusion is based on one-dimensional one from the entry side to the exit side. In the case of flow-micro DS cell, however, the electrode surface area of hydrogen exit side is not equal to that of hydrogen entry side and hydrogen diffusion seems to be three-dimensional and somewhat spherical. In addition, since the steel sheet is polycrystalline in general, it is obviously inhomogeneous in a microscopic viewpoint. It can be approximated to be macroscopically homogeneous if the sheet

is composed of a lot of fine grains. However, the coarse-grained sheet used in the study, whose grain size is larger than the thickness, is inhomogeneous also from the macroscopic viewpoint. Only a limited number of researches dealing the effect of inhomogeneity in metal on diffusion coefficient is reported and no report exists for the sinusoidal perturbation method. Therefore, no theoretical equation can interpret the phase shift for such an inhomogeneous specimen. These problems are remained as subject on the study of the sinusoidal perturbation method and are dealt with in Chapter 3.

2.4. Conclusions

Many researchers reported the different values of hydrogen diffusion coefficient D in pure iron measured using DS cells under different conditions. The bibliographic research on the past reports revealed the several requirements such as specimen preparation conditions and acidity of the solution for each cell to evaluate D properly.

DS cells are widely utilized not only for the quantification of D but also for the acquisition of distinctive information of hydrogen penetration behavior. Some unique and remarkable variants of DS cells were briefly introduced with their outcomes. A flow-micro DS cell was specified as one of the variants capable of local measurement of hydrogen penetration. In this context, it was pointed out that the analysis on the hydrogen penetration considering the inhomogeneity in the specimen or the electrode surface area is lacking. These problems are dealt with in Chapter 3.

2.5. References

M.A.V. Devanathan and Z. Stachurski, *Proc. R. Soc. A Math. Phys. Eng. Sci.* **270**, 90 (1962).

K. Kiuchi and R.B. McLellan, *Acta Metall.* **31**, 961 (1983).

W. Beck, J.O'M. Bockris, J. McBreen and L. Nanis, *Proc. R. Soc. A Math. Phys. Eng. Sci.* **290**, 220 (1966).

A.J. Kumnick and H.H. Johnson, *Metall. Trans.* **5**, 1199 (1974).

S. Asano, K. Hara, Y. Nakai and N. Ohtani, *J. Japan Inst. Met.* **38**, 626 (1974).

M. Nagano, Y. Hayashi, N. Ohtani, M. Isshiki and K. Igaki, *Trans. Japan Inst. Met.* **22**, 423 (1981).

K. Yamakawa, T. Tsuruta and S. Yoshizawa, *Corros. Eng.* **30**, 501 (1981).

H. Hagi, *J. Japan Inst. Met.* **57**, 742 (1993).

P. Atkins and J. de Paula, Atkins' Physical Chemistry, 7th ed. (W. H. Freeman, New York, 2002).

Z. Qi, J. Volkl, R. Lasser and H. Wenzl, *J. Phys. F Met. Phys.* **13**, 2053 (1983).

H. K. Birnbaum and C. A. Wert, *Ber Bunsenges. Phys. Chem.* **76**, 806 (1972).

W.M. Robertson, *Z. Metallk.* **64**, 436 (1973).

T. Tsuru, Y. Huang, M.R. Ali and A. Nishikata, *Corros. Sci.* **47**, 2431 (2005).

E. Akiyama, S. Li, T. Shinohara, Z. Zhang, and K. Tsuzaki, *Electrochim. Acta* **56**, 1799 (2011).

S. Ootsuka, S. Fujita, E. Tada, A. Nishikata and T. Tsuru *Corros. Sci.* **98**, 430 (2015).

S. Evers, C. Senöz and M. Rohwerder, *Sci. Technol. Adv. Mater.* **14**, 014201 (2013).

H. Katayama, *ISIJ Int.* **56**, 478 (2016).

Y. Sugawara, Y. Sakaizawa, A. Shibata, I. Muto and N. Hara, *ISIJ Int.* **58**, 1860 (2018).

K. Fushimi, M. Jin, T. Nakanishi, Y. Hasegawa, T. Kawano and M. Kimura, *ECS Electrochem. Lett.,* **3**, C21 (2014).

T. Suter and H. Böhni, *Electrochim. Acta* **42**, 3275 (1997).

K. Fushimi, M. Jin, Y. Kitagawa, T. Nakanishi, and Y. Hasegawa, *ISIJ Int.*, **56**, 431 (2016).

K. Sekine, *Chem. Lett.,* **4**, 841 (1975).

Table 2.1. Reported temperature dependence of hydrogen diffusion coefficient in annealed iron. The Arrhenius plot is also shown in Fig. 2.2.

Ref.	Purity / %	Thickness / um	Anneal temp. / K	Anneal duration / h	Final polish	Surface treatment for exit side	Measure-ment method	Solution for entry side	Entry current density / mA cm^{-2}	Solution for exit side	Dislocation density / m^{-2}	Temp. region / K	D_0 / m^2 s^{-1}	E_a / J mol^{-1}
Beck et al., 1966	99.85	770	873	2	H_2SO_4 etching	Pd (in situ)	step	0.05 M H_2SO_4	8.1	0.2 M NaOH + Pd nitrite complex	not provided	283-348	6.00E-08	5565
Kumnick et al., 1974	99.85	630	1123	4	as annealed	Pd	step	0.1 M NaOH	1.8	0.1 M NaOH	not provided	278-329	1.25E-06	17000
Asano et al., 1974	98.95	300	1073	5	chemical polish	Pd	step (transient)	0.5 M H_2SO_4 +5 mg/l As_2O_3	0.85-1.13	0.2 M NaOH	not provided	286-357	1.05E-07	7531
Nagano et al., 1981	99.999	500	1073	24	as annealed	Pd	sinusoidal	0.5 M H_2SO_4 +MeOH (1:1)	not provided	1 M KOH	not provided	222-322	4.90E-08	4200
Yamakawa et al., 1981	99.98	1000	1123	1	electro-chemical polish	Ni	step	0.05 M H_2SO_4	30	1 M NaOH	1.00E+13	283-343	6.20E-08	4853
Hagi, 1993	99.99	1000	1173	3	as annealed	Pd	step	0.5 M H_2SO_4	not provided	0.2 M NaOH	1.30E+11	278-318	6.40E-08	4700
Hagi, 1993	99.98	1000	1223	3	as annealed	Pd	step	0.5 M H_2SO_4	not provided	0.2 M NaOH	6.00E+10	278-318	6.00E-08	4500
Hagi, 1993	99.98	1000	1173	3	as annealed	Pd	step	0.5 M H_2SO_4	not provided	0.2 M NaOH	2.50E+11	278-318	8.00E-08	5300
Hagi, 1993	99.99	1000	973	3	as annealed	Pd	step	0.5 M H_2SO_4	not provided	0.2 M NaOH	7.00E+10	278-318	4.70E-08	4000
Hagi, 1993	99.94	1000	1173	3	as annealed	Pd	step	0.5 M H_2SO_4	not provided	0.2 M NaOH	1.80E+11	278-318	7.70E-08	5100
Hagi, 1993	99.83	1000	1173	3	as annealed	Pd	step	0.5 M H_2SO_4	not provided	0.2 M NaOH	4.40E+11	278-318	1.35E-07	7000

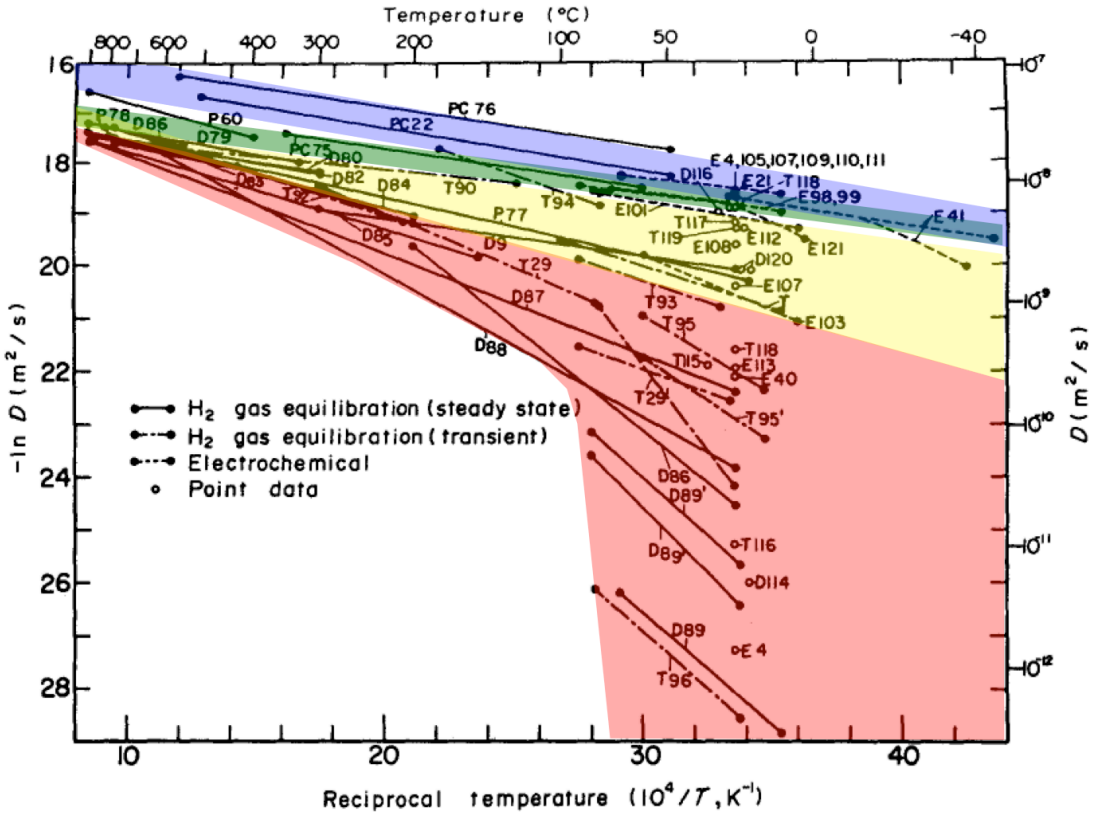

Fig. 2.1. Reported values of hydrogen diffusion coefficient in annealed iron at varying temperature. Annotations PC, P, D, T denote the data obtained by gas-phase penetration while E denotes the data obtained by liquid-phase (electrochemical) penetration. The data annotated with PC has been obtained using Pd-coated specimens. The following numbers in the annotations denote the reference number in the original paper. The overlaid colors representing the experimental conditions in the region are made from another figure in the paper: "Pd coated, UHV (H_2-gas equilibration)" (blue), "Electrochemical" (green), "H_2-gas equilibration (bare metal)" (yellow), and "Data obtained from specimens containing defects or surface trapping sites which produced unsatisfactory results" (red). The data in the red-colored region are assumed to be obtained for pure iron specimens not fully annealed.

This figure was reprinted from the following paper: K. Kiuchi and R.B. McLellan, *Acta Metall.* **31**, 961 (1983).

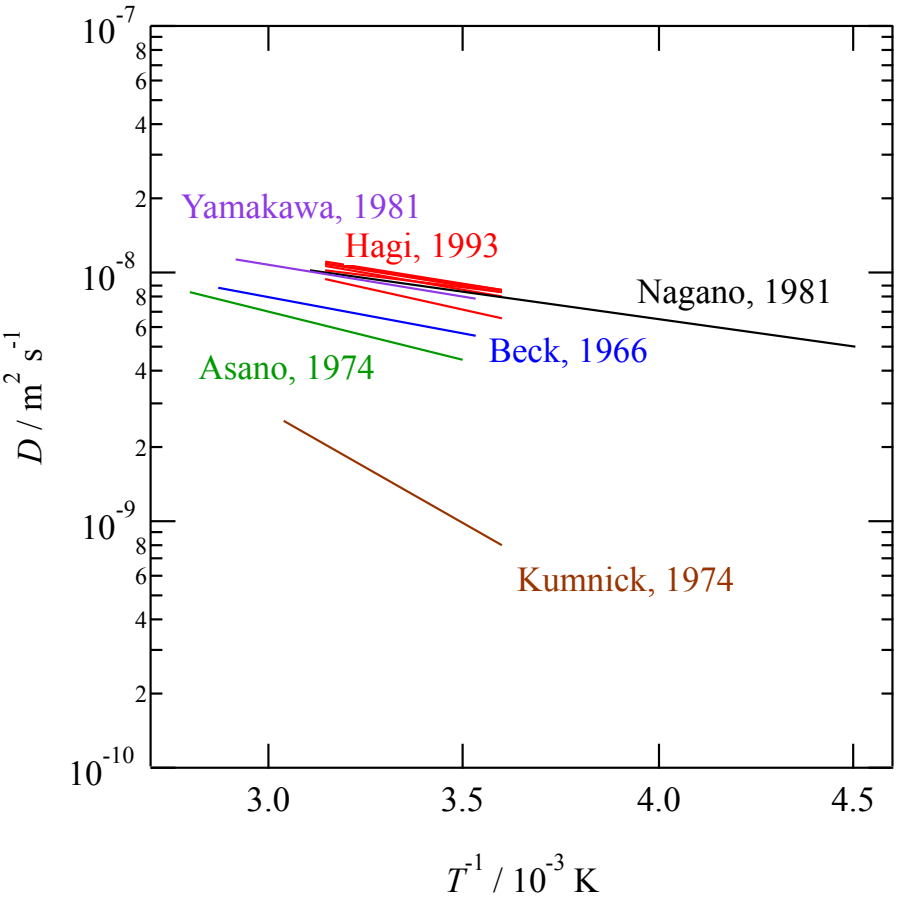

Fig. 2.2. Arrhenius plot of reported temperature dependence of hydrogen diffusion coefficient in annealed iron. Only family name of the first author is written in the annotations. Experimental conditions for each plot are listed in Table 2.1.

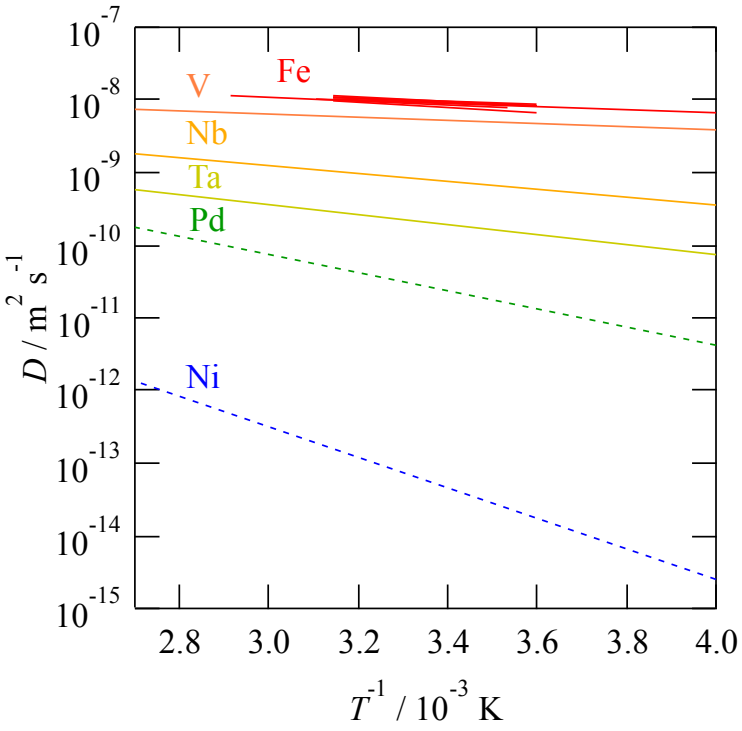

Fig. 2.3. Hydrogen diffusion coefficient in various metals. Solid lines represent the data of bcc metals while broken lines represent the data of fcc metals.

This data plotted in the figure was obtained from the following paper:

[Fe] M. Nagano, Y. Hayashi, N. Ohtani, M. Isshiki and K. Igaki, *Trans. Japan Inst. Met.* **22**, 423 (1981).

[Fe] K. Yamakawa, T. Tsuruta and S. Yoshizawa, *Corros. Eng.* **30**, 501 (1981).

[Fe] H. Hagi, *J. Japan Inst. Met.* **57**, 742 (1993).

[V, Nb, Ta] Z. Qi, J. Volkl, R. Lasser and H. Wenzl, *J. Phys. F Met. Phys.* **13**, 2053 (1983).

[Pd] H. K. Birnbaum and C. A. Wert, *Ber Bunsenges. Phys. Chem.* **76**, 806 (1972).

[Ni] W.M. Robertson, *Z. Metallk.* **64**, 436 (1973).

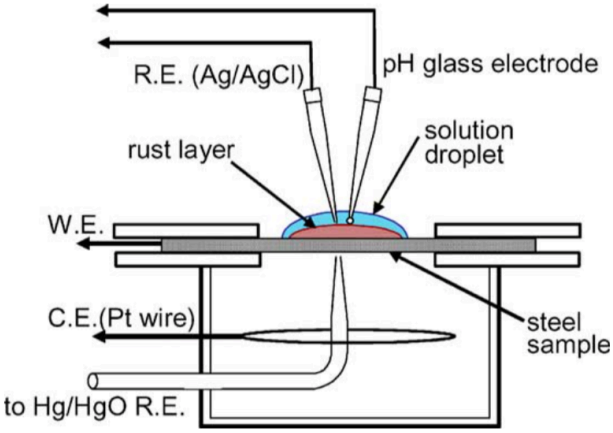

Fig. 2.4. Schematic drawing of modified DS cell with atmospheric corrosion cell.

This figure was reprinted from the following paper: T. Tsuru, Y. Huang, M.R. Ali, and A. Nishikata, *Corros. Sci.* **47**, 2431 (2005).

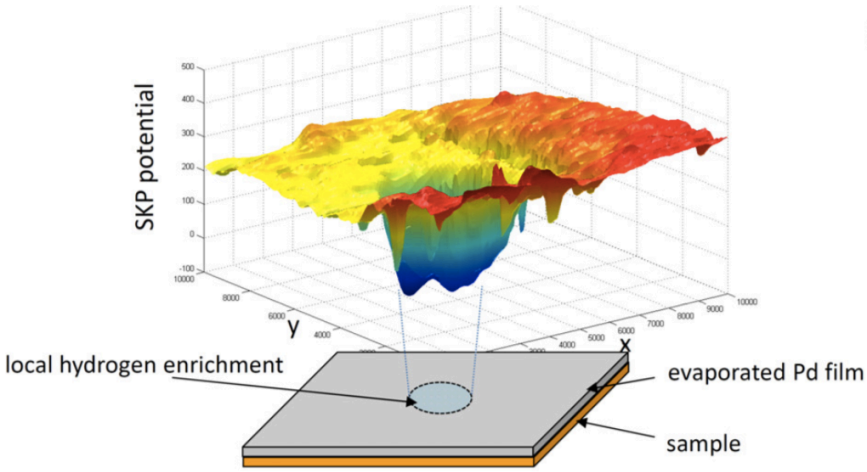

Fig. 2.5. Map of work function distribution on the surface of a 100 nm thin palladium film evaporated on an iron sample that was locally charged with hydrogen, measured by SKP microscopy in a dry nitrogen gas atmosphere.

This figure was reprinted from the following paper: S. Evers, C. Senöz and M. Rohwerder, *Sci. Technol. Adv. Mater.* **14**, 014201 (2013).

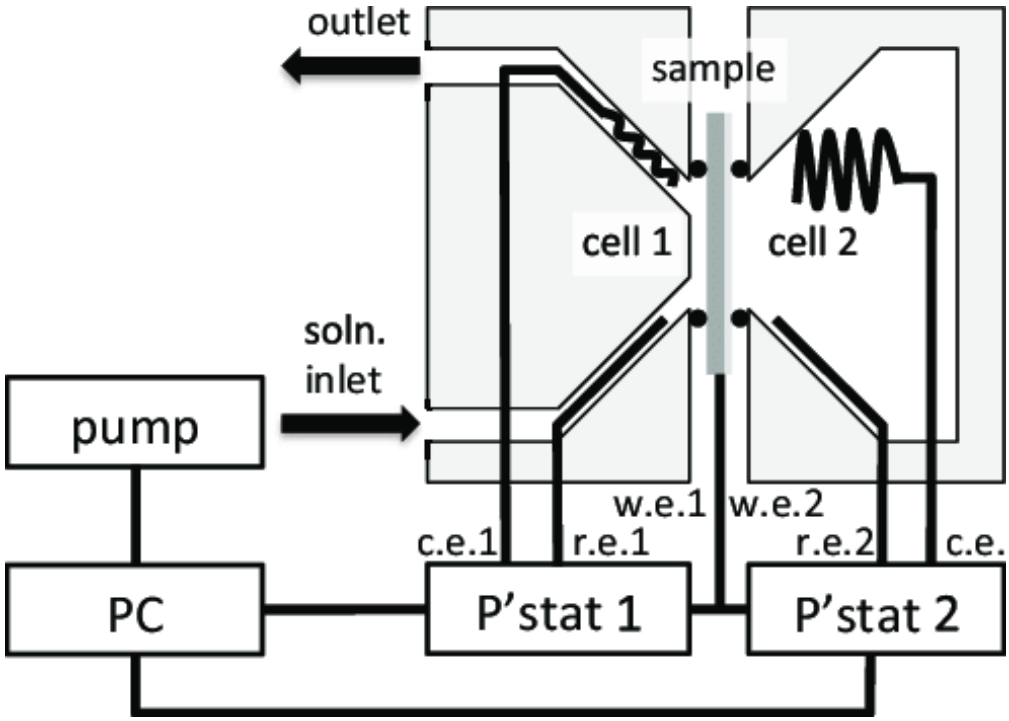

Fig. 2.6. Schematic diagram of Devanathan-Stachurski cell with a flow cell.

This figure was reprinted from the following paper: K. Fushimi, M. Jin, T. Nakanishi, Y. Hasegawa, T. Kawano and M. Kimura, *ECS Electrochem. Lett.,* **3**, C21 (2014).

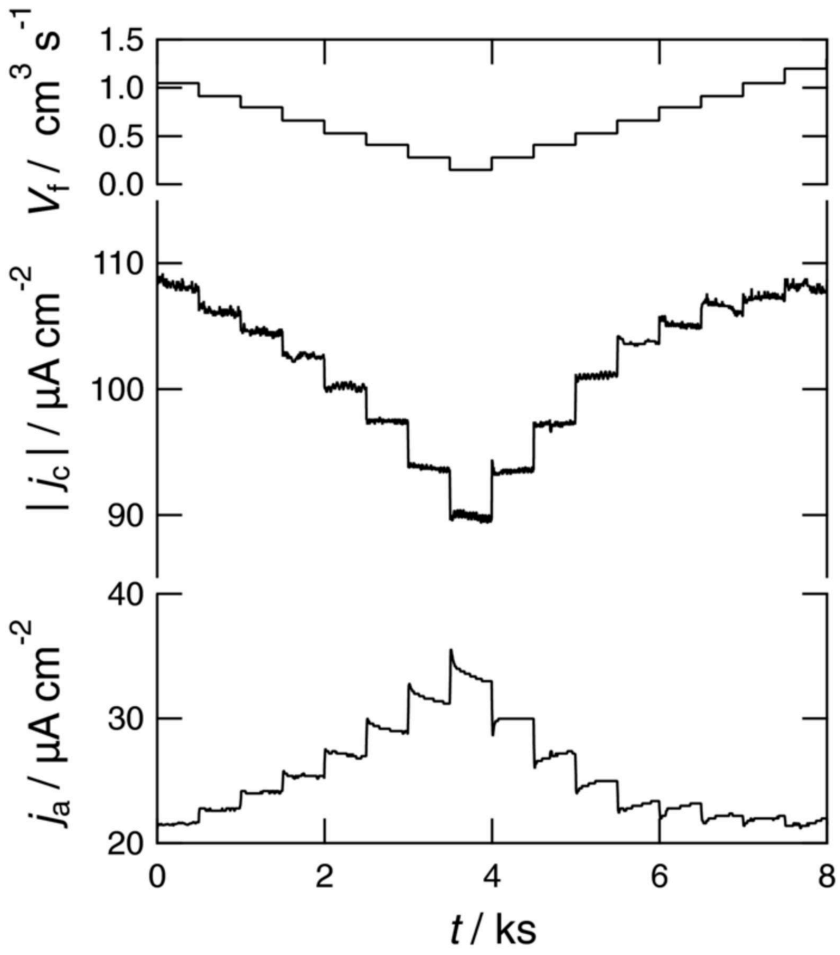

Fig. 2.7. Time-transient of currents j_c and j_a flowing through the hydrogen entry electrode and hydrogen exit electrode, respectively, at electrolyte flow rate V_f of the hydrogen entry cell. The electrode was polarized at –1.0 and 0.4 V_{SHE} for hydrogen entry and exit, respectively.

This figure was reprinted from the following paper: K. Fushimi, M. Jin, T. Nakanishi, Y. Hasegawa, T. Kawano and M. Kimura, *ECS Electrochem. Lett.,* **3**, C21 (2014).

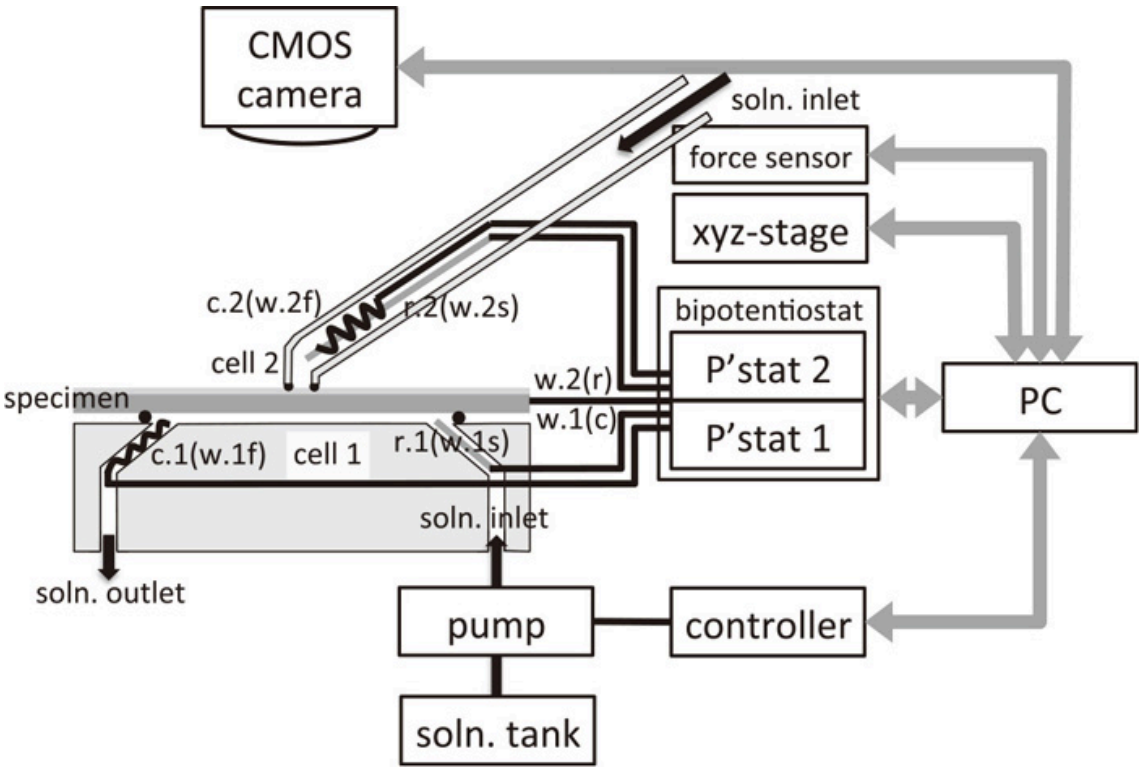

Fig. 2.8. Schematic diagram of Devanathan-Stachurski cell with a flow cell and a micro-capillary cell.

This figure was reprinted from the following paper: K. Fushimi, M. Jin, Y. Kitagawa, T. Nakanishi and Y. Hasegawa, *ISIJ Int.*, **56**, 431 (2016).

Chapter 3:
FEM Analysis for Hydrogen Penetration as Multi-dimensional Diffusion

3.1. Introduction

Fushimi et al. developed a modified DS cell with flow channel at the entry side and tested the effect of controlling electrolyte flow rate during hydrogen penetration [Fushimi et al., 2014]. It was reported that sinusoidal perturbation of the electrolyte flow rate in the hydrogen-entry side of the DS cell induced an exit current wave as well as an entry current wave. A phase shift of the exit current from the entry current observed during the perturbation of the hydrodynamic condition in the modified DS cell was proposed to be a new factor for evaluating hydrogen penetration into steel. In this background, observation of a phase shift in local measurement using a DS cell combined with an MCC was successfully conducted [Fushimi et al., 2016]. It was also reported that the hydrogen diffusivity in a region with two single crystal grains and a grain boundary was at least two-times larger than that in a region with a single grain. However, there are some problems to interpret the results. Since a macro cell for hydrogen entry side and a micro cell for exit side cell have been used, the hydrogen diffusion inside the sheet cannot be assumed to be one-dimension. As discussed in Chapter 1, hydrogen penetration measurement is mainly based on the diffusion of hydrogen in the specimen sheet. To simplify the discussion, most of reported analytical consideration for hydrogen penetration assumed one-dimensional diffusion. One-dimensional diffusion model is suitable for uniform penetration of hydrogen in thin sheets where the concentration gradient along the in-plane direction can be ignored. Generally, an analytical solution of a partial differential equation can be obtainable only under strict conditions. In most cases, it is unable to

solve two- or three-dimensional diffusion problems analytically, which is essential for local or heterogeneous hydrogen penetration of a non-uniform substrate and/or environment. The discussion of local or heterogeneous hydrogen penetration has made little progress. It is thought that numerical calculation is helpful to obtain approximate solution of the problem and to improve remarkably in the discussion.

In this chapter, a finite element method (FEM) is applied to solve one- and two-dimensional diffusion problems and to simulate the hydrogen concentration gradient in metal. Phase shifts and hydrogen flux are obtained during local penetration measurement with a DS-micro-capillary cell for the first time. Moreover, the difference between diffusion coefficients of hydrogen in a single grain and grain boundary is discussed using the results from a series of FEM calculations.

3.2. Governing equations and boundary conditions for hydrogen penetration

Hydrogen diffusion inside a metal sheet can be described by Fick's laws (Eqs. 1.3.1 and 1.3.3). Geometry discussed in this section is schematically illustrated in Fig. 3.1. If the hydrogen entry reaction and exit reaction occur on whole surface of the both sides of an uniform sheet, absorbed hydrogen linearly diffuses from the entry side surface to the exit side. In such a case, hydrogen diffusion is expressed by an one-dimensional equation as same as Eq. 1.4.1:

$$\mathbf{J} = -D\frac{\partial C}{\partial z}, \qquad \text{Eq. 3.2.1}$$

$$\frac{\partial C}{\partial t} = D\frac{\partial^2 C}{\partial z^2}. \qquad \text{Eq. 3.2.2}$$

Here z is defined as coordinate in the direction of sheet thickness. A pair of one-dimensional equations is adopted only for verifying the validity of calculation result. A sheet with heterogeneity along in-plane direction cannot be expressed in the one-dimensional diffusion model and should be considered as a two- or three-dimensional problem. The pair of

three-dimensional diffusion equations (Eqs. 1.3.1 and 1.3.3) is the most general form but needs more computational resource to solve. Hence in this study, the system expressed in two-dimensional coordinates is chosen. Two-dimensional equations are expressed as follows:

$$\mathbf{J} = -D\left(\frac{\partial}{\partial x} + \frac{\partial}{\partial z}\right)C, \quad \text{Eq. 3.2.3}$$

$$\frac{\partial C}{\partial t} = D\left(\frac{\partial^2}{\partial x^2} + \frac{\partial^2}{\partial z^2}\right)C, \quad \text{Eq. 3.2.4}$$

where x is coordinate for in-plane-direction of the sheet. In one- and two-dimensional diffusion problems, the sheet with a thickness of L and width of w can be regarded as a line with a length of L and a rectangle with side lengths of L and w, respectively.

Three-dimensional diffusion equations (Eqs. 1.3.1 and 1.3.3) in cylindrical coordinates system are also be expressed as follows:

$$\mathbf{J} = -D\left(\frac{\partial}{\partial z} + \frac{\partial}{\partial r} + \frac{\partial}{r\partial \varphi}\right)C, \quad \text{Eq. 3.2.5}$$

$$\frac{\partial C}{\partial t} = D\left(\frac{\partial^2}{\partial z^2} + \frac{\partial^2}{\partial r^2} + \frac{\partial}{r\partial r} + \frac{\partial^2}{\partial \varphi^2}\right)C, \quad \text{Eq. 3.2.6}$$

where r is distance from the center of the rotational axis and φ is azimuth angle around the rotational axis. In the case of rotational symmetry, the equations can be simplified to two-dimensional as follows:

$$\mathbf{J} = -D\left(\frac{\partial}{\partial z} + \frac{\partial}{\partial r}\right)C, \quad \text{Eq. 3.2.7}$$

$$\frac{\partial C}{\partial t} = D\left(\frac{\partial^2}{\partial z^2} + \frac{\partial^2}{\partial r^2} + \frac{\partial}{r\partial r}\right)C, \quad \text{Eq. 3.2.8}$$

Eqs. 3.2.7-3.2.8 have been adopted for the calculation of systems with rotational symmetry.

Hydrogen diffusion coefficients in steel sheets are widely distributed depending on the specifications of the sheets such as chemical compositions and the density of dislocations as discussed in Chapter 2. Since the aim of this chapter is not an accurate quantification of phase shift but qualitative discussion, the value of D used for calculations is considered not to be significant. From the previous report [Fushimi et al., 2016], the diffusion coefficient of hydrogen in the steel sheet used in the local penetration experiment was estimated as $D = 1.2\times10^{-9}$ m^2 s^{-1}. In the following discussion, therefore, the value of 10^{-9} m^2 s^{-1} is used for a basic hydrogen diffusion coefficient of a steel sheet.

As described in Section 1.6, absorbed hydrogen concentrations $C_{x=0}$ and $C_{x=L}$ at the

entry side interface and the exit side interface, respectively, can be expressed as same as Eqs. 1.6.1 and 1.6.2.

$$C_{x=0} = C_0 + \Delta C \sin(2\pi f t), \quad \text{Eq. 3.2.9}$$

$$C_{x=L} = 0, \quad \text{Eq. 3.2.10}$$

While the flux of hydrogen on the entry or exit electrode surface is expressed by Eqs. 3.2.9 and 3.2.10, no flux passes through the boundary other than electrode surfaces. Any boundaries other than the hydrogen entry or exit side are treated as isolation wall and no flux passes through the boundary whose normal vector is **N**.

$$\mathbf{N} \cdot \mathbf{J} = 0. \quad \text{Eq. 3.2.11}$$

No flux also passes through any symmetric lines, and therefore Eq. 3.2.11 is also adopted for the periodic boundary condition and a boundary condition for rotational symmetry. Currents flowing through the entry and exit side electrodes are products of fluxes that have passed through the electrodes and Faraday constant, as the hydrogen adsorption/desorption reaction is one-electron transfer reaction (Eq. 1.2.1).

3.3. FEM calculation

Diffusion equations (Eqs. 3.2.1-3.2.8) are regarded as governing equations of hydrogen penetration and then approximated forms of the equations are solved by FEM. All of the finite element calculations presented in this dissertation were performed by COMSOL Multiphysics® 5.0 running on a Windows PC equipped with 3.5 GHz Intel® Xeon® CPU E3-1241 v3 and with 32 GB RAM.

3.4. Results and discussion

3.4.1. One-dimensional diffusion problem

Primarily, the validity of the calculation method of the diffusion problem was checked by one-dimensional FEM calculation. In the case of one-dimensional diffusion of hydrogen in a homogeneous sheet with a sinusoidal perturbation at the entry side interface, the

hydrogen concentration at the exit side interface becomes a function of the following five parameters: mean concentration C_0 and concentration amplitude ΔC of hydrogen at the entry side, thickness L of the sample sheet, diffusion coefficient D of hydrogen in the sheet and frequency f of perturbation in the entry side concentration. One of them was used as a variable, while the other four parameters were fixed. The following default values were used: C_0 = 1 mol m^{-3}, ΔC = 0.1 mol m^{-3}, $L = 10^{-4}$ m, $D = 10^{-9}$ m^2 s^{-1} and f = 0.01 Hz. An example of calculated waveforms of entry flux and exit flux is shown in Fig. 3.2. At the earliest stage of the penetration, hydrogen entry flux is abnormally large since the sheet is empty of hydrogen. The penetration seems to become in quasi-steady state within 100 s under the default condition. The phase shift θ between the entry and the exit flux has been quantified to be 17.66º in this case. Fig. 3.3 shows a series of dependencies of phase shift θ, which is the difference of the exit flux wave from the entry flux wave, on the five parameters used in the calculations. It is obvious that the phase shift is independent of the values of C_0 and ΔC (Figs. 3.3a and 3.3b), though the amplitude of the exit flux wave was strongly dependent on these values. This means that the calculated result of phase shift is also independent of irregular change of the hydrogen entry or signal noise, suggesting that phase shift measurement is useful for investigating hydrogen penetration. On the other hand, the values of L, D and f strongly affect θ as shown in Figs. 3.3c-3.3e. The value of θ increases with increases in L and f, and with decrease in D. It is clear that the diffusion phenomenon is dependent on these parameters. In order to normalize these dependencies, the parameter α is defined by Eq. 1.6.4. Fig. 3.4 shows the relation between θ and α. θ increases exponentially with increase in α with slopes of 2 at $\alpha < 1$ and of 1 at $\alpha > 1$. θ at the cross point of the slopes is 57.29º, which is equivalent to 1 rad. It is obvious that the relation as a function of L, D or f coincides with the algebraic result reported by Sekine [1975], which is an inverse trigonometric function for the tangent of the product of the tangent and hyperbolic tangent of α as described in Eq. 1.6.3. This agreement verifies the results of the FEM calculation for the one-dimensional diffusion problem of hydrogen penetration in this thesis. In the following calculations, C_0 = 1 mol m^{-3}, ΔC = 0.1 mol m^{-3}, $L = 10^{-4}$ m, $D = 10^{-9}$ m^2 s^{-1} and f =

0.01 Hz are used as default parameters.

3.4.2. Local measurement with a micro-capillary cell

The use of a small electrode or microelectrode is effective to investigate the microelectrochemical property of material surface. Fushimi et al. investigated the local penetration of hydrogen in a steel sheet using a DS cell combined with a micro-capillary cell [2016]. In that case, the hydrogen exit side of the micro-cell was smaller than that of the hydrogen entry side because the diameters of them were 2.5×10^{-4} m and 8.0×10^{-3} m, respectively. In addition, the measurement system can be well described by cylindrical geometry, as both the hydrogen entry and exit side electrode areas are concentric circles. Hydrogen penetration during local measurement, therefore, was simulated with FEM calculation in a two-dimensional, axis-symmetrical diffusion problem (Eqs. 3.2.7-3.2.8). The boundary conditions were defined to simulate the experimental system by Fushimi et al. Fig. 3.5a shows a cross-sectional distribution of hydrogen concentration in the steel. The slope of the gradient of hydrogen concentration means the flux of hydrogen according to Eq. 3.2.7. It is confirmed that the diffusion layer (or depletion layer in this case) is mainly formed below the exit side interface. However, local hydrogen flux at the exit edge ($r = 1.25\times10^{-4}$ m) is higher than that at any other exit interface as shown in Fig. 3.5b, indicating that the micro-cell can detect hydrogen diffused not only from just below the exit side but also from the outer part. The resolution of local measurement with the micro-capillary cell, which is a ratio of hydrogen flux from the entry side plane just below the cell to that of the exit side plane, was estimated to be 47.5%.

Although the experiment might be very difficult to carry out, local measurements of hydrogen penetration with an inversed set-up of the micro-capillary cell combined with the DS cell, in which the hydrogen entry was the micro-cell and smaller than that of the hydrogen exit, and with a DS set-up using a double micro-capillary cell, in which the entry and exit cells were two micro-cells with a same diameter, were employed in the FEM calculation. Broadening of

hydrogen diffusion from the entry side interface in the steel was confirmed in both the inversed set-up and the double micro-cell set-up as shown in Figs. 3.6a and 3.7a, respectively. The hydrogen distribution in the sheet in Fig. 3.6a was as same as that of the reversed distribution in Fig. 3.5a. Thus, hydrogen flux in Fig. 3.6b also absolutely coincided with that of the inversed relation in Fig. 3.5b. At the entry edge, the flux shows a maximum, indicating active diffusion in the sheet bulk. On the other hand, local flux in the case of the double micro-cell was smaller than that of only the micro-cell for the exit side as shown in Fig. 3.7b. The peak flux at the entry edge in the double micro-cell is 66.3% of that in the single micro-cell, suggesting that hydrogen diffusion outside of the micro-cell interface decreases the resolution of local measurement. The ratio would be increased with increase in diameter of the capillary cell and with decrease in thickness of the sheet.

3.4.3. Two-dimensional diffusion problem

In general, a steel sheet is polycrystalline and has a heterogeneous structure including a number of single grains and grain boundaries. The diffusion problem of hydrogen in heterogeneously structured sheets has frequently been discussed. However, it is difficult to obtain a rigid solution for hydrogen penetration in a heterogeneous structure even in the case of a sheet with uniform thickness because multi-dimensional diffusion problems need to be solved. In order to tentatively analyze the penetration in a heterogeneous structured sheet, the geometry of the specimen sheet is simplified perpendicularly as shown in Fig. 3.8. The sheet is a lamella composed of two domains of A and B with diffusion coefficients of D_A and D_B and with widths of $2w_A$ and $2w_B$, respectively. Since the boundary planes of the domains are perpendicular to both the entry and exit surfaces, a periodic boundary condition, in which hydrogen flux becomes symmetric at the center plane, is effective. Thus, a two-dimensional diffusion problem, in which w_A and w_B are the periodic boundary condition, was carried out as shown in Fig. 3.9a. In the case of $w_B = w_A$, θ calculated at $D_B = D_A$ is 17.62º, which corresponds to the phase shift θ_0 for a homogeneous sheet. θ decreases with increase in D_B, though the value is asymptotically

approaching the critical values θ_H and θ_L, which are θ calculated for homogeneous sheet, i.e., θ_H = 32.34º at smaller D_B and θ_L = 0º at larger D_B. The value θ_H is strongly dependent on width w_B. When D_B is smaller than D_A, θ_H decreases with decrease in w_B and approaches the value of θ_0, indicating that the diffusion phenomenon in the sheet is dominated by that of larger domains. When D_B is larger than D_A, however, the value of θ for a fixed value of D_B increases with decrease in width w_B. At $D_B = 10^{-7}$ m^2 s^{-1} and $w_B = w_A$ /100, θ is 9.02º, which is almost half of θ_0. This suggests that the presence of a domain with a significantly large diffusivity affects hydrogen diffusion in the sheet. Fig. 3.9b is a double logarithmic plot of the relation between D_B and w_B, where the sinusoidal entry perturbation leads to hydrogen penetration with a half phase shift of θ_0. It is obvious that D_B increases with decrease in w_B with a slope of 1 at w_B smaller than 10^{-5} m. The smaller slope at large w_B suggests that the hydrogen diffusion in not only perpendicular direction but also the horizontal direction affects the hydrogen penetration in a sheet with a heterogeneous structure composed of comparable domains. The plots coincide with the calculated results from the reported relation [Sekine, 1975] using a mean diffusion coefficient D_{mean} as follows:

$$D_{\mathrm{mean}} = \frac{D_A w_A + D_B w_B}{w_A + w_B}. \qquad \text{Eq. 3.4.2}$$

The grain boundary is a steric mismatch of lattices and the boundary width is considered to be in atomic scale. Assuming that $w_B = 10^{-9}$ m for the grain boundary width, the value of $D_B = 10^{-4}$ m^2 s^{-1} can be estimated for the hydrogen diffusion coefficient of the grain boundary. Although the value is five orders in magnitude larger than that of single grains, it is in good agreement with the value reported previously [Hart, 1957].

As discussed above, FEM calculation is effective to simulate hydrogen diffusion in both the grain and boundary. In this chapter, the diffusion problem in a sheet with heterogeneity in in-plane direction is treated. FEM calculation is applicable to differently structured sheets if necessary. For example, a galvanized steel sheet would be modeled as layered structure. A concave structure of the grain boundary may collect hydrogen flux and play the role of a so-called hydrogen trap. In order to clarify the effects of these structures in detail, more

complicated calculations in three dimensions are necessary.

3.5. Conclusions

Local hydrogen penetration and hydrogen penetration in heterogeneous specimen was simulated by FEM calculation as multi-dimensional diffusion. In the case of penetration with sinusoidal perturbation in a homogeneous sheet, the result coincided with the analytical solution reported by Sekine. Simulation of localized hydrogen penetration using a micro-capillary cell resulted in detecting resolution of 47.5%. In the case of penetration in a heterogeneous sheet with two domains, the penetration behavior was characterized by a mean diffusion coefficient. Assuming a grain boundary width of 10^{-9} m, the diffusion coefficient in the grain boundary was estimated to be 10^{-4} m^2 s^{-1}, which was five orders in magnitude larger than that in the grain. The results in this indicated that the validity and usefulness of FEM calculation on analysis of hydrogen diffusion in metal.

3.6. References

K. Fushimi, M. Jin, T. Nakanishi, Y. Hasegawa, T. Kawano and M. Kimura, *ECS Electrochem. Lett.*, **3**, C21 (2014).

K. Fushimi, M. Jin, Y. Kitagawa, T. Nakanishi, and Y. Hasegawa, *ISIJ Int.* **56**, 431 (2016).

K. Sekine: *Chem. Lett.*, **4**, 841 (1975).

R.N. Iyer, H.W. Pickering, M. Zamanzadeh: *J. Electrochem. Soc.*, **136**, 2463 (1989).

H. Hagi: *Mater. Trans. JIM*, **35**, 112 (1994).

E.W. Hart: *Acta Metall.*, **5**, 597 (1957).

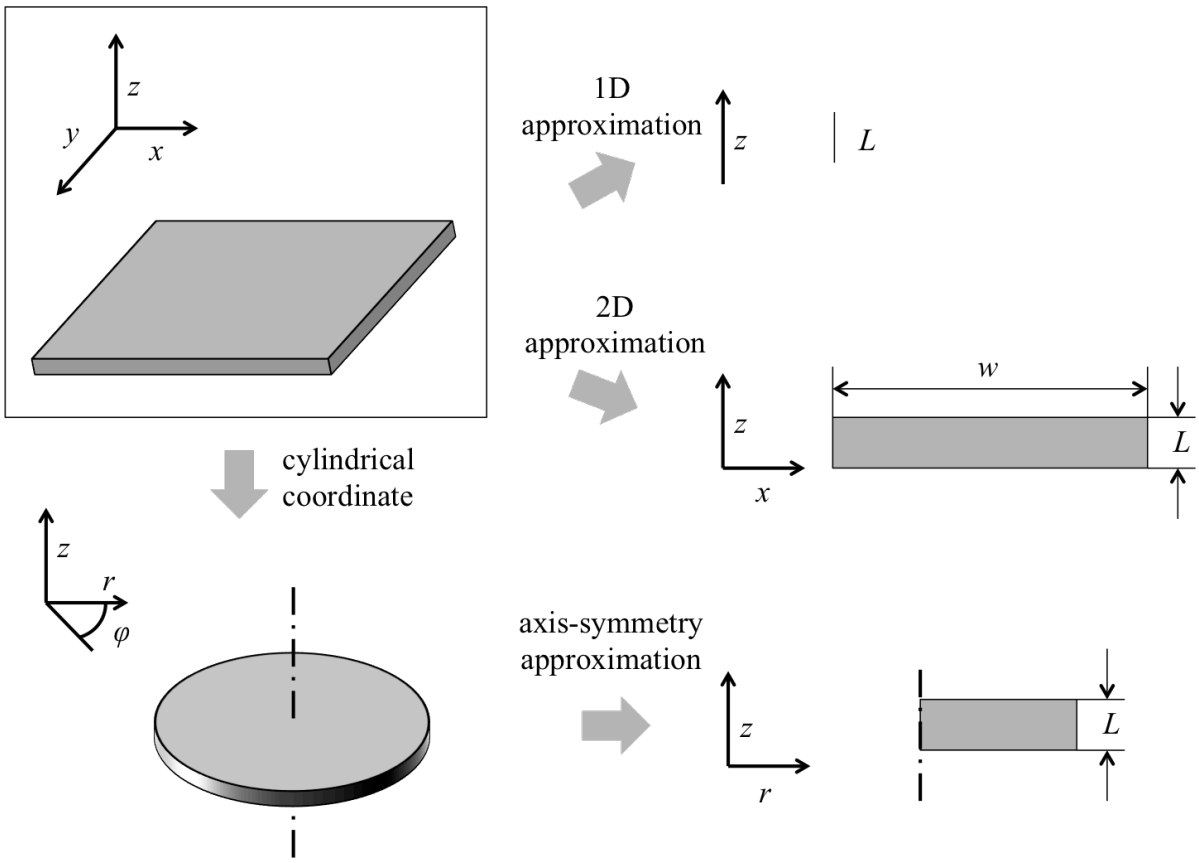

Fig. 3.1. Schematic illustrations of geometric approximation of a steel sheet where hydrogen penetration take places.

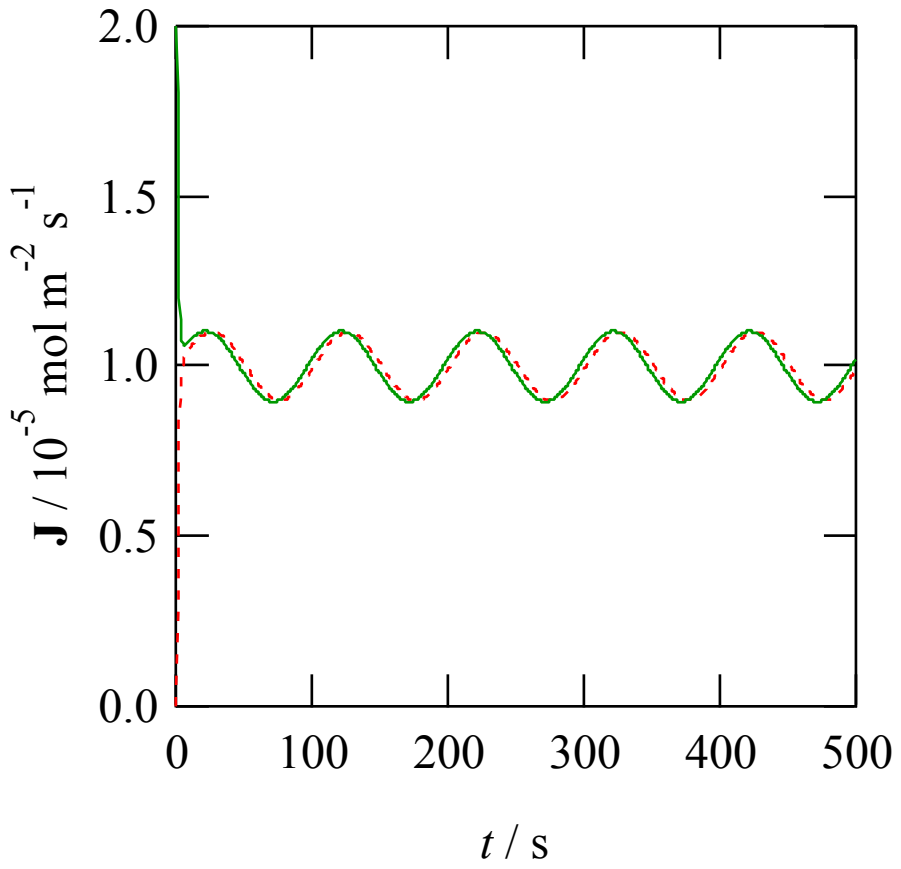

Fig. 3.2. Example of calculated waveforms of hydrogen flux passing through the entry side surface (green solid line) and the exit side surface (red broken line). C_0 = 1 mol m^{-3}, ΔC = 0.1 mol m^{-3}, $L = 10^{-4}$ m, $D = 10^{-9}$ m^2 s^{-1} and f = 0.01 Hz.

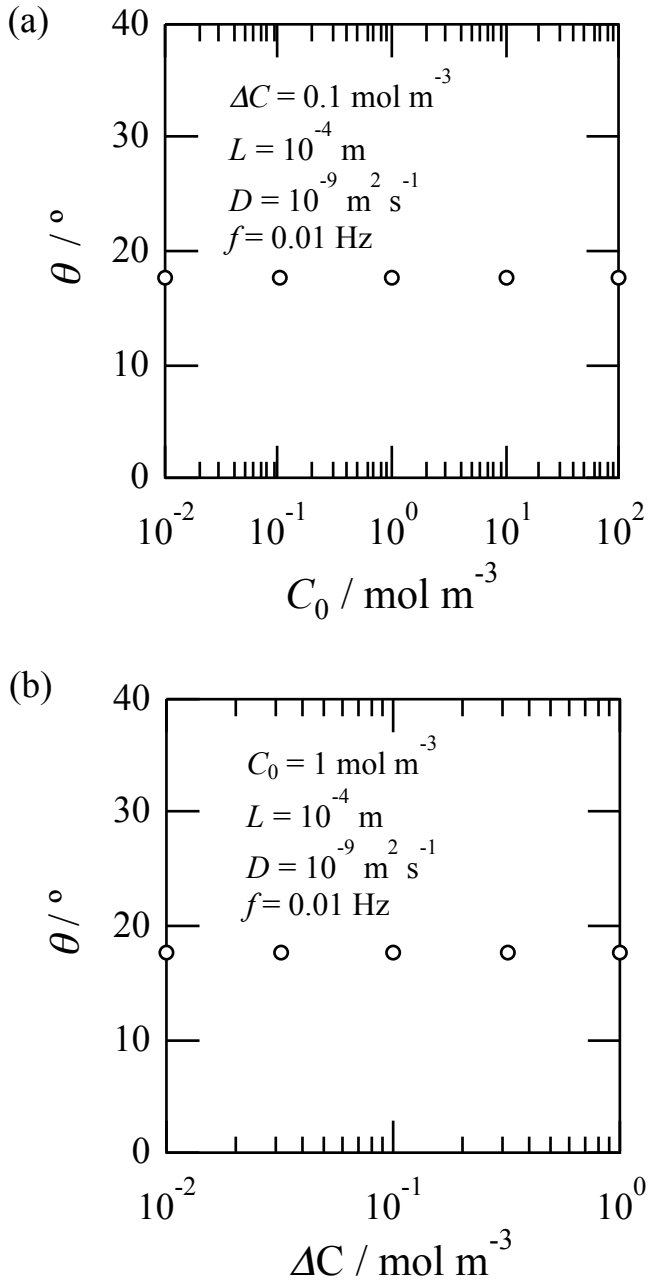

Fig. 3.3. Dependencies of phase shift θ on (a) mean concentration C_0 and (b) concentration amplitude ΔC of hydrogen at the entry side, (c) thickness L of the sample sheet, (d) diffusion coefficient D of hydrogen in the sheet and (e) frequency f of entry perturbation. The values of C_0 = 1 mol m^{-3}, ΔC = 0.1 mol m^{-3}, L = 10^{-4} m, D = 10^{-9} m^2 s^{-1} and f = 0.01 Hz were used as default values.

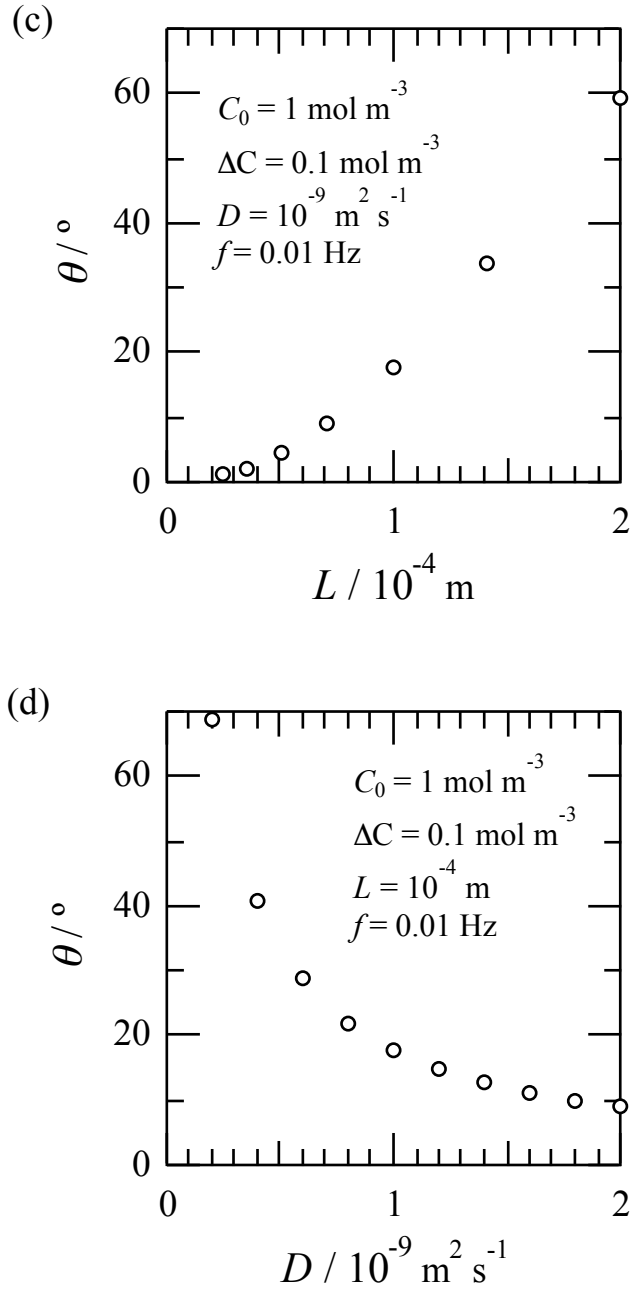

Fig. 3.3. (Continued from the previous page) Dependencies of phase shift θ on (a) mean concentration C_0 and (b) concentration amplitude ΔC of hydrogen at the entry side, (c) thickness L of the sample sheet, (d) diffusion coefficient D of hydrogen in the sheet and (e) frequency f of entry perturbation. The values of C_0 = 1 mol m^{-3}, ΔC = 0.1 mol m^{-3}, L = 10^{-4} m, D = 10^{-9} m^2 s^{-1} and f = 0.01 Hz were used as default values.

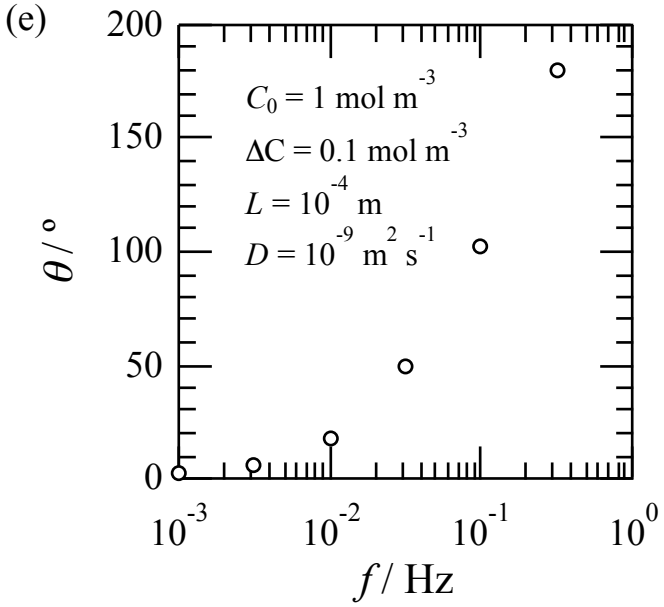

Fig. 3.3. (Continued from the previous page) Dependencies of phase shift θ on (a) mean concentration C_0 and (b) concentration amplitude ΔC of hydrogen at the entry side, (c) thickness L of the sample sheet, (d) diffusion coefficient D of hydrogen in the sheet and (e) frequency f of entry perturbation. The values of C_0 = 1 mol m^{-3}, ΔC = 0.1 mol m^{-3}, L = 10^{-4} m, D = 10^{-9} m^2 s^{-1} and f = 0.01 Hz were used as default values.

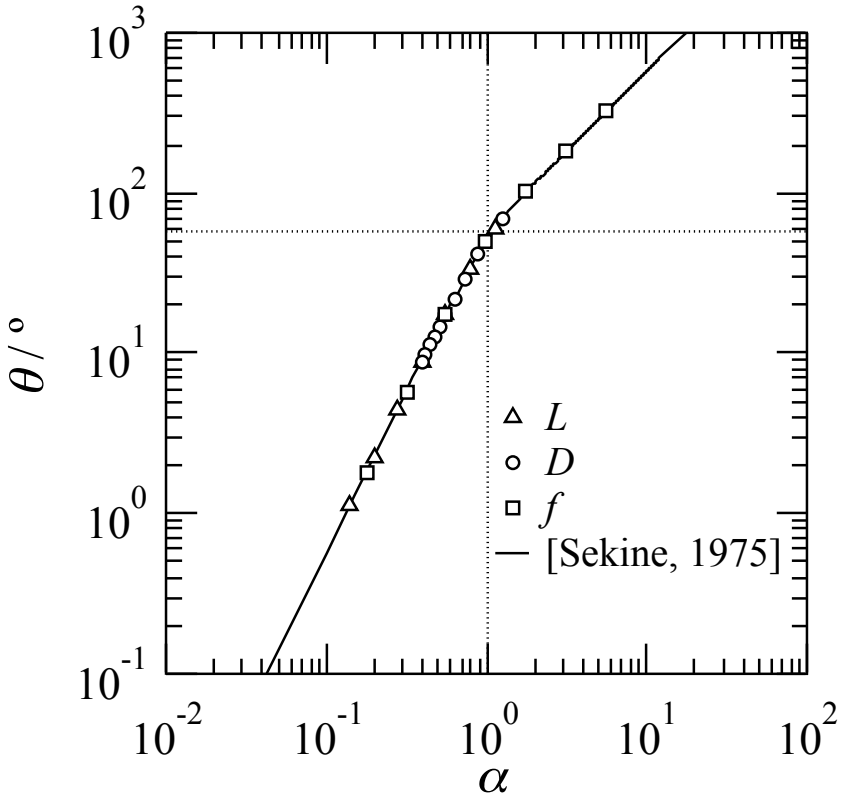

Fig. 3.4. Relations between θ and α when L, D or f was changed from default values of $L = 10^{-4}$ m, $D = 10^{-9}$ m^2 s^{-1} and $f = 0.01$ Hz. The relation reported by Sekine [1975] was also plotted as a solid line. $\alpha = (\pi f L^2/D)^{1/2}$.

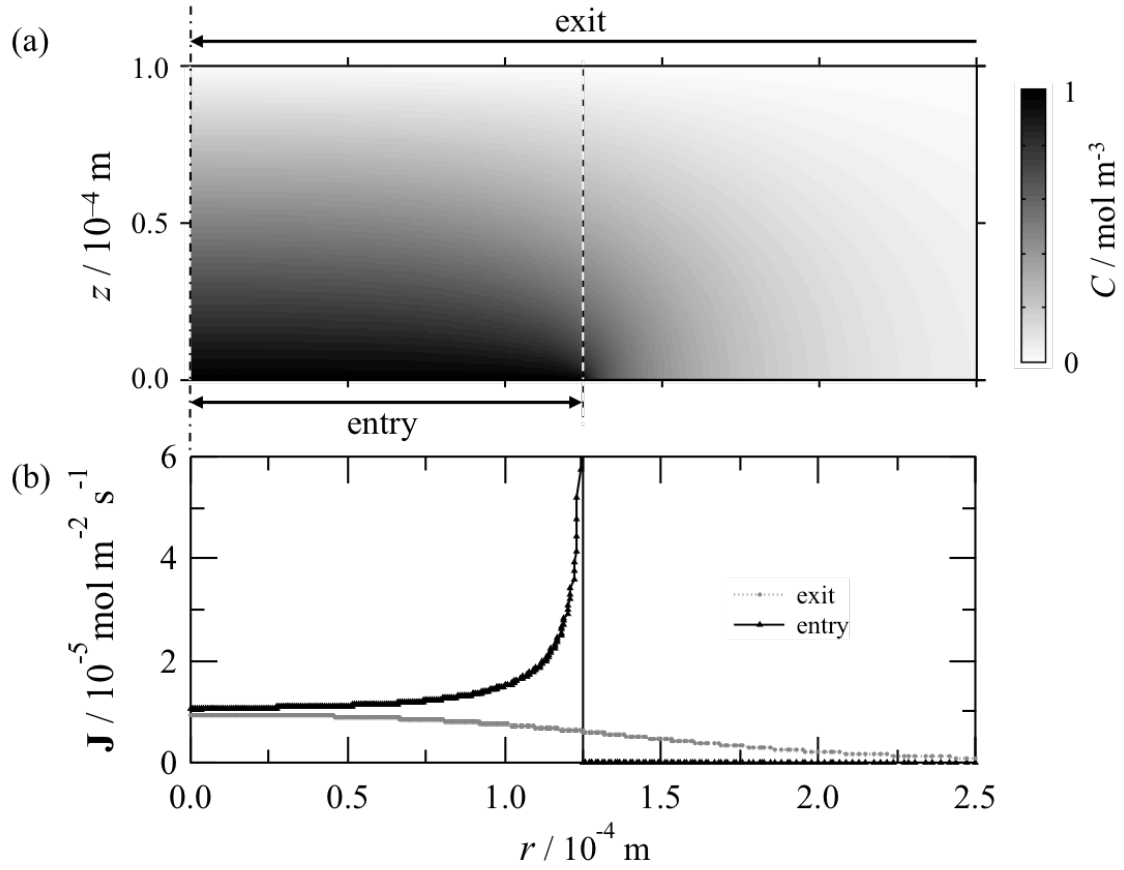

Fig. 3.5. (a) Cross-sectional distribution of hydrogen in the sheet and (b) local current of the exit side during hydrogen penetration when the entry and exit sides were 8×10^{-3} m and 2.5×10^{-4} m in diameter, respectively. The diffusion coefficient of the sheet was 10^{-9} m^2 s^{-1}.

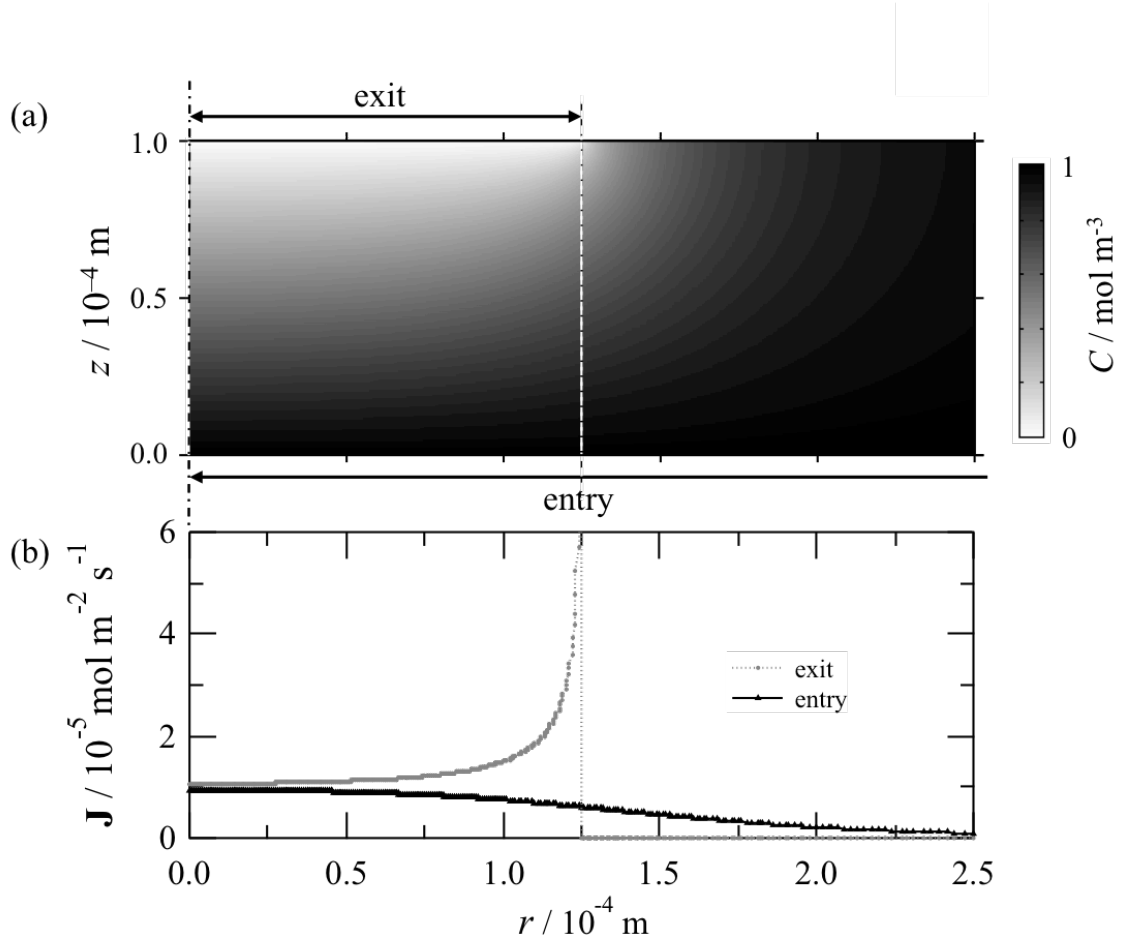

Fig. 3.6. (a) Cross-sectional distribution of hydrogen in the sheet and (b) local current of the entry side during hydrogen penetration when the entry and exit sides were 2.5×10^{-4} m and 8×10^{-3} m in diameter, respectively. The diffusion coefficient of the sheet was 10^{-9} m^2 s^{-1}.

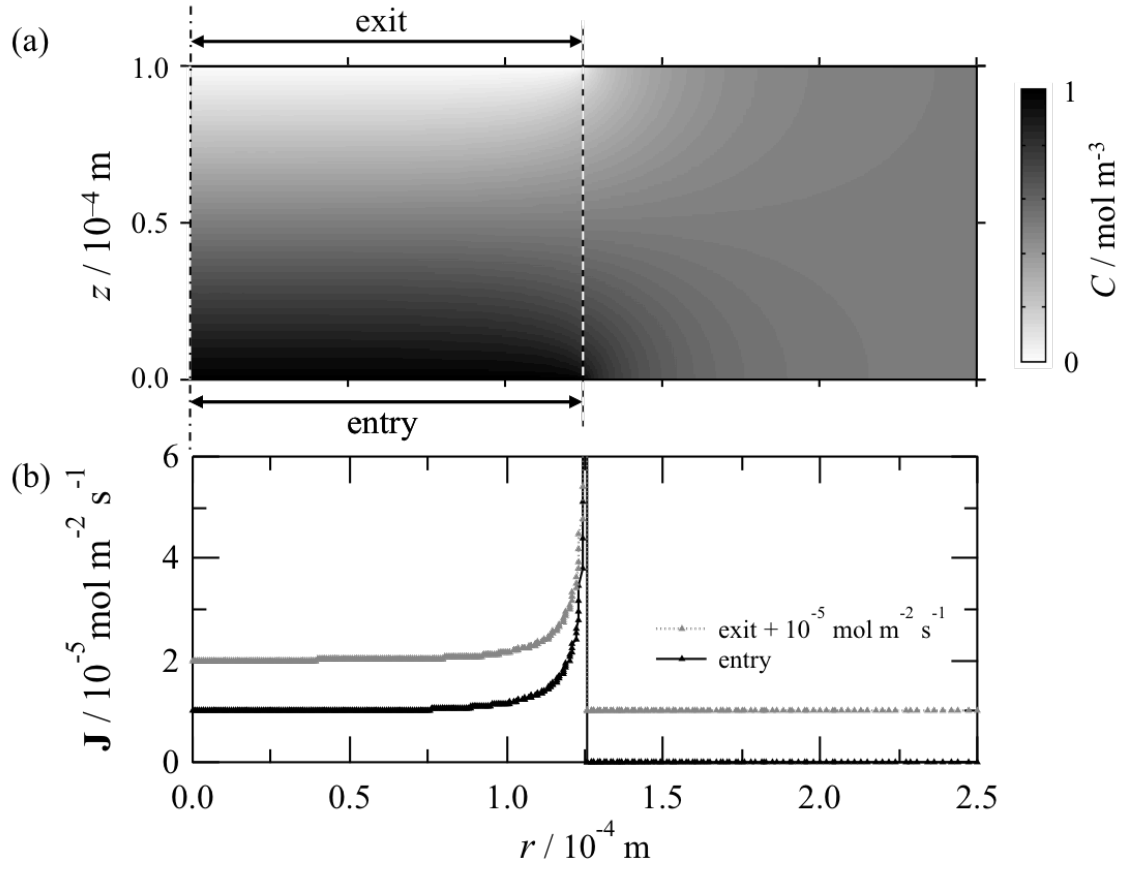

Fig. 3.7. (a) Cross-sectional distribution of hydrogen in the sheet and (b) local current of the entry side during hydrogen penetration when both the entry and exit sides were 2.5×10^{-4} m in diameter, respectively. The diffusion coefficient of the sheet was 10^{-9} m^2 s^{-1}.

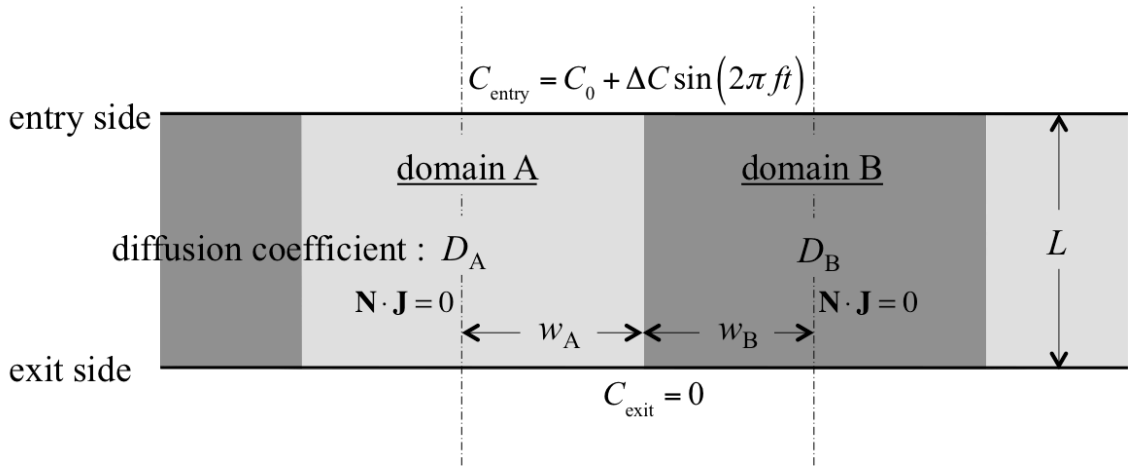

Fig. 3.8. Schematic diagrams of a heterogeneous sheet composed of domains used for a two-dimensional diffusion problem. Lamella of domains with different diffusivities was located perpendicularly with different width or thickness, respectively. A dotted line indicates the symmetric center of the domain for the periodic boundary condition of FEM calculation used.

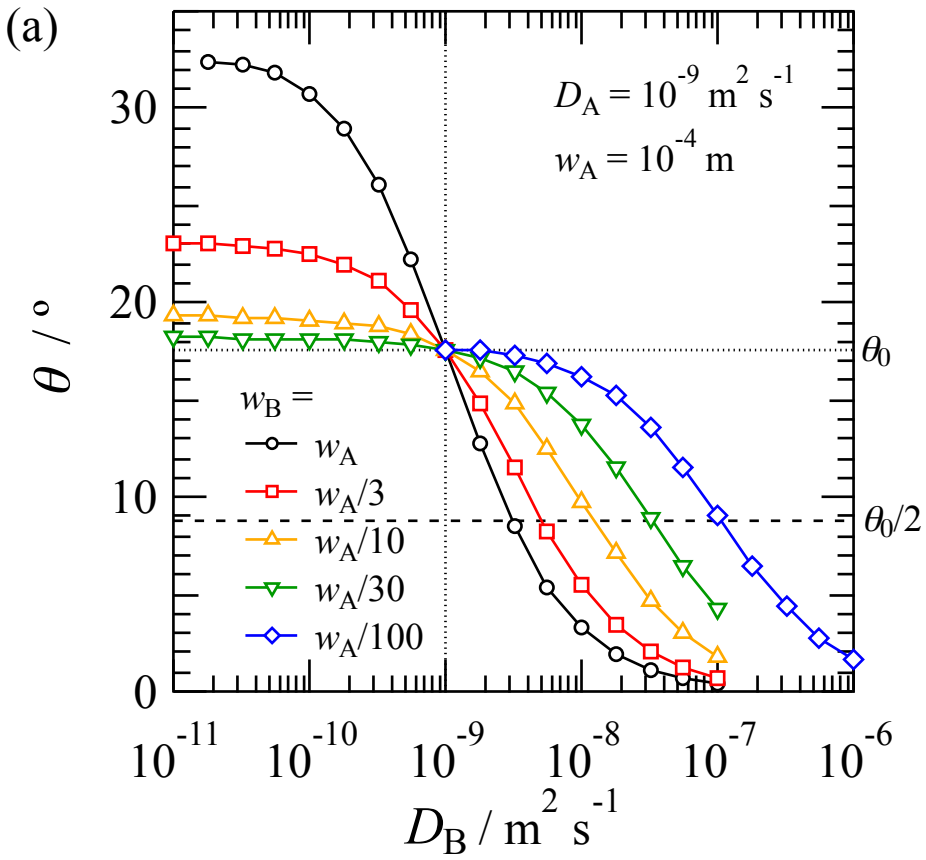

Fig. 3.9. (a) Relation between θ and diffusion coefficient D_B of domain B in a heterogeneous sheet with $L = w_A = 10^{-4}$ m, $D_A = 10^{-9}$ m^2 s^{-1}, and $f = 0.01$ Hz when the width w_B of domain B was changed. (b) Plot of $D_B(\theta_0/2)$, showing a half of θ_0 obtained in the homogeneous sheet, as a function of w_B. The relation calculated from Sekine [1975] was also plotted as a solid line.

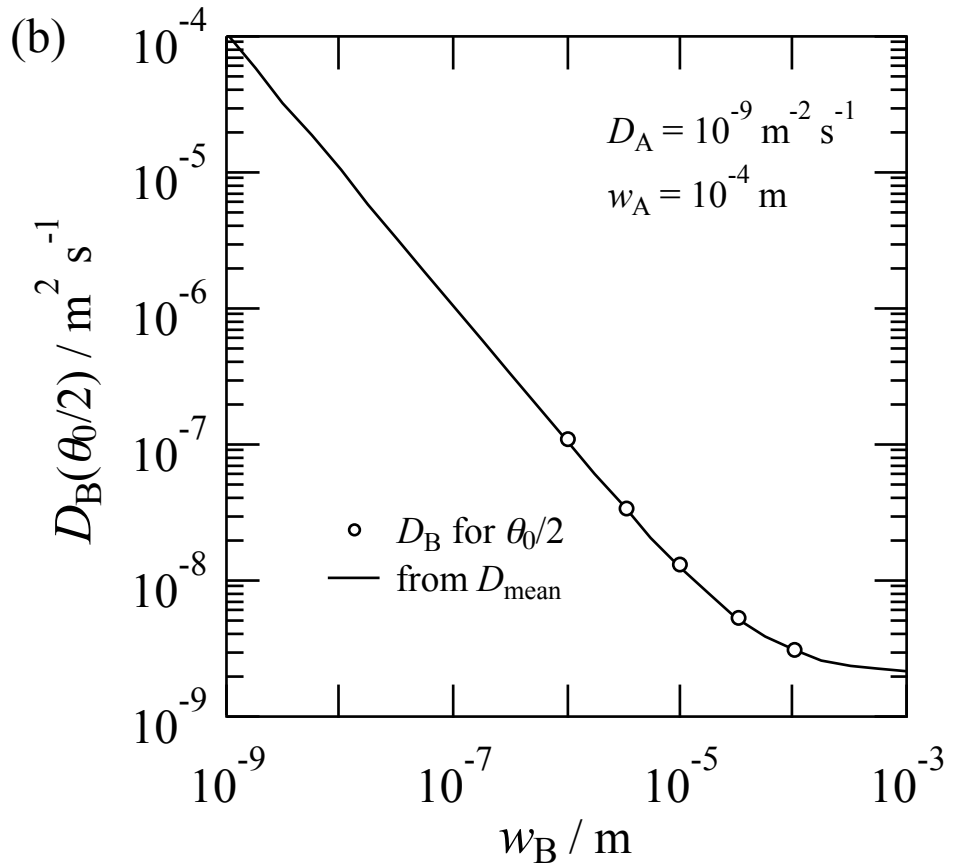

Fig. 3.9. (Continued from the previous page) (a) Relation between θ and diffusion coefficient D_B of domain B in a heterogeneous sheet with $L = w_A = 10^{-4}$ m, $D_A = 10^{-9}$ m^2 s^{-1}, and $f = 0.01$ Hz when the width w_B of domain B was changed. (b) Plot of $D_B(\theta_0/2)$, showing a half of θ_0 obtained in the homogeneous sheet, as a function of w_B. The relation calculated from Sekine [1975] was also plotted as a solid line.

Chapter 4:
Time-Dependent Measurement of Hydrogen Penetration into Iron Sheets from a Borate Buffer Solution Using FFT Analysis

4.1. Introduction

As mentioned in Section 1.6, the sinusoidal perturbation method has potential advantages even in the data processing. The observed hydrogen entry- and exit-current waveforms containing AC signals are decomposed into a frequency domain by a Fourier transform to yield amplitude and phase spectra, which are highly useful in evaluating the phase shift between hydrogen entry- and exit-current waveforms. In addition, the relationship between the phase shift and hydrogen diffusion coefficient is written in identical equations (Eqs. 1.6.3-1.6.4). Therefore, the sinusoidal perturbation method can provide a systematic automation procedure for the derivation of the hydrogen diffusion coefficient. Furthermore, the procedure enables the evaluation of temporal changes in the phase shift. It is useful in practical measurement, in which the conditions at the entry side interface will vary with time due to occurrence of surface reaction such as a corroding surface. In this manner, it is expected that the sinusoidal perturbation method is effective in obtaining further information on surface reaction as well as the hydrogen penetration behavior.

In this chapter, the fast Fourier transform (FFT) technique is combined with the sinusoidal perturbation method in order to automate the derivation process of the phase shift and the hydrogen diffusion coefficient. A series of electrochemical hydrogen penetration measurement with a sinusoidal perturbation on polarization potential at the entry side cell is conducted on pure iron sheet specimens under the controlled environmental conditions.

Subsequently, the temporal response of the phase shift and resulting hydrogen diffusion coefficient are evaluated to show the usefulness of the FFT technique. A pH 8.4 boric acid-borate buffer is used as the electrolyte solution in the entry side cell to maintain the stability of the surface during time-dependent measurement.

4.2. Experimental

4.2.1. DS measurement with flow rate perturbation

All the iron sheet specimens used in this chapter were sourced from pure iron sheets (99.99% Fe, 200, 500, and 800-μm thick, Nilaco). Each sheet was cut into 12 mm × 15 mm rectangular pieces. In vacuum (~10^{-3} Pa), the sheets were heated at 1173 K for 1 h to remove internal stress and to grow crystal grains of up to ~100 μm in diameter; later, they were furnace-cooled down to room temperature. Each sheet was electro-polished in a Jacquet solution (18.5 vol% perchloric acid (purity 70%) + 76.5 vol% anhydrous acetic acid + water) cooled by ice for 600 s with a current density of 60 mA cm^{-2} [Jacuqet, 1956] to ensure a flat and clean surface. The resulting thickness of the sheet specimen was measured by a micrometer prior to electrochemical measurements. One side of each specimen was electroplated with nickel to prevent corrosion at the exit side surface. Nickel electroplating was conducted in an ordinary Watts bath (1 M nickel sulfate + 0.2 M nickel chloride + 0.6 M boric acid) at 4 mA cm^{-2} for 600 s at room temperature [Yoshizawa et al., 1975]. Assuming that the Faradaic efficiency was as same as the reported value (~40%), the thickness of resulting nickel layer was calculated to be ~0.3 μm.

Electrochemical hydrogen penetration measurement was conducted in a modified DS cell with double flow channel as mentioned in Chapter 2. A schematic diagram of the measurement system is shown in Fig. 4.1. Each cell has a three-electrode configuration,

composed of an iron sheet specimen as the working electrode (WE, common), a Pt wire as the counter electrode (CE), and an Ag/AgCl electrode connected via an agarred KNO_3 salt bridge as the reference electrode (RE). The surface area of the WE was determined using an O-ring with an inner diameter of 8.0 mm, resulting in an electrode area of ~0.50 cm^2 for each side. A 0.3 M boric acid-borate buffer solution (pH 8.4) and a 0.2 M sodium hydroxide solution were used as the electrolyte solutions in the entry side cell and exit side cell, respectively. Both electrochemical cells were equipped with an independent circulating flow path flowing the internal electrolyte using a bimorph pump (BPS-215i, Nitto Kohki) driven by a variable-frequency alternating current source (FCA-100, Nitto Kohki) to remove reaction products from the vicinity of the electrode surface. The flow rate u_{entry} at the entry side cell was controlled at 0.25 to 1.5 $cm^3\ s^{-1}$ in a laminar flow condition, while the flow rate u_{exit} at the exit side was set at a constant value of 0.625 $cm^3\ s^{-1}$. The temperature of both electrolytes was controlled at 1 to 70°C with a thermostat (NCB-1200, EYELA) and measured using a type-K thermocouple built in the flow path of the entry side cell. Electrochemical polarization was achieved using a dual-potentiostat (SDDP-212m, Syrinx). The polarization potential E_{entry} at the entry side was sinusoidally perturbed at $E_{entry,0}$ of –0.60 to –1.00 V_{SHE} with an amplitude ΔE of 5 to 10 mV and frequency f of 1 to 50 mHz, whereas the potential E_{exit} at the exit side was kept constant at 0.20 V_{SHE}.

The entry side surface of the specimen after the measurement was observed by X-ray photoelectron spectroscopy (XPS; JPS-9200, JEOL). Photoelectron spectra were recorded with Al-Kα radiation from an X-ray tube operated at the tube voltage of 10 kV and the tube current of 10 mA. The obtained spectra were decomposed using a SpecSurf software (JEOL).

4.2.2. Derivation of the diffusion coefficient using FFT

Data samples of the recorded currents I_{entry} and I_{exit} containing several cycles of sinusoidal perturbation were extracted for the following data processing operation. The direct current components were eliminated using a high-pass filter with a cut-off frequency of $f/2$. FFT was performed on the filtered data samples to yield spectra of amplitude and phase simultaneously. Since the peak frequency of amplitude spectra corresponds to f, the phase shift θ between I_{entry} and I_{exit} was obtained from a difference between phases at f in the phase spectra. D was calculated from α using the inverse interpolation of θ in Eq. 1.6.3 (Fig. 4.1) and Eq. 1.6.4 when f and L were known. All the derivation processes were automated by a computer program on LabVIEW (National Instruments) shown in Appendix 1.

4.3. Results and discussion

4.3.1. Actual illustration of FFT processing

Fig. 4.2a shows a typical variation in currents I_{entry} and I_{exit} at the entry and exit sides, respectively, with respect to time when the entry side potential E_{entry} was perturbed at (–0.95 ± 0.01) V_{SHE} at 10 mHz. The length of the extracted data samples affected the determining stability and response speed of D. The value of D determined from a large sampling was stabilized, while the temporal response was found to be sluggish in the case of large sampling. In the following steps, FFT processing on 10 cycles of the sampled data was carried out. Fig. 4.2b shows the amplitude and phase spectra, which are the Fourier-transformed forms of the currents in Fig. 4.2a. The main peak of I_{entry} is apparently observed at f = 10 mHz and minor peaks at 20, 30 and 40 mHz are also seen as harmonic signals. They are caused by waveform distortion from the input sine wave. Although the distortion seems to originate from the slight nonlinearity in the relationship between E_{entry} and I_{entry}, it did not matter during the

quantification of the phase shift θ between I_{entry} and I_{exit} and hence was ignored.

4.3.2. Frequency dependence

Fig. 4.3 shows typical time variations of I_{entry}, I_{exit}, θ, and D for a 785 μm thick specimen when the perturbation frequency f of E_{entry} was increased stepwise from 1 to 5 mHz. It is clear that I_{entry} and I_{exit} exhibited sinusoidal waveforms and their frequencies changed with changes in f. It is noteworthy that the θ obtained by FFT is relatively stable even though the apparent signal-to-noise ratio of I_{exit} is not so good, demonstrating the previously mentioned advantage of the sinusoidal perturbation method in Section 1.6. The value of θ increased with increase in f as expected from Eqs. 1.6.3 and 1.6.4. Regardless of f, the value of D ranges from 4.2 to 5.0 × 10^{-9} m^2 s^{-1} except for the artificial noises formed before and after frequency changes. Ignoring the data sampled within 500 s before and after the frequency transitions, the mean value of D was calculated at 4.5 × 10^{-9} m^2 s^{-1}.

Although the value of D could be determined from α using Eq. 1.6.4 as shown in Fig. 4.3, the dependence of α^2 on f also yields the value of D, since it is proportional to $\pi L^2/D$ [Nagano et al., 1981]. Fig. 4.4 shows the relationship between α^2 and f. It is apparent that the relationship shows a good proportionality with a slope of 429.9 s. The slope provides D = 4.5 × 10^{-9} m^2 s^{-1}, which is in good agreement with the values of D in Fig. 4.3. It is suggested that both determination methods are effective and result in the same value of D. Although the latter method seems to provide more precise values, it needs a longer time to sweep f in the measurement. Therefore, the former method is adopted to determine the value of D in the following experiments. The proportional relationship shown in Fig. 4.4 also confirms that D is independent of f, even when the former determination method is adopted. The obtained D is

smaller than the diffusion coefficient of 9.0-9.8 × 10^{-9} m^2 s^{-1} at room temperature reported for annealed pure iron specimens in acids [Nagano et al., 1981; Hagi, 1993]. This difference can be attributed to differences in the experimental conditions, such as the residual internal stress of the specimen and surface barrier layer, which will also be discussed in the following sections.

4.3.3. Dependence of *D* on specimen thickness and potential

The values of *D* for specimens with thicknesses of 190, 485, and 785 μm were tentatively measured using the sinusoidal perturbation method at f = 5 mHz. However, the θ of the 190 μm thick specimen was nearly zero at f = 5 mHz and it was difficult to obtain the value of *D* with a good reproducibility. Although the f affects the relationship between α and *D* (Eq. 1.6.4), the *D* was independent of f as explained in Section 4.3.2. So, the *D* values of the 190 and 485-μm thick specimens were measured at frequencies of 50 and 10 mHz, respectively.

Fig. 4.5a shows the dependence of *D* on the specimen thickness when the entry side electrode was polarized at –0.95, –0.90, –0.85, and –0.80 V_{SHE}. It is obvious that the *D* increases with increase in the specimen thickness depending on the polarization potential, which is inconsistent with the assumption introduced in the derivation process of Eqs. 1.6.3-1.6.4 and the independence of *D* from specimen thickness. Although the intercept value of *D* (~1.0 × 10^{-9} m^2 s^{-1}) at L = 0 seems to correspond to some parameters related to hydrogen penetration other than specimen bulk, the value of *D* should be constant and higher than those obtained in Fig. 4.5a. This inconsistency in thickness dependence indicates that the measured phenomena of hydrogen penetration include not only simple diffusion of hydrogen through the bulk of the specimen but also other processes causing penetration delays.

In the derivation of Eqs. 1.6.3 and 1.6.4, hydrogen diffusion is assumed to be

significantly slower than other processes and the rate of hydrogen penetration is determined only by the diffusion of hydrogen in the homogeneous bulk of the metal specimen. However, it is thought that the assumption is excessively simple and needs to be modified. The most probable reason why D depends on the specimen thickness is related to the surface processes of the specimen. In Eq. 1.6.1, surface processes of Eqs. 1.2.1-1.2.6 are assumed to be sufficiently fast compared to hydrogen diffusion and cause no delay for the hydrogen diffusion. In this measurement, however, a pH 8.4 boric acid-borate buffer was used as the entry side solution. Although the buffer is effective to prevent the iron surface from corroding, it is difficult to keep a completely bare surface exposing in a neutral and/or weakly alkaline solution even during cathodic polarization at sufficient overpotentials. The existence of barrier layers such as an oxide or hydroxide on the surface might decrease the reaction activity or reaction areas available for Eqs. 1.2.1-1.2.6, resulting in a relatively small value of D owing to the suppressed surface processes, which are comparably slow with the diffusion process. The relative effect of surface processes on hydrogen penetration becomes larger in thinner specimens. Although the delaying effect of the surface processes seems to be negligible in the case of the 785 μm thick specimen, the use of thicker specimens would be helpful in simplifying the model of hydrogen penetration in the following experiments.

Fig. 4.5b shows the dependence of D on the mean polarization potential $E_{\mathrm{entry},0}$. D increases as $E_{\mathrm{entry},0}$ becomes less noble. This dependence could be observed, regardless of specimen thickness. It is also attributed to the surface effect as the driving forces for Eqs. 1.2.1-1.2.4 are activated by an increase in cathodic overpotential. Electrochemical activation of Eqs. 1.2.1-1.2.4 indirectly accelerates the hydrogen absorption reaction (Eq. 1.2.6). If the iron specimen surface is covered with a native oxide film, absorbed hydrogen reduces the oxide and

forms a non-stoichiometric oxide/hydroxide mixture, thus affecting the reaction activities of the surface processes (Eqs. 1.2.1-1.2.6) [Modiano et al., 2008]. It is likely that the polarization potential affects the surface processes by changing the chemical composition and/or reaction activity, causing additional delays in hydrogen penetration.

The appropriate thickness for the determination of D in bulk specimens might be dependent on the experimental conditions including electrode potential. It was reported that a 500-μm thick annealed pure iron sheet was thick enough to determine D in bulk specimens by the perturbation method in 0.5 M sulfuric acid [Nagano et al., 1981]. It is also suggested that solution acidity affects the determination of D in bulk specimens as a larger value of D is obtained in more acidic solutions. A solution with a high concentration of H^+ ions allows the reactions of Eqs. 1.2.1 and 1.2.3 rather than those in Eqs. 1.2.2 and 1.2.4. Moreover, iron at potentials lower than 0.00 V_{SHE} in solutions of pH < 4 is stable in the form of Fe^0 or Fe^{2+} [Pourbaix, 1974] (The pourbaix diagrams of iron in acidic environment and in basic environment, and the cathodic dynamic polarization curve in pH 8.4 borate buffer solution are shown in Appendix 2), supporting the exposure of bare iron surface. Considering the experimental conditions adopted in this chapter, iron at –0.95 V_{SHE} in pH 8.4 is stable as Fe^0. However, it can be occurred that the reaction is not rapid and the native oxide remains over the hydrogen penetration.

In order to confirm the effect of the native oxide on surface, tentative hydrogen penetration measurement was conducted in 0.05 M sulfuric acid solution (pH~1) with a 780 μm thick specimen. The other parameters for the measurement were as follows; u_{entry} = 1.5 cm^3 s^{-1}, $E_{entry,0}$ = –0.35 V_{SHE}, ΔE = 5 mV, f = 5 mHz, and T = 298 K. In this acid, a bare surface of the specimen might be exposed without any oxides [Pourbaix, 1974]. This measurement provided a

hydrogen diffusion coefficient of 7.2×10^{-9} m^2 s^{-1}, which is apparently larger than that determined in pH 8.4 buffer and is closer to the reported value [Nagano et al., 1981; Hagi, 1993]. This result stands as an evidence for the existence of some barrier layer on the surface, which inhibits hydrogen penetration through the specimen in pH 8.4 buffer solution and results in small apparent values of D. The entry side of the specimen in the acid, however, exhibited an obvious dissolution of ~30 μm per day, while no dissolution of the specimen was observed in pH 8.4 buffer solution even after a week of measurement. Usage of such a strong acid might be suitable for short-term measurement but not for long-term measurement. Although the existence of barrier layers on the surface in pH 8.4 buffer solution affects the hydrogen penetration by reducing the apparent hydrogen diffusion coefficient and/or variation in the rate of hydrogen evolution, it would be better to use this solution for reproducible hydrogen penetration measurement.

4.3.4. Flow-rate dependence

Fig. 4.6 shows the dependence of D on the electrolyte flow rate u_{entry} in the entry side cell. It is clear that the D is independent of u_{entry} regardless of the specimen thickness, though an increase in u_{entry} led to an increase in I_{entry} and a decrease in I_{exit} as reported previously [Fushimi et al., 2014]. It is suggested that u_{entry} mostly affects the reaction rates of Eqs. 1.2.1-1.2.4 and little affects the stability of the surface layer on the entry side surface. This is unlike the effect of polarization potential on D discussed in Section 4.3.3.

When the electrolyte flow rate u_{exit} in the exit side cell was varied, it was found that the D obtained was also independent of u_{exit}. On the other hand, Ceballos et al. reported the contrasting result that D was dependent on u_{exit} using a pH 8.4 boric acid-borate buffer solution

in the exit side cell [Ceballos et al., 2014]. This inconsistence seems to be due to the difference of electrolyte used in the exit side cell. A 0.2 M sodium hydroxide was used for the experiment in this chapter. As described in Section 2.2, the use of a strong alkaline solution for the exit side cell seems to be essential for the establishment of the constant concentration boundary condition (Eq. 1.6.2) and the proper measurement of D. This would be the origin of the apparent dependence of D on u_{exit} reported by Ceballos et al.

4.3.5. Time-dependent measurement

As mentioned in Section 1.7, one of the most significant advantages of the sinusoidal perturbation method is the possibility of time-dependent evaluations of the phase shift and hydrogen diffusion coefficient. The native oxide on the entry side surface would cause a delay addition to the hydrogen penetration process as mentioned in 4.3.3. In this case, the D obtained by sinusoidal perturbation is regarded as an apparent value that deviates from the actual hydrogen diffusion coefficient of the specimen. As the apparent D contains quantitative information on the delay caused by surface-related processes, it is thought that the time-dependent measurement of hydrogen penetration is useful in evaluating the temporal changes on the surface.

Fig. 4.7 shows a result of time-dependent measurement of hydrogen diffusion coefficient. During the measurement, the temperature was maintained at a constant value of 298 K. Although the apparent value of D is almost constant at 6.7×10^{9} m^2 s^{-1} throughout the measurement, $|I_{entry}|$ decreases and I_{exit} increases. The absorption efficiency (Eq. 1.5.1) increased with time, even though the hydrogen penetration process expressed by D did not change. It is thought that the decrease in $|I_{entry}|$ with increasing absorption efficiency is correlated with the

deterioration of the surface layer [Modiano et al., 2008].

4.3.6. Temperature dependence

In microscopic perspective, hydrogen diffusion in metal lattice is expressed by a repetition of jump between adjacent troughs of energy as described in Section 1.2. It is considered that the depth of the trough equals to the activation energy of hydrogen diffusion. Since the trough depth corresponds to the strength of the interaction between a hydrogen atom and the lattice, the temperature dependence of hydrogen diffusion coefficient (Eq. 1.3.5) reflects the strength of the interaction. In this viewpoint, the temperature dependence is an important factor in evaluating hydrogen penetration behavior.

A series of hydrogen penetration measurement at different temperatures was conducted to evaluate the temperature dependence of D. Fig. 4.8 is a typical result showing time variation of I_{entry}, I_{exit}, θ, absorption efficiency and D when temperature was changed from 285 to 325 K. It is apparent that both currents I_{entry} and I_{exit} increase with increase in temperature, indicating the activation of both hydrogen evolution and hydrogen penetration. The phase shift gradually decreases with time. It clearly corresponds to the increase of hydrogen diffusion coefficient, which is expected from Eq. 1.3.5. The absorption efficiency also changes with temperature. However, temperature dependence of absorption efficiency is a kind of meaningless; the absorption efficiency is affected not only by the rate of hydrogen evolution/absorption reactions but also by the hydrogen diffusion coefficient, since hydrogen penetration is diffusion-controlled process. Temperature affects both the rate of the surface reactions and the hydrogen diffusion coefficient. For the evaluation of hydrogen adsorption reaction (Eq. 1.2.6), hydrogen absorption efficiency should be measured under a condition

where the parameters affecting hydrogen diffusion process are kept constant. However, it is noteworthy that the value of absorption efficiency drastically increased sudden after the spike noise in I_{entry}. The origins of this phenomenon and of the noise itself are not clear. Anyway, it seems not to affect the calculation result of D.

Fig. 4.9 shows an Arrhenius plot of the measured temperature dependence of D. The Arrhenius parameters obtained by a linear-least-square fitting are listed in Table 4.1. Although the D value obtained at room temperature in this work is of the same order as the reported values for annealed 99.99% iron, the E_a estimated is slightly greater than the reported values, 4.2 kJ mol^{-1} [Nagano et al., 1981] and 4.0-5.3 kJ mol^{-1} [Hagi, 1993]. It is thought that this is also due to the synergistic effect of the surface barrier layer on hydrogen penetration as mentioned in Sections 4.3.4 and 4.3.5.

4.3.7. X-ray photoelectron spectroscopy

In the above sections, it was suggested that a surface barrier layer, which affects hydrogen penetration behavior, exists on the entry side surface of the specimens in the hydrogen penetration measurement using pH 8.4 boric acid-borate buffer solution. In order to investigate the barrier products existing on the surface, XPS was conducted on the entry side surface of an iron specimen after hydrogen penetration measurement, in which the entry side surface was polarized at a constant potential E_{entry} = –0.95 V_{SHE} in 0.3 M boric acid-borate buffer for 200 ks under flow rate u_{entry} = 1.5 cm^3 s^{-1} and temperature T = 298 K.

Figs. 4.10 and 4.11 show Fe $2p_{3/2}$ and O 1s photoelectron spectra, respectively, obtained from the surfaces of the polarized area and not-polarized area of the specimen. It is clear in Fig. 4.10 that two peaks are observed at ~707 and ~711 eV on both measurement areas.

The low binding energy peak corresponds to metallic Fe (Fe^0) [Sinha et al., 1987; Andersson et al., 1989; Powell et al., 2012] while the high binding energy peak would be originated from mixture of some oxides and/or hydroxides of Fe. Some compounds can be candidates for the oxide and/or hydroxide such as Fe_2O_3 (710.7-710.97 eV) [Asami et al., 1977; Mathiew et al., 1986; Andersson et al., 1989], Fe_3O_4 (709.2-710.95 eV) [Asami et al., 1977; Tan et al., 1990; Marcus et al., 1992] and FeOOH (711.44-711.60 eV) [Asami et al., 1977; Tan et al., 1990]. However, it was difficult for the spectra to be deconvoluted with these compounds clearly. Therefore, the spectra were curve-fitted with two components of metal and oxide-hydroxide mixture. The peak area ratio of metallic Fe to the total of metal and the mixture on the surface area where hydrogen penetration had been conducted was 11.2%, which was smaller than 23.4% obtained on the area where hydrogen penetration had not been conducted.

In Fig. 4.11, at least two components can also be distinguished at 530.5 and 531.5 eV. It was reported that the peak at 531.4-531.7 eV corresponds to hydroxide state of O in FeOOH [Asami et al., 1977; Tan et al., 1990] while the peaks emerge from O existing as oxide such as Fe_2O_3 (529.8-529.98 eV) [Asami et al., 1977; Paparazzo et al., 1988, Tan et al., 1990; Rueda et al., 1996], Fe_3O_4 (529.7-530.7 eV) [Asami et al., 1977; Tan et al., 1990; Marcus et al., 1992; Allen et al., 1996], FeO (529.8-530.1 eV) [Allen et al., 1974; McIntyre et al., 1977] and FeOOH (529.7-530.3 eV) [Asami et al., 1977; Tan et al., 1990]. Although the exact identification of the two peaks is also difficult similar to the case of Fe $2p_{3/2}$, the spectra is curve-fitted with two components of hydroxide with high binding energy and oxide with low binding energy. The peak area ratio of hydroxide to the total of hydroxide and oxide on the hydrogen-penetrated area is 86.1%, which is apparently larger than 73.6% measured on the area where hydrogen penetration had not been conducted.

The result of XPS suggests that the entry side of the iron specimen is not completely bare. The cathodic polarization for hydrogen entry reaction could not reduce a native layer of iron oxide and/or hydroxide originally covered on the surface to metal and formed hydroxide significantly. Moreover, the hydrogen penetration measurement seems to increase the layer thickness since metallic Fe peak is smaller than the mixture peak. One of the reasons why the layer thickness increases during the hydrogen penetration measurement might be the reduction of oxide to hydroxide due to cathodic polarization and hydrogen uptake. The increase of the ratio of hydroxide in the surface layer may result in the decrease of the density of the layer. In any case, the existence of hydroxide layer on iron specimens undergoing hydrogen penetration in the buffer solution supports the measurement obtaining apparent small values of D discussed in previous sections, especially in Section 4.3.5 where the deterioration of the layer during the hydrogen penetration was discussed.

Summarizing all the obtained facts, a model describing the mechanism how the hydrogen absorption efficiency increased over three days during hydrogen penetration measurement is proposed as depicted in Fig. 4.12. The specimen surface was originally covered by a surface layer composed of some mixture of iron oxides and hydroxides. The content of hydroxide in the surface layer was increased owing to the hydrogen insertion during the hydrogen penetration. Such deterioration of the surface layer may have caused the decrease in the reaction activity of the hydrogen gas evolution (forward reactions of Eqs. 1.2.4-1.2.5), resulting in the accumulation of H_{ads} on the entry side surface. As described in Eqs. 1.2.14-1.2.17, the enrichment of H_{ads} on the entry side surface (increased $\theta_{coverage}$) promotes hydrogen entry reaction (forward reaction of Eq. 1.2.6) and therefore the hydrogen exit current increased. The enrichment of hydroxide also caused thickening of the layer since the density of

hydroxide is lower than that of oxide.

It is remarkable that the sinusoidal perturbation method separately enables the extraction of the amount of hydrogen uptake and the temporal delay during penetration. In this manner, the sinusoidal perturbation method combined with FFT provides a way to study in detail the effect of the deteriorating surface barrier layer and assists in the elucidation of the mechanism. Taking all factors into account, time-dependent hydrogen penetration measurement by the sinusoidal perturbation method combined with FFT exhibits their usefulness for the evaluation of hydrogen penetration as well as the deterioration of the surface barrier layer.

4.4. Conclusions

A new methodology for time-dependent measurement of hydrogen penetration by sinusoidal perturbation in a combination with FFT was introduced. Hydrogen penetration into annealed pure iron sheets from a pH 8.4 boric acid-borate buffer solution was investigated using a modified DS cell with individual flow paths. The dependence of phase shift between the hydrogen entry and exit currents and the hydrogen diffusion coefficient on specimen thickness, polarization potential, electrolyte flow rate, time and temperature were examined thoroughly. The dependence on specimen thickness and polarization potential suggests the presence of a surface barrier layer on the entry side surface of the specimen, which causes an additional delay in the hydrogen penetration processes. The electrolyte flow rate in the entry side cell or in the exit side cell did not affect the apparent value of the hydrogen diffusion coefficient. The detail examinations of temporal change in the phase shift and hydrogen diffusion coefficient indicated deterioration of the barrier layer on the entry side surface. XPS revealed that the deterioration was due to the reduction of a native oxide to hydroxide. The time-dependent hydrogen

penetration measurement method was proven to be useful in evaluating the deterioration of the barrier layer and its effect on the hydrogen penetration behavior.

4.5. References

M. Nagano, Y. Hayashi, N. Ohtani, M. Isshiki and K. Igaki, *Trans. Japan Inst. Met.,* **22**, 423 (1981).

K. Fushimi, M. Jin, Y. Kitagawa, T. Nakanishi and Y. Hasegawa, *ISIJ Int.*, **56**, 431 (2016).

P.A. Jacquet, *Metall. Rev.,* **1**, 157 (1956).

S. Yoshizawa, T. Tsuruta and K. Yamakawa, *Corros. Eng*., **24**, 511 (1975).

H. Hagi, *J. Japan Inst. Met.*, **57**, 742 (1993).

S. Modiano, J. A. V. Carreño, C. S. Fugivara, R. M. Torresi, V. Vivier, A. V. Benedetti and O. R. Mattos, *Electrochim. Acta*, **53**, 3670 (2008).

M. Pourbaix, *Atlas of Electrochemical Equilibria in Aqueous Solution*, 2nd ed., p. 307, National Association of Corrosion Engineering, Houston (1974).

K. Fushimi, M. Jin, T. Nakanishi, Y. Hasegawa, T. Kawano and M. Kimura, *ECS Electrochem. Let*t., **3**, C21 (2014).

A. M. P. Ceballos, J. A. C. Gutierrez and O. R. Mattos, *Dyna*, **81**, 152 (2014).

M. Nagumo, *Fundamentals of Hydrogen Embrittlement*, 1st ed., p. 58, Uchida Rokakuho Publishing, Tokyo (2008) (Japanese).

K. Asami and K. Hashimoto, *Corros. Sci.* **17**, 559 (1977).

S. Sinha, S. Badrinarayanan and A.P.B. Sinha, *J. Less Common Met.* **125**, 85 (1986).

S.L.T. Andersson and R.F. Howe, *J. Phys. Chem.* **93**, 4913 (1989).

C.J. Powell, *J. Electron Spectros. Relat. Phenomena* **185**, 1 (2012).

H.J. Mathieu and D. Landolt, Corros. Sci. **26**, 547 (1986).

B.J. Tan, K.J. Klabunde and P.M.A. Sherwood, *Chem. Mater.* **2**, 186 (1990).

P. Marcus and J.M. Grimal, *Corros. Sci.* **33**, 805 (1992).

E. Paparazzo, *Surf. Interface Anal.* **12**, 115 (1988).

F. Rueda, J. Mendialdua, A. Rodriguez, R.Casanova, Y. Barbaux, L. Gengembre and L. Jalowiecki, *J. Electron Spectros. Relat. Phenomena* **82**, 135 (1996).

G.C. Allen and K.R. Hallam, *Appl. Surf. Sci*. **93**, 25 (1996).

G.C. Allen, M.T. Curtis, A.J. Hooper and P.M. Tucker, *J. Chem. Soc., Dalt. Trans.* **0**, 1525 (1974).

N.S. McIntyre and D.G. Zetaruk, *Anal. Chem.* **49**, 1521 (1977).

Table 4.1. Temperature dependence of the hydrogen diffusion coefficient of a pure iron sheet.

Reference	Thickness / μm	Heat treatment	D_0 / m^2 s^{-1}	E_a / kJ mol^{-1}	D @ R.T.[a] / m^2 s^{-1}
Present work	190	900°C, 3.6 ks	3.6×10^{-8}	8.1	1.4×10^{-9}
Present work	785	900°C, 3.6 ks	6.6×10^{-7}	13	4.2×10^{-9}
[Hagi, 1993]	1000	900°C, 10.8 ks	6.4×10^{-8}	4.7	9.6×10^{-9}

[a] R.T.: Room temperature

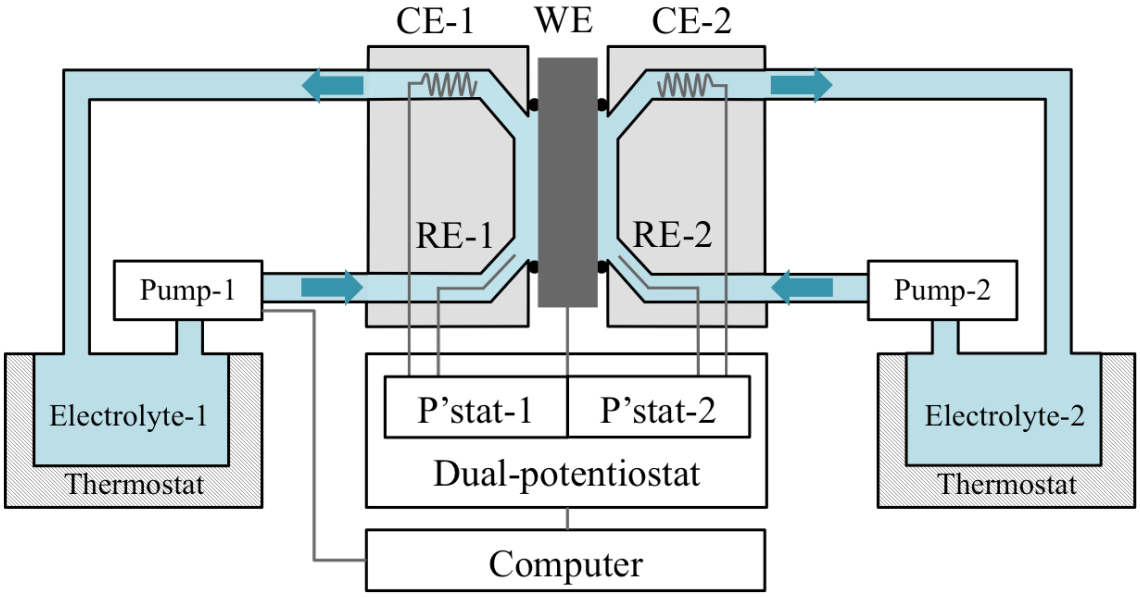

Fig. 4.1. Schematic of the set-up of the hydrogen penetration measurement system used in this study.

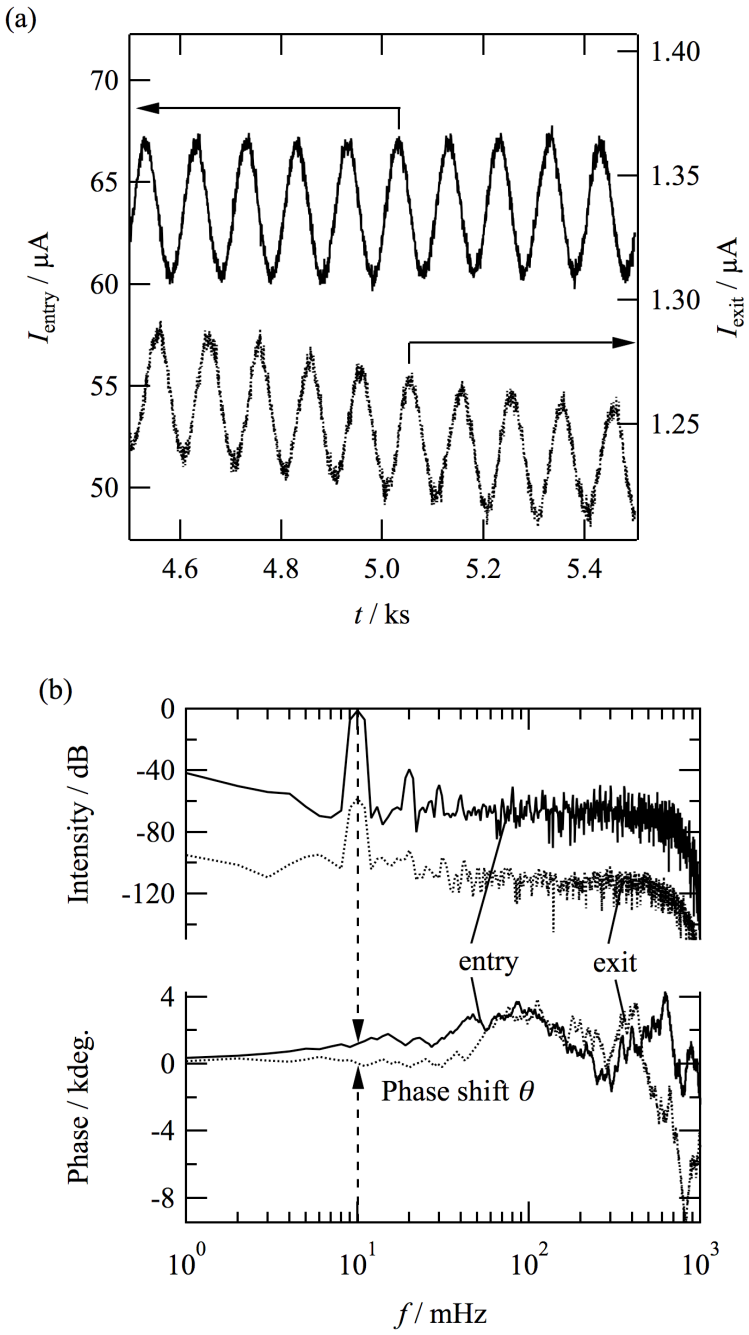

Fig. 4.2. (a) Extracted time variation of the entry side current I_{entry} and exit side current I_{exit} when the entry side electrode of the specimen with a thickness of 785 μm was polarized at (–0.95 ± 0.005) V_{SHE} with f = 10 mHz. (b) Amplitude and phase spectra after FFT processing of the data in Fig. 4.2a.

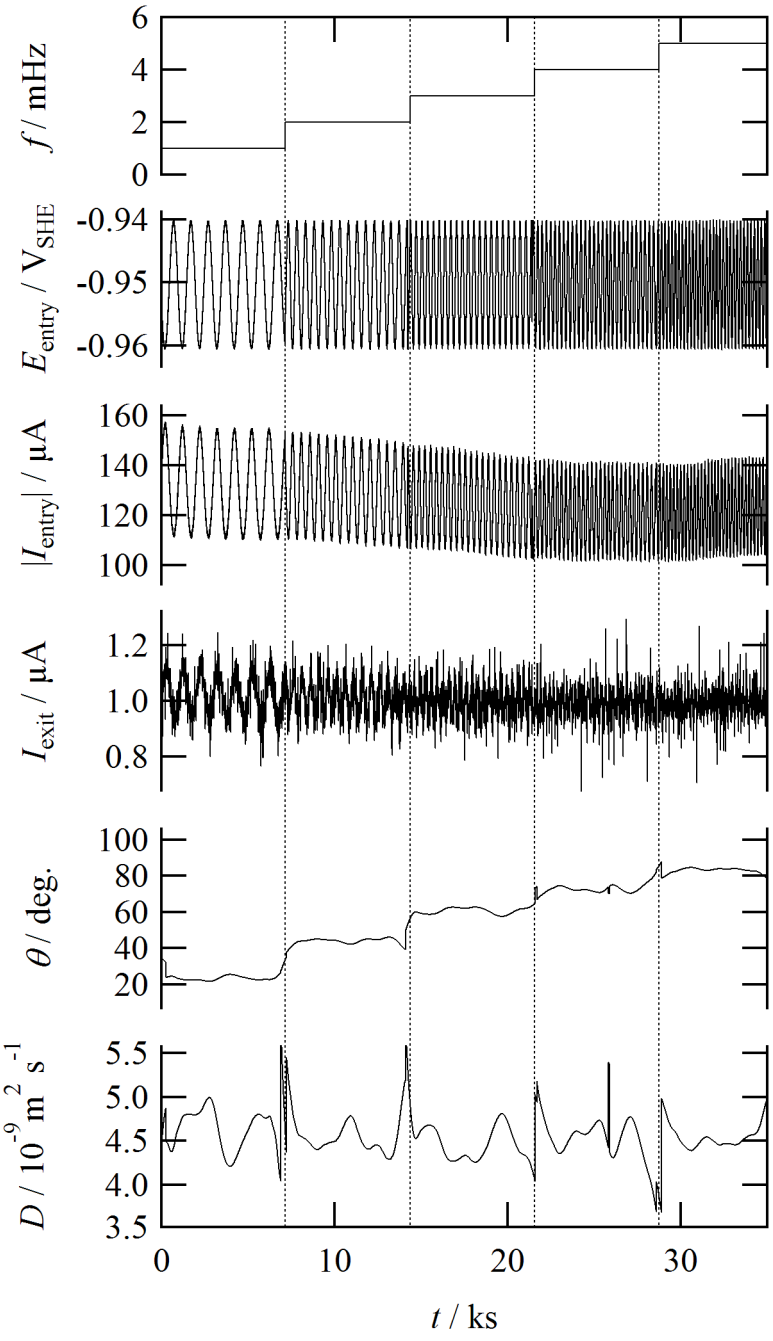

Fig. 4.3. Time variation of I_{entry}, I_{exit}, θ, and D for a 785 μm thick specimen when the perturbation frequency f of E_{entry} (= (–0.95 ± 0.01) V_{SHE}) was increased stepwise from 1 to 5 mHz; u_{entry} = 1.5 $cm^3\ s^{-1}$ and T = 298 K.

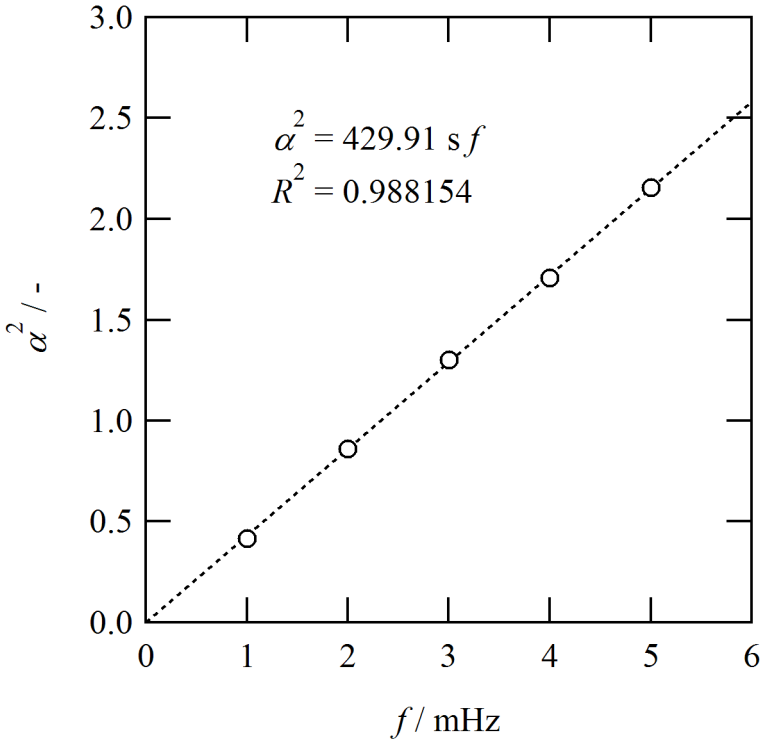

Fig. 4.4. Relationship between the hydrogen diffusion parameter α^2 and frequency f (Fig. 4.2). The plot was fitted by a line crossing the origin.

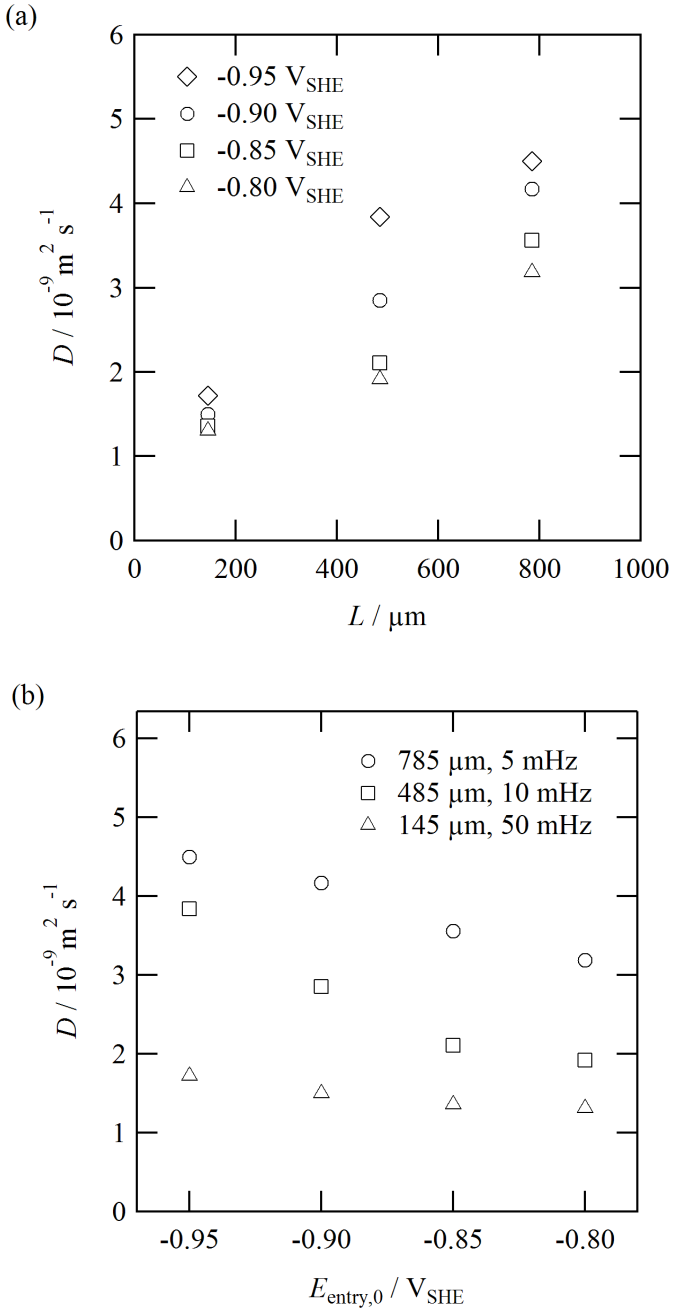

Fig. 4.5. (a) Relationship between D and specimen thickness and (b) relationship between D and polarization potential $E_{entry,0}$ of the entry side electrode when it was polarized at –0.95, –0.90, –0.85, or –0.80 V_{SHE} with an amplitude of 5 mV. f was varied between 50, 10, and 5 mHz for specimens with thickness of 190, 485, and 785 μm, respectively. u_{entry} = 1.5 cm^3 s^{-1} and T = 298 K.

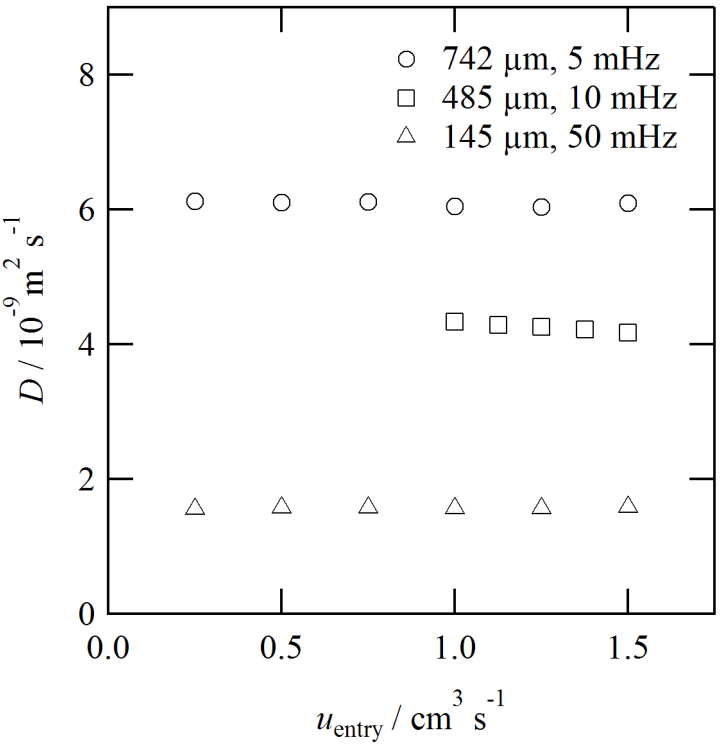

Fig. 4.6. Relationship between D and flow rate u_{entry} in the entry side cell at E_{entry} = (–0.95 ± 0.005) V_{SHE} and T = 298 K.

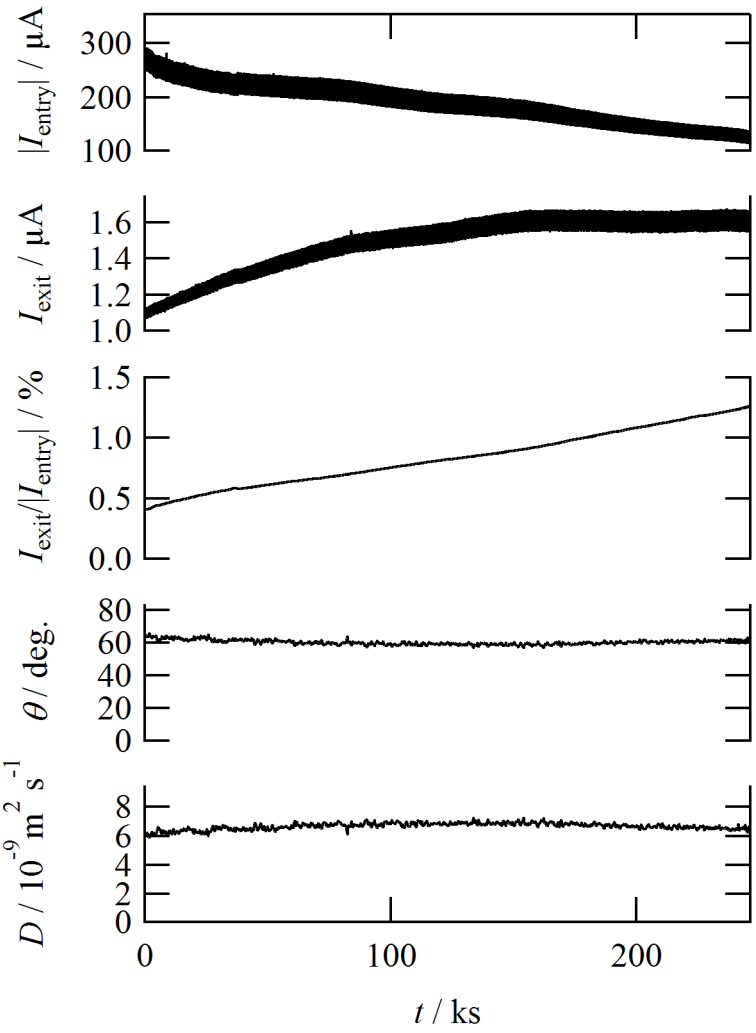

Fig. 4.7. Time variation of I_{entry}, I_{exit}, θ, and D during hydrogen penetration into iron in the borate buffer solution. The hydrogen absorption efficiency, $I_{exit}/|I_{entry}|$, is also shown in the middle. L = 742 μm, u_{entry} = 1.5 cm^3 s^{-1}, $E_{entry,0}$ = –1.00 V_{SHE}, ΔE = 5 mV, f = 5 mHz, and T = 298 K.

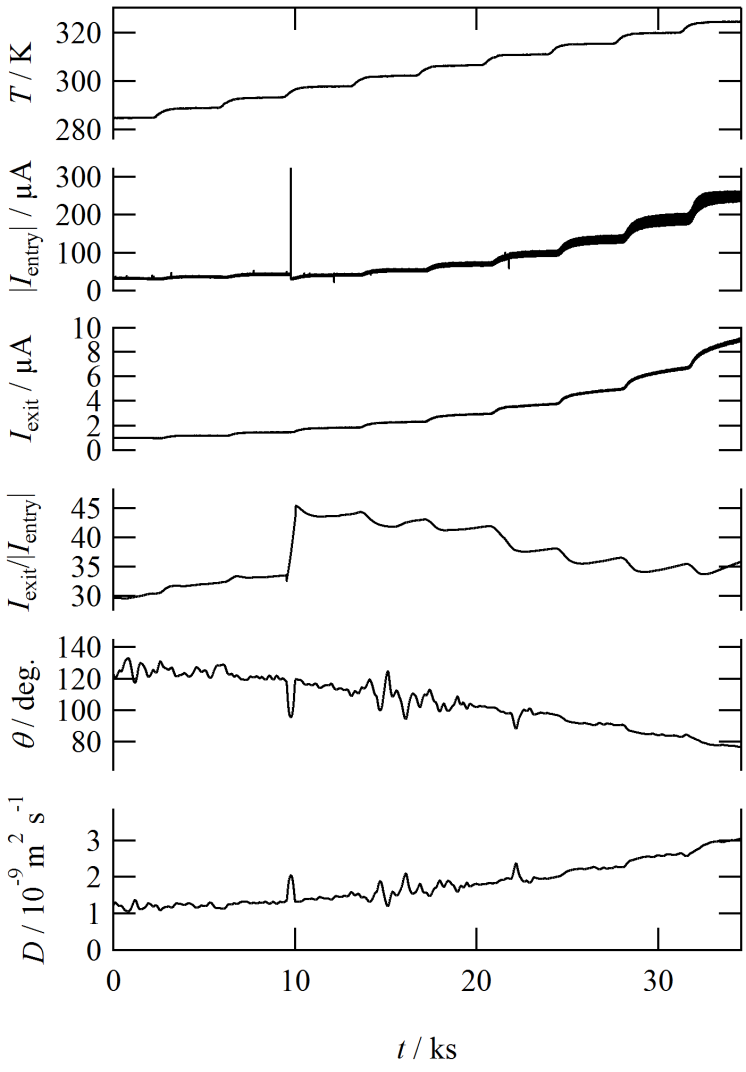

Fig. 4.8. Time variation of I_{entry}, I_{exit}, absorption efficiency, θ, and D during hydrogen penetration into iron in the borate buffer solution under step-wise temperature control. L = 190 μm, u_{entry} = 1.5 cm^3 s^{-1}, $E_{entry,0}$ = –0.90 V_{SHE}, ΔE = 5 mV, f = 50 mHz.

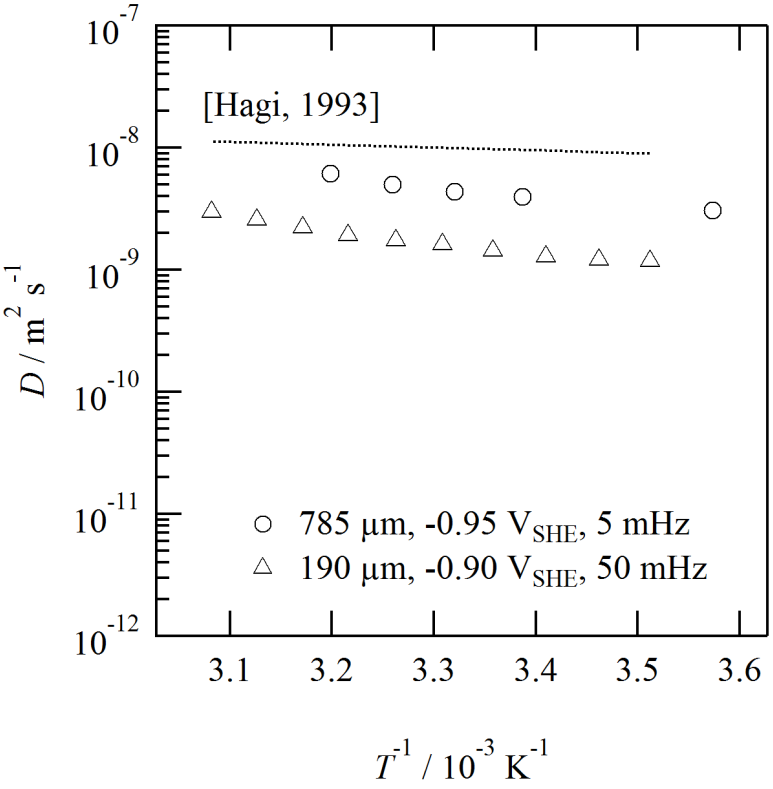

Fig. 4.9. Dependence of D on the temperature of the entry side cell. E_{entry} = (0.95 ± 0.005) V_{SHE} and u_{entry} = 1.5 $cm^3\ s^{-1}$.

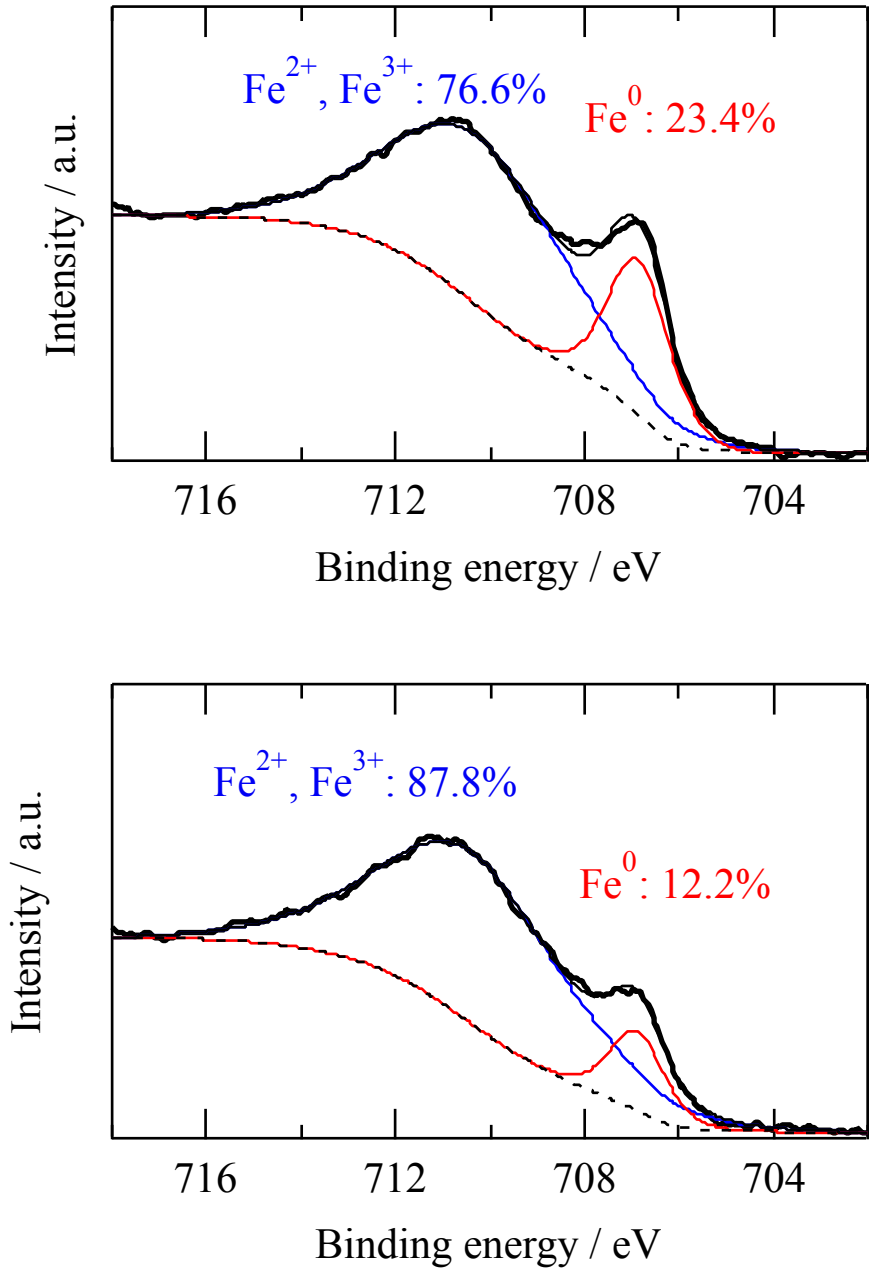

Fig. 4.10. Fe $2p_{3/2}$ photoelectron spectra of iron specimen after hydrogen penetration for 2 days in 0.3 M borate buffer solution at E_{entry} = –0.95 V_{SHE}, u_{entry} = 1.5 cm^3 s^{-1} and temperature T = 298 K. Each experimental spectrum (black bold) has been obtained for (upper) not-polarized area and (lower) polarized area and deconvolved by two components; oxides (blue) and metal (red) after subtraction of background (black dashed) by Shirley's method, yielding total fit (black solid).

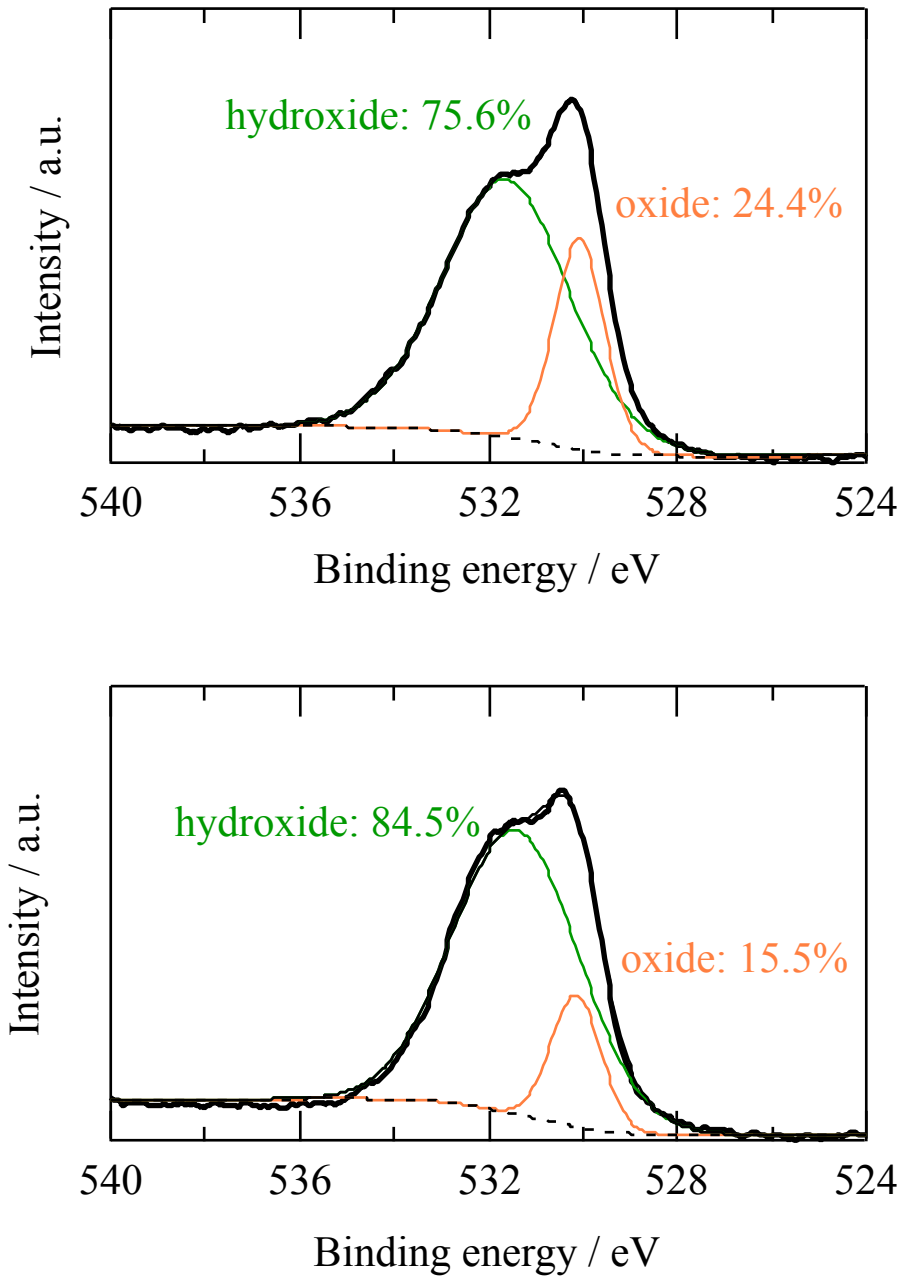

Fig. 4.11. O 1s photoelectron spectra of iron specimen after hydrogen penetration for 2 days in 0.3 M borate buffer solution at E_{entry} = –0.95 V_{SHE}, u_{entry} = 1.5 cm^3 s^{-1} and temperature T = 298 K. Each experimental spectrum (black bold) has been obtained for (upper) not-polarized area and (lower) polarized area and deconvolved by two components; hydroxide (blue) and oxide (red) after subtraction of background (black dashed) by Shirley's method, yielding total fit (black solid).

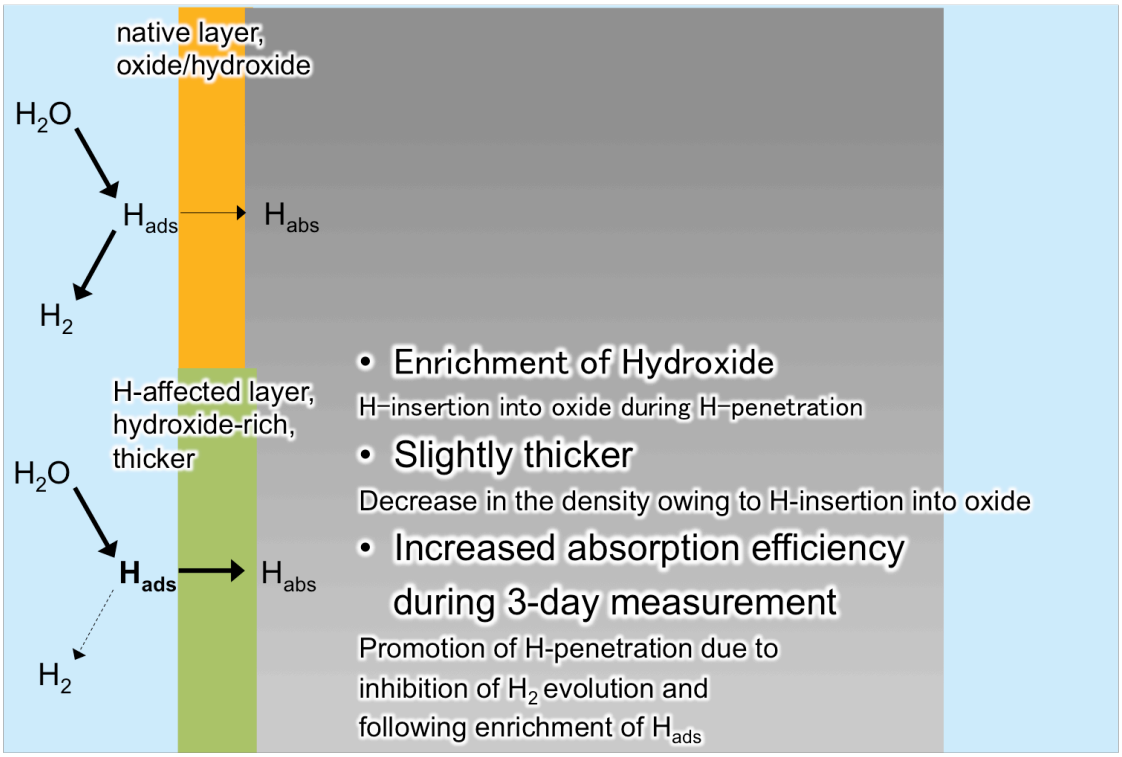

Fig. 4.12. Schematic illustration of proposed mechanistic model for deterioration of surface layer on the entry side surface during hydrogen penetration measurement.

Chapter 5: Summary

Hydrogen penetrated in iron and steel causes hydrogen embrittlement, which threatens the safety use of these materials. Although there have already been long history of hydrogen penetration study, the detailed mechanism and kinetics of hydrogen penetration is not fully elucidated. Especially, time-dependent measurement method for evaluation of hydrogen penetration behavior has been lacking. This dissertation aims to enable time-dependent hydrogen penetration measurement by utilization of sinusoidal perturbation method. The emphasis has also been put on the verification of the applicability of this method to local measurement and to the measurement on heterogeneous specimens.

In Chapter 1, the background of the study and the mechanisms of existing measurement methods for hydrogen penetration were reviewed, and the aim of the dissertation was described.

In Chapter 2, previous studies on hydrogen penetration and its measurement method were introduced with the characteristic design of DS cells developed. For some types of modified DS cell, the potential problems originated from the peculiarity of the measurement method and the cell design were described.

In Chapter 3, the analysis of hydrogen penetration in multi-dimensional geometry was conducted using numerical calculations. Local hydrogen penetration in a homogeneous specimen and hydrogen penetration in heterogeneous specimen were simulated by FEM calculation of diffusion problem in two-dimension. In the case of hydrogen penetration with sinusoidal perturbation in a homogeneous steel sheet, the calculated dependence of phase shift coincided with the algebraic equation reported by Sekine. In the case of hydrogen penetration in a heterogeneous steel sheet with two domains having different diffusion coefficients, the

penetration behavior was characterized by a mean diffusion coefficient of two domains. The result of simulation for reported local hydrogen penetration with a micro-capillary cell showed that the detection resolution was limited to below 50%.

In Chapter 4, a new methodology for time-dependent measurement of hydrogen penetration by a combination of sinusoidal perturbation and FFT was introduced. It was utilized for the investigation of hydrogen penetration into annealed pure iron sheets from a borate buffer solution. The measured dependence of phase shift on specimen thickness and polarization potential suggested the presence of a surface barrier layer on the entry side surface of the specimen. Temporal changes in the phase shift and hydrogen-diffusion coefficient were examined in detail; they indicated deterioration of the barrier layer during electrochemical hydrogen penetration in the borate buffer solution. The time-dependent hydrogen-penetration measurement method was proven to be useful in evaluating the deterioration of the barrier layer and its effect on the hydrogen-penetration behavior.

In Chapter 5, the conclusions obtained in each chapter have been summarized and outlook for the study is shown.

Through the dissertation, the range of hydrogen penetration measurement has been enhanced by introduction of the concept of time-dependent measurement. This measurement method is considered to be useful to trace temporal change of hydrogen penetration behavior into corroding metal, since the method is capable of separating the change of hydrogen diffusivity and the change in hydrogen absorption efficiency. The method makes it easier to understand which factor is responsible for the change in electrochemical response in electrochemical hydrogen penetration.

Appendix

1 – LabVIEW program to calculate phase shift using FFT

The front pane and the brock diagram is shown in Fig. A1.1 and Fig A1.2, respectively. This program conduct fast Fourier transform (FFT) for the input currents waveforms and calculate the phase shift between them. This program requires a plot data of Sekine's equation (Eq. 1.6.3) as "sekine_function.csv" to work.

Input data: 5 column CSV (comma–separated values) file; time, E_{entry}, I_{entry}, E_{exit}, I_{exit}. The data should be obtained at regular interval. The starting time of the measurement must be given in the filename as "YYYYMMDDhhmmss.csv"; for example, "20181128210532.csv" for the data obtained by a measurement started from 2018/11/28 21:05:32. Some information must be input on the front panel; number of samples for a single processing, f, L, temporal interval of input data in seconds.

Output data: 15 column CSV file; time, I_{entry}, I_{exit}, E_{entry}, E_{exit}, θ, UNIX time (the elapsed seconds from 1899/12/30 00:00:00), temporal mean of I_{entry}, perturbation amplitude of I_{entry}, temporal mean of I_{exit}, perturbation amplitude of I_{exit}, absorption efficiency, amplitude ratio of I_{exit} to I_{entry}, D.

Fig. A1.1. Front panel of the program.

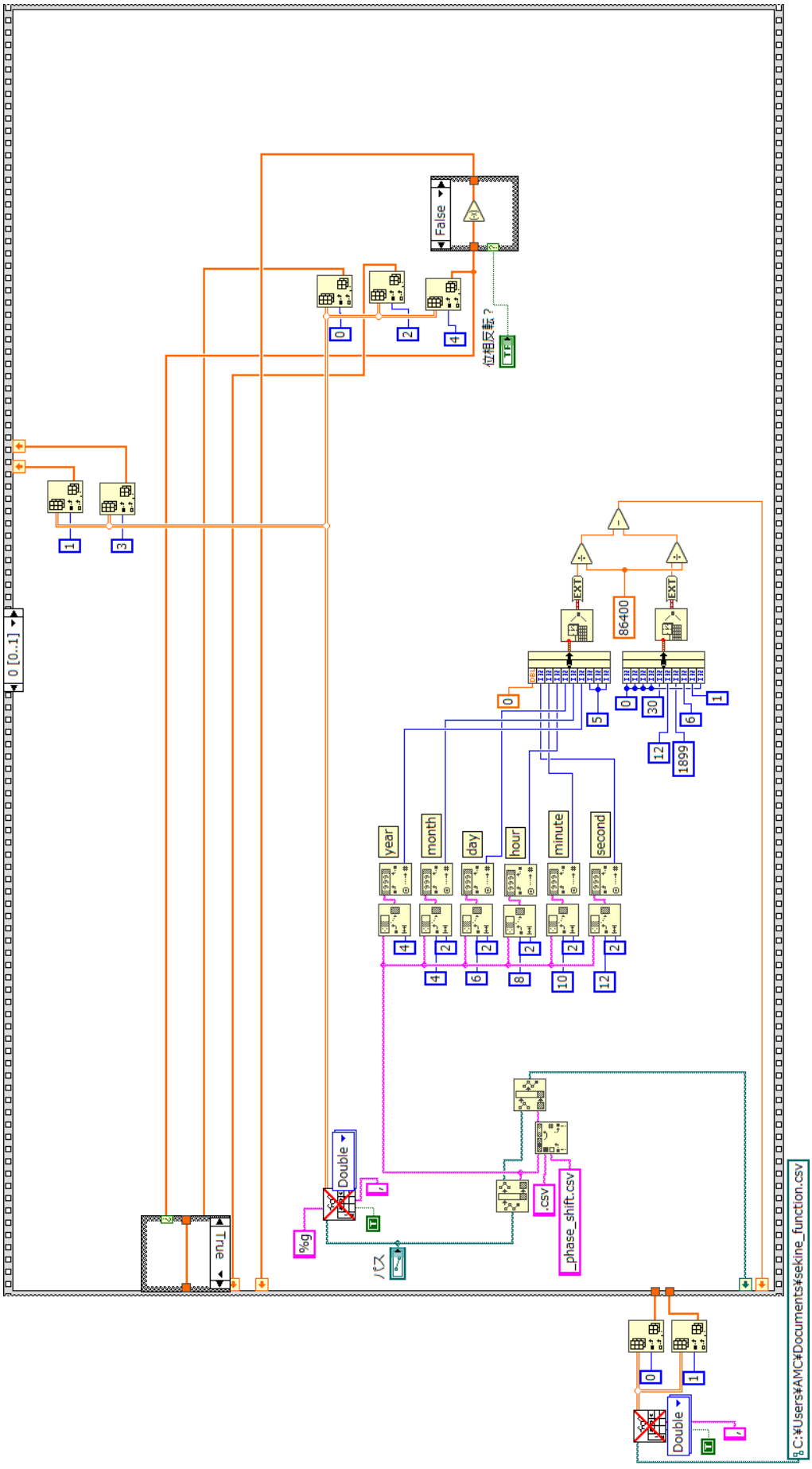

Fig. A1.2. The block diagram of the program (1/2).

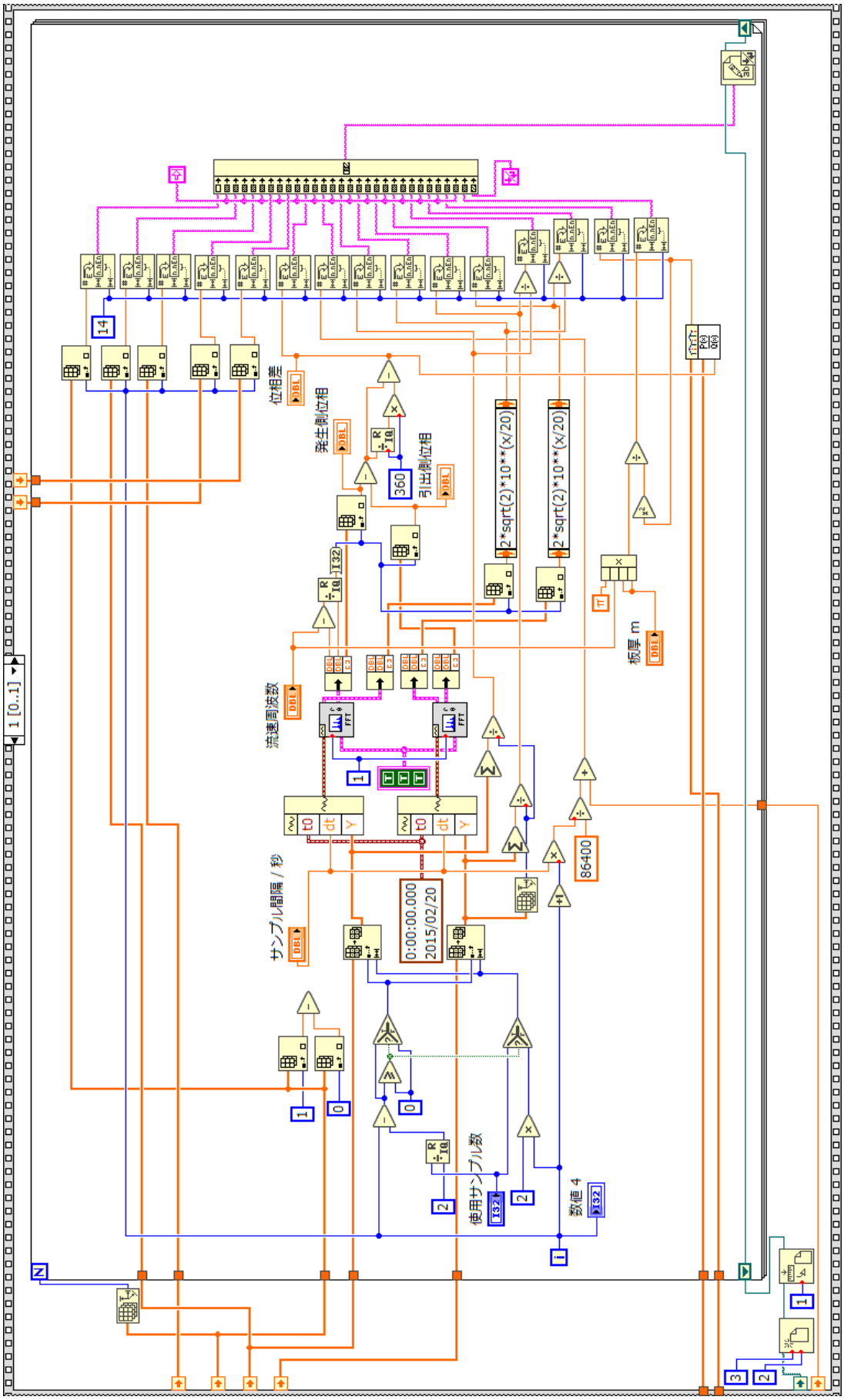

Fig. A1.2 (continued from the previous page). The block diagram of the program (2/2).

2 – Pourbaix diagram and cathodic dynamic polarization curve of iron

Figs. A2.1, A2.2 show the pourbaix diagrams of iron in acidic environment and in basic environment, respectively. The cathodic potentiodynamic polarization curve in pH 8.4 borate buffer solution are also shown in Fig A2.2.

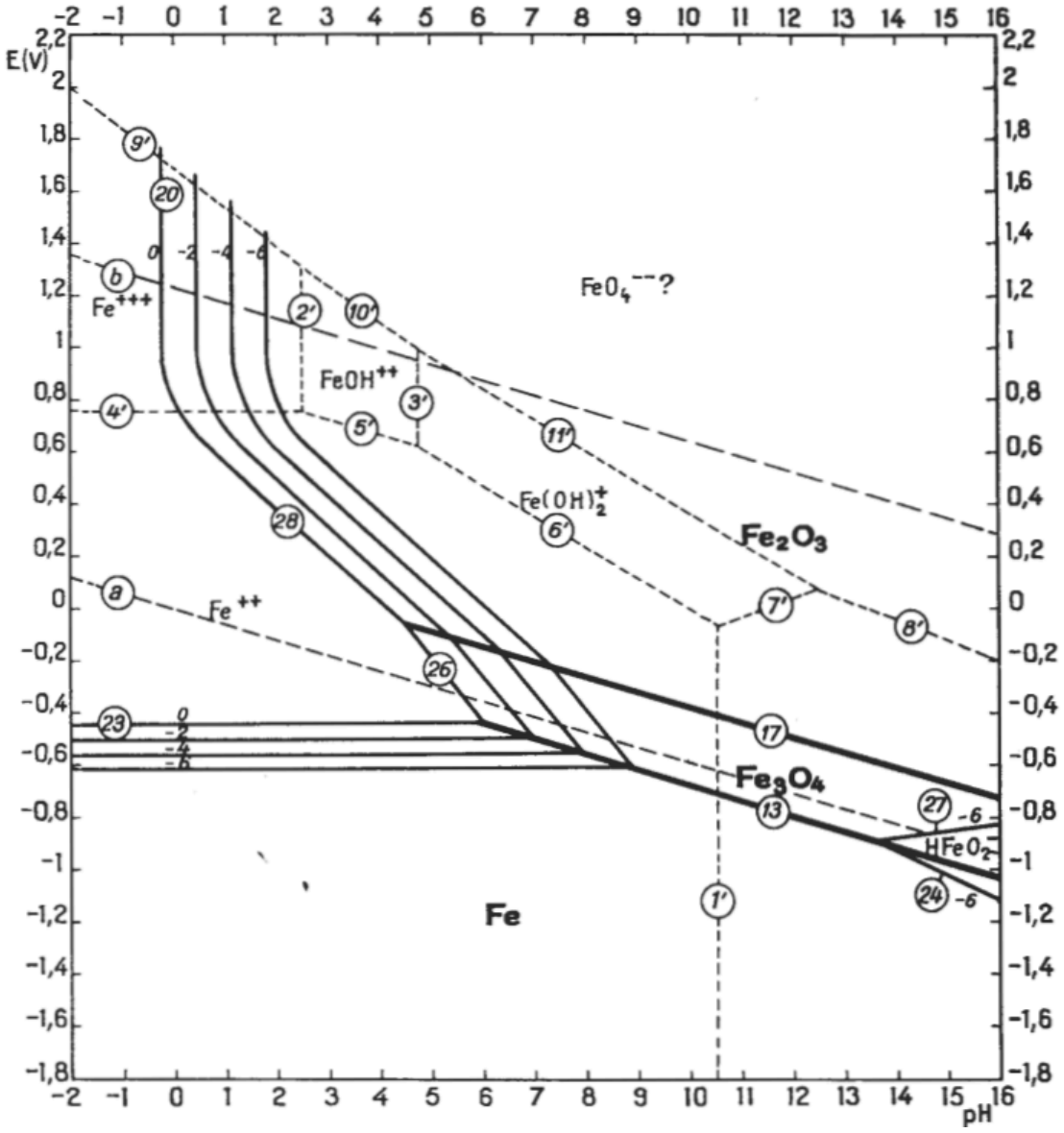

Fig. A2.1. Potential–pH equilibrium diagram for the system iron–water, at 25ºC [considering as solid substances only Fe, Fe_3O_4 and Fe_2O_3].

This figure was reprinted from the original literature: M. Pourbaix, *Atlas of Electrochemical Equilibria in Aqueous Solution*, 2nd ed. (National Association of Corrosion Engineering, Houston, 1974).

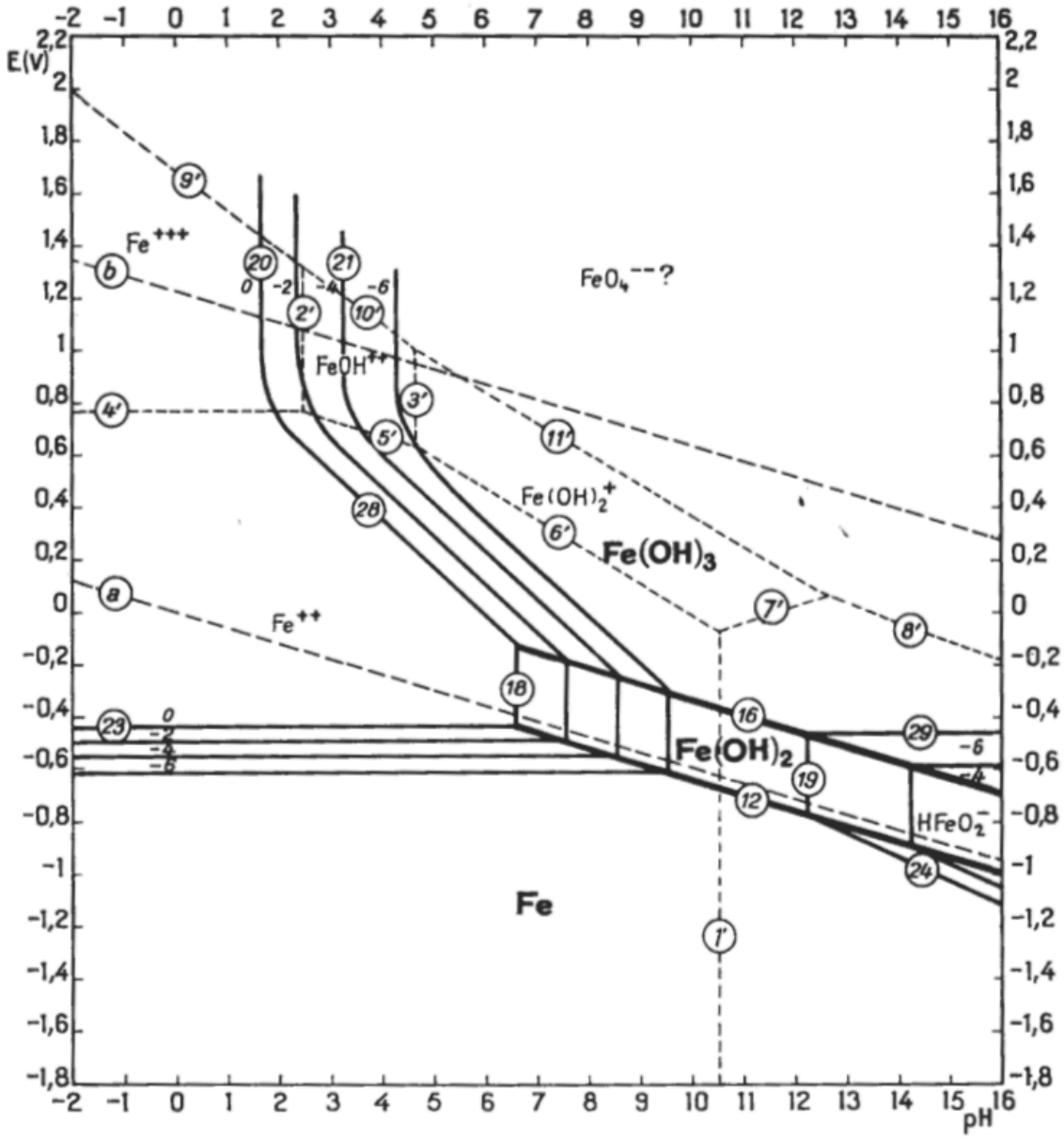

Fig. A2.2. Potential–pH equilibrium diagram for the system iron–water, at 25ºC [considering as solid substances only Fe, $Fe(OH)_2$ and $Fe(OH)_3$].

This figure was reprinted from the original literature: M. Pourbaix, *Atlas of Electrochemical Equilibria in Aqueous Solution*, 2nd ed. (National Association of Corrosion Engineering, Houston, 1974).

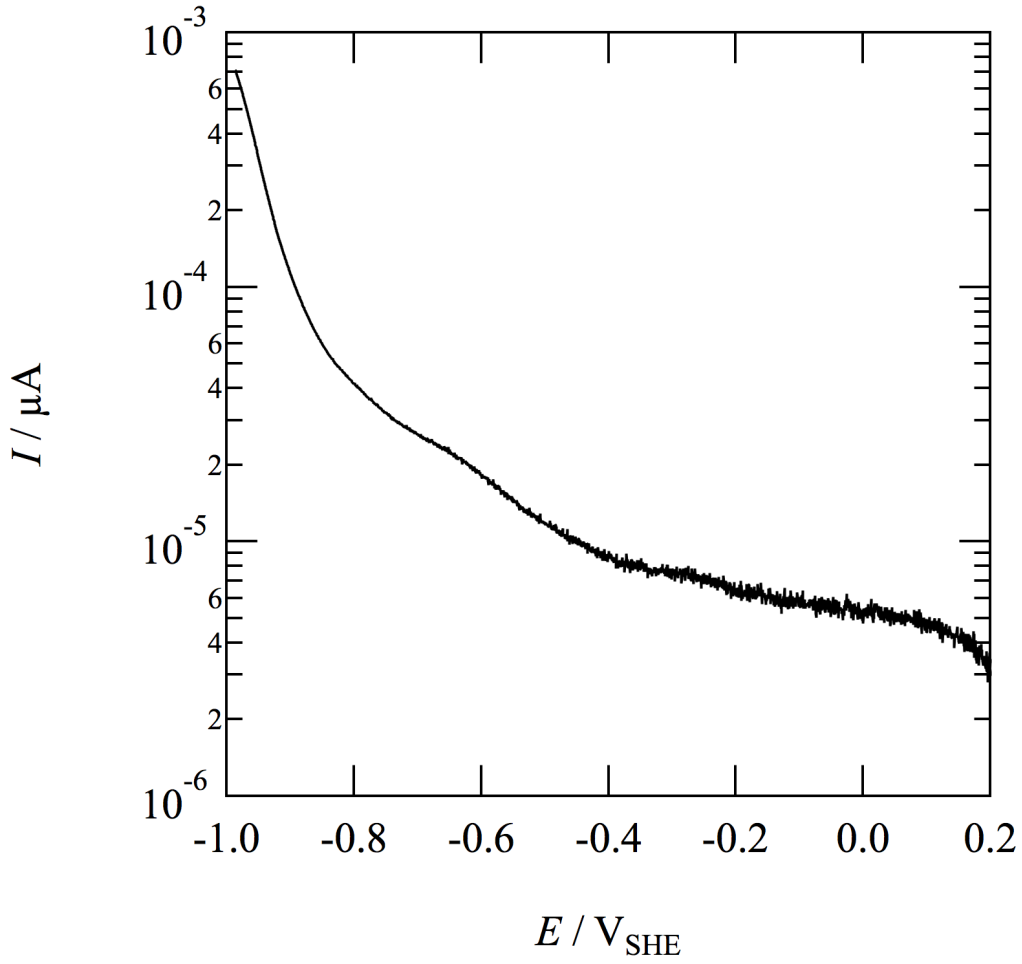

Fig. A2.3. Cathodic potentiodynamic polarization curve of iron in 0.3 M boric acid–borate buffer solution deaerated with Ar. The potential sweep rate was 1 mV s^{-1}.

3 – List of symbols used in this dissertation

All the symbols used in this dissertation are shown in Table A1.

Table A1. List of symbols used in this dissertation.

Symbol	Dimensions	Meaning
A	–	Perturbation amplitude ratio of hydrogen entry flux to the exit flux
a_i	–	Activity of a chemical species i in solution
C	mol m^{-3}	Concentration
C_0	mol m^{-3}	Hydrogen concentration at the entry side surface
C_{lattice}	mol m^{-3}	Hydrogen concentration in interstitial positions of a regular lattice
$C_{t=0}$	mol m^{-3}	Initial hydrogen concentration
C_{trap}	mol m^{-3}	Hydrogen concentration in trap sites
$C_{x=0}$	mol m^{-3}	Hydrogen concentration at the entry side surface
$C_{x=L}$	mol m^{-3}	Hydrogen concentration at the exit side surface
D	m^2 s^{-1}	Diffusion coefficient
D_0	m^2 s^{-1}	Maximum value of D at high temperature
D_{A}	m^2 s^{-1}	Diffusion coefficient of hydrogen in domain A
D_{B}	m^2 s^{-1}	Diffusion coefficient of hydrogen in domain B
D_{lattice}	m^2 s^{-1}	Hydrogen diffusion coefficient in a regular lattice
D_{mean}	m^2 s^{-1}	Mean diffusion coefficient of hydrogen in heterogeneous matrix
E	V	Electrode potential
E_0	V	Equilibrium potential
E_{a}	J mol^{-1}	Activation energy for the diffusion of hydrogen
E_{entry}	V	Polarization potentialat the entry side cell
$E_{\text{entry,0}}$	V	Mean polarization potentialat the entry side cell
E_{exit}	V	Polarization potentialat the exit side cell

Table A1. (Continued from the previous page) List of symbols used in this dissertation.

Symbol	Dimensions	Meaning
F	A s mol^{-1}	Faraday constant
f	s^{-1}	Frequency of sinusoidal perturbation
i	A m^{-2}	Current density
i_0	A m^{-2}	Exchange current density
I_{entry}	A	Current at the entry side cell
I_{exit}	A	Current at the exit side cell
$\mathbf{J}$	mol m^{-2} s^{-1}	Diffusive flux of substance
$\mathbf{J}_{x=0}$	mol m^{-2} s^{-1}	Hydrogen mass flux passing through the entry side surface
$\mathbf{J}_{x=L}$	mol m^{-2} s^{-1}	Hydrogen mass flux passing through the exit side surface
k	–	Probability of trapping
$k_{-\mathrm{H}}$	mol m^{-2} s^{-1}	Backward reaction rate constant of Heyrovsky step in acidic solution
$k_{-\mathrm{T}}$	mol m^{-2} s^{-1}	Backward reaction rate constant of Tafel step in acidic solution
$k_{-\mathrm{V}}$	mol m^{-2} s^{-1}	Backward reaction rate constant of Volmer step in acidic solution
$k'_{-\mathrm{H}}$	mol m^{-2} s^{-1}	Backward reaction rate constant of Heyrovsky step in basic or neutral solution
$k'_{-\mathrm{V}}$	mol m^{-2} s^{-1}	Backward reaction rate constant of Volmer step in basic or neutral solution
k'_{H}	mol m^{-2} s^{-1}	Forward reaction rate constant of Heyrovsky step in basic or neutral solution
k'_{V}	mol m^{-2} s^{-1}	Forward reaction rate constant of Volmer step in basic or neutral solution
k_{H}	mol m^{-2} s^{-1}	Forward reaction rate constant of Heyrovsky step in acidic solution
k_{T}	mol m^{-2} s^{-1}	Forward reaction rate constant of Tafel step in acidic solution
k_{V}	mol m^{-2} s^{-1}	Forward reaction rate constant of Volmer step in acidic solution
L	m	Thickness of specimen sheet
N	mol m^{-3}	Concentration of trapping site
n	–	Occupancy of trapping site
n_{trap}	–	Fractional occupancy of hydrogen trap sites

Table A1. (Continued from the previous page) List of symbols used in this dissertation.

Symbol	Dimensions	Meaning
p	–	Probability of de–trapping
R	J K^{-1} mol^{-1}	Gas constant
T	K	Absolute temperature
t	s	Time
t_{break}	s	Breakdown time of hydrogen mass flux at the exit side surface
t_{lag}	s	Lag time of hydrogen mass flux at the exit side surface
u_{entry}	m^3 s^{-1}	Flow rate of solution in the entry side cell
u_{exit}	m^3 s^{-1}	Flow rate of solution in the exit side cell
w_A	m	Width of domain A
w_B	m	Width of domain B
z	–	Number of electrons transferred by the reaction
α	–	Variable related to phase shift in sinusoidal perturbation method (equals to $(\pi f l^2/D)^{1/2}$)
α_A	–	Electron transfer coefficient of the oxidation reaction
ΔC	mol m^{-3}	Perturbation amplitude of absorbed hydrogen concentration at the entry side interface
ΔE	V	Amplitude of perturbation applied in polarization potential at the entry side cell
ΔG	J mol^{-1}	Gibbs free energy change
ΔG_0	J mol^{-1}	Standard Gibbs free energy change
ΔH	J mol^{-1}	Enthalpy change
ΔH_0	J mol^{-1}	Standard enthalpy change
ΔS	J mol^{-1}	Entropy change
ΔS_0	J mol^{-1}	Standard entropy change
η	V	Overpotential

Table A1. (Continued from the previous page) List of symbols used in this dissertation.

Symbol	Dimensions	Meaning
θ	degree	Phase shift between hydrogen mass flux passing through the entry side and hydrogen mass flux at the exit side surface
$\theta_{coverage}$	–	Surface coverage of adsorbed hydrogen
$\mu_{0,i}$	J mol^{-1}	Standard chemical potential of a chemical species *i*
μ_i	J mol^{-1}	Chemical potential of a chemical species *i*
v	mol m^{-3} s^{-1}	Reaction rate
v_{-H}	mol m^{-2} s^{-1}	Backward reaction rate of Heyrovsky step in acidic solution
v_{-T}	mol m^{-2} s^{-1}	Backward reaction rate of Tafel step in acidic solution
v_{-V}	mol m^{-2} s^{-1}	Backward reaction rate of Volmer step in acidic solution
v'_{-H}	mol m^{-2} s^{-1}	Backward reaction rate of Heyrovsky step in basic or neutral solution
v'_{-V}	mol m^{-2} s^{-1}	Backward reaction rate of Volmer step in basic or neutral solution
v'_{H}	mol m^{-2} s^{-1}	Forward reaction rate of Heyrovsky step in basic or neutral solution
v'_{V}	mol m^{-2} s^{-1}	Forward reaction rate of Volmer step in basic or neutral solution
v_H	mol m^{-2} s^{-1}	Forward reaction rate of Heyrovsky step in acidic solution
v_T	mol m^{-2} s^{-1}	Forward reaction rate of Tafel step in acidic solution
v_V	mol m^{-2} s^{-1}	Forward reaction rate of Volmer step in acidic solution
φ	–	Hydrogen absorption efficiency

List of Publications

– Publications related to the dissertation:

[1] Yudai Yamamoto, Yuichi Kitagawa, Takayuki Nakanishi, Yasuchika Hasegawa and Koji Fushimi, "FEM Analysis for Sinusoidal Perturbation of Hydrogen Permeation into a Steel Sheet", *ISIJ International* **56**, 472 (2016).

[2] Yudai Yamamoto, Yuichi Kitagawa, Yasuchika Hasegawa and Koji Fushimi, "Time-Dependent Measurement of Hydrogen Penetration into Iron Sheets from a Borate Buffer Solution Using FFT Analysis", *Journal of the Electrochemical Society,* **165**, C900 (2018).

– Other publications:

[1] Koji Fushimi, Kazunori Kurauchi, Yudai Yamamoto, Takayuki Nakanishi, Yasuchika Hasegawa and Toshiaki Ohtsuka, "Growth and Degradation of an Anodic Oxide Film on Titanium in Sulphuric Acid Observed by Ellipso-microscopy", *Electrochimica Acta* **144**, 56 (2014).

Acknowledgements

First of all, I sincerely express my deepest gratitude to my supervisor Assoc. Prof. Koji Fushimi for ceaseless support and kind coaching throughout the whole doctoral studentship.

I appreciate the insightful comments and from Prof. Kazuhisa Azumi, Prof. Yasuchika Hasegawa and Prof. Kei Murakoshi as advisors for the dissertation. The appreciation also goes to Assoc. Prof. Masatoshi Sakairi and Asst. Prof. Yuichi Kitagawa.

I would also like to thank all the members and ex-members of Advanced Materials Chemistry Laboratory, Graduated school of Chemical Sciences and Engineering, Hokkaido University, Japan, who had kindly helped my research and daily life.

Finally, I gratefully acknowledge the financial support from the Japan Society for the Promotion of Science (JSPS) as “Grant-in-Aid for JSPS Research Fellow” and from the Ministry of Education, Culture, Sports, Science and Technology through Program for Leading Graduate Schools (Hokkaido University "Ambitious Leader’s Program").

February 2019,

Yudai Yamamoto